DEVELOPING INNOVATIVE GEOSPATIAL TECHNIQUES FOR ASSESSING THE SURFACE IN ALPINE SETTINGS: SAN JUAN MOUNTAINS, CO AND PATAGONIA ICE FIELD, ARGENTINA

A Dissertation

by

PANSHU ZHAO

Submitted to the Graduate and Professional School of
Texas A&M University
in partial fulfillment of the requirements for the degree of

DOCTOR OF PHILOSOPHY

Chair of Committee,	John R. Giardino
Committee Members,	John J. Vitek
	Kevin R. Gamache
	Hongbin Zhan
Head of Department,	Ronald Kaiser

December 2021

Major Subject: Water Management and Hydrological Science

ABSTRACT

Geospatial technology has rapidly developed over the past ten years and is making substantial impacts in geomorphology. The new techniques, which have been developed, require high computational ability to produce in-depth analysis, accurate mapping, and precise characterization of details. Thus, geospatial technology is an excellent technology for completing sophisticated tasks in geomorphology. Unfortunately, existing commercial software coupled with traditional geomorphological methods do not adequately satisfy the demands of geomorphologists today. In addition, current geospatial technology consistently lags behind the technology advancement in other relevant domains (e.g., computer vision and digital image processing). It also appears many geomorphologists because of their lack of training in computational programming skills, are forced to use only commercially available software. Unfortunately, this leads to inadequate and incomplete analysis because many of the commercial software, in many instances, are too generalized to address specific geomorphological problems. To overcome the above-mentioned limitations in geomorphologic studies, this dissertation focuses on designing multiple, innovative geospatial algorithms for mapping and studying in the alpine and glacial environments.

The objective of this dissertation was to 1) develop an ANN (artificial neural network) based protocol to map basic geomorphology in the alpine and glacial environments; 2) create a protocol by using graph theory with object-oriented analysis to quantify changes in the surface structure of glaciers.

Two study sites were selected for this research: the San Juan Mountains in Southwestern Colorado and the Southern Patagonia Ice Field, Argentina. Results from the ANN analysis of the San Juan Mountains suggest that the combination of ANN and innovative topographic indices can facilitate the geomorphology mapping in alpine settings.

Secondly, this dissertation focused on two glaciers in Patagonia: the Glacier Perito Moreno (GPM) and Glacier Ameghino (GA) for the period 2000-2011, which was the best available DEMs to study the area. GPM has been stable since the first *in situ* field measurement in Patagonia, whereas GA has been retreating during the same time. Thus, this dissertation suggests that a stable terminus does not necessarily represent a stable supra-glacier surface structure or a decrease in the dynamic activities of a glacier. The result suggests that the surface structure of GPM has more rapidly transitioned into a more fragmented system when compared to GA. Four underlying reasons could account for this contrasting pattern: solar panel effect, prehistorical landslide relict, glacier orientation shift, and AAR (accumulation area ratio) difference. Both glaciers are located side-by-side and flow in the same direction.

This dissertation does not diminish the need for field work but does facilitate study of areas of extreme accessibility.

DEDICATION

This work is dedicated to the people who have come to America with big dreams.

No matter where you originally come from, YOU CAN MAKE IT!

AMERICA IS GREAT BECAUSE OF YOU!

ACKNOWLEDGEMENTS

I am very grateful for Dr. Giardino's guidance for my dissertation and my Ph.D. life. As a graduate student, I have been in too many situations that were not limited to academia but also include immigration and social issues. Dr. Giardino has always led me to the right directions and most of all, he never gave up on me. Without Dr. Giardino being my advisor, I would not have finished my dissertation or become a proud U.S. citizen.

I would also like to thank Dr. Gamache for contributing to my publication record and giving me very sincere advice on the due process during my legal proceedings with the U.S. Army and the United States Citizenship and Immigration Services (USCIS).

In addition, thank you Dr. Vitek, Dr. Zhan, and Dr. Owens for reviewing and editing my dissertation.

I am also very grateful to Attorney Margaret Stock and Nio class-action attorneys for helping me to obtain justice as an immigrant solder in the U.S. Army.

I would like to extend my acknowledgement to the friends I made since I landed in the United States, including Chris Madeira, Billy Hales, Seth Adams, Chris Norman, Dan Quinn, the Loder Family, the Hatch Family, the Nixon Family, the Bagby Family, my battle buddies in 321st Combat Engineering Company, and other friends who helped me relentlessly.

Finally, thanks to my mother, father, and my brother for their encouragement and support. I love my family!

CONTRIBUTORS AND FUNDING SOURCES

Contributors

This work was supervised by a dissertation committee consisting of Dr. John R. Giardino (committee chair) of the Department of Water Management and Hydrological Sciences, Dr. John J. Vitek of the Department of Geology and Geophysics, Dr. Kevin R. Gamache of the Bush School of Government and Public Service and Dr. Hongbin Zhan of Department of Water Management and Hydrological Sciences.

Funding Sources

This dissertation research is funded by multiple funding resources, including fellowships and scholarships from Texas A&M University, investment profits under supervision of U.S. Securities and Exchange Commission (SEC), stipends from the U.S. Army, and family educational foundation.

TABLE OF CONTENTS

Page

ABSTRACT ii

DEDICATION iv

ACKNOWLEDGEMENTS v

CONTRIBUTORS AND FUNDING SOURCES vi

TABLE OF CONTENTS vii

LIST OF FIGURES viii

LIST OF TABLES xi

1. INTRODUCTION 1

2. TECHNIQUES FOR STUDYING SURFACE CHANGE 6

3. CONTRASTING PATTERNS OF GLACIER ACTIVITIES IN THE SOUTH PATAGONIAN ICEFIELD 60

4. THE STRATIFICATION OF AUTOMATED SURFACE EXPRESSIONS USING NEW TOPOGRAPHC INDICS AND ARTIFICIAL NEURAL NETWORKS 134

5. CONCLUSIONS 160

LIST OF FIGURES

Page

Figure 1. An example of an artificial neural network. 11

Figure 2. Typical neighborhood in image processing 12

Figure 3. A typical FCM architecture. 13

Figure 4. The THMS. 14

Figure 5. A traditional semivariogram 27

Figure 6. Strahler stream order 40

Figure 7. The topomap of study area 42

Figure 8. FFT, Wedge, and ring. 44

Figure 9. FFT analysis results. 45

Figure 10. Illustration of original classification based on landform 47

Figure 11. Landform classification map of the San Juan Mountains. 48

Figure 12. Surface roughness in the San Juan Mountains. 49

Figure 13. Illustration of the convergence and divergence concepts. 50

Figure 14. The divergence index image and the convergent index image. 51

Figure 15. The exponential decay function used in fuzzy classification. 52

Figure 16. The results from the thresholding method at different values. 53

Figure 17. The results from the fuzzy classification at different powers 54

Figure 18. The Patagonia Icefields map. 63

Figure 19. The GPM and the GA map 66

Figure 20. The conceptual model of glacier dynamics 68

Figure 21. Basic weather data for Patagonia Ice Field 71

Figure 22. The study area map with field photoes. 73

Figure 23. Surface-elevation changes over GPM and GA from 2000 to 2011. 77
Figure 24. Surface elevation change in GA and GPM along the central flowlines 78
Figure 25. The hypsometry curves for SRTM and ASTER DEMs.. 79
Figure 26. Schematic figure for this index.. 80
Figure 27. Convergence index computed based on Equation. 82
Figure 28. Segmentation results. 83
Figure 29. Network analysis conceptual diagram 85
Figure 30. Centroid analysis.....86
Figure 31. The semantics of how to calculate Topographic Exposure Index.. 88
Figure 32. Comparisons with LANDSAT Image.....90
Figure 33. Network analysis results for both SRTM and ASTER imageries.. 92
Figure 34. Cross-comparisons of center-line profiles.. 93
Figure 35. The topographic exposure results 95
Figure 36. TOPEX analysis for GA and GPM.....97
Figure 37. Field photo of the GPM terminus 105
Figure 38. Segmentation results from ASTER DEM before and after noise removal…107
Figure 39. Convergence images, segmentation images and link images. 112
Figure 40. Post analysis of link images. 114
Figure 41. “Solar Effect”.....116
Figure 42. The North-facing inspection angle image.....117
Figure 43. The high resolution image. 119
Figure 44. GA and GPM centerlines overlaid on topographic exposure image. 122
Figure 45. The study area of Chapter 4. 142
Figure 46. An example of an artificial neural network 144

Figure 47. Surface expressions based on processes. 145
Figure 48. The basic three input layers. 148
Figure 49. The additional basic input layers. 149
Figure 50. Height above Nearest Drainage. 150
Figure 51. The futher additional basic input layers. 151
Figure 52. Surface-expression objects 152
Figure 53. Spatial distribution of sampling points across the region. 154
Figure 54. The comparison between ANN mapping and Kelkar's mapping 156

LIST OF TABLES

Page

Table 1. NOAA precipitation and cloud radars.....9

Table 2. Six examples of satellites,.....17

Table 3. Biophysical indices can be calculated from remote sensing image. 18

Table 4. Online climate-data sources. 22

Table 5. Evaluation on Lidar input, GPS tracks, Spatial Analysis and Spatial Interpolation.....33

Table 6. Evaluation on Geostatistics, Image filters, and Image transformation. 34

Table 7. Evaluation on Image enhancement, Geodatabase, Classification, and Segmentation. 35

Table 8. Evaluation on Pattern recognition, Terrain analysis, and Raster analysis. 36

Table 9. Evaluation on Vector analysis, 3D visualization, Scripting functionality, and Batch processing.....37

Table 10. Url for each software package.....38

Table 11. Uniqueness of some software.....39

Table 12. Detailed information for glacier-surface changes. 98

Table 13. Details about how GA and GPM surface structure changes over time.....113

1. INTRODUCTION

A geomorphology map contains exponentially more information than plain words (Vitek et al., 1996). For almost every geomorphological project, an accurate, visual depiction of the study area could help the map end-user gain a basic geospatial sense of the study interest at first glance, including size, shape, orientation, scale, spatial complexity, texture, and patterns (Whitmeyer et al., 2010). A more comprehensive understanding of the study interest, such as existing landforms, dominant processes, underlying Quaternary geomorphic evidence, can also be obtained by the analyzing an accurate map (Walsh et al., 1998). Thus, an accurate geomorphology map is imperative for undertaking any fundamental and/or applied geoscience study (Williams et al., 2018).

The advent of Geography Information Systems (GIS) in 1960s has enhanced traditional field mapping that relies on accurate identification and representation (Goodchild et al., 2007). GIS can assist mapping geomorphology in various ways, from data acquisition and storage to spatial analysis and product visualization (Bubniak et al., 2020). To undertake a more sophisticated geomorphological or hydrological science projects, however, GIS itself can not satisfy the need because of the following four reasons:

i. GIS has limited geo-computation capacities. A civilian GIS system today significantly depends on the computational capacity. Thus, supercomputer and cloud computation are important for mass-data processing (Wang, 2010).

ii. GIS is limited when addressing digital image processing and computer vision. Raster and vector are two basic data formats in a GIS setting. With LiDAR and UAV data acquisition used to generate high-resolution images and DEMs, the existing raster-based algorithm is not sufficient for geomorphologic studies, however, many raster-based algorithms can be directly adapted from image processing and computer vision to fulfill this need (Weickert, 2000).

iii. GIS users are more frequently locked in a tight coupling GIS setting, as an echo chamber. A loose GIS coupling environment is more powerful than a tight coupling GIS setting when dealing with a geomorphic phenomenon because these processes are more complicated than an individual commercial software can handle (Eldrandaly et al., 2005).

iv. Artificial intelligence has minimal application in the current GIS environment. Not matter if it is Artificial Neural Network or Machine Learning, the existing artificial intelligence has been proven highly efficient and accurate in numerous geomorphologic studies, including landform classification, pattern recognition, feature extraction, and change detection (Openshaw, 1992; Basu, et al., 2019).

Geomorphometry, which is the science and the methodology to characterize Earth surface from process-based point of view, uses mathematical, statistical, and computational solutions to quantify hydrological, morphological, ecological, and other aspects of land surfaces. This approach is optimal for geomorphic mapping and research (Evans, 2019). To overcome the existing issues listed above for a traditional GIS mapping framework, this dissertation focuses on integrating geomorphometry with a

newly developed, innovative algorithm designed to address unique geomorphologic problems in alpine and glacial settings. Specifically, my dissertation contains four major research objectives:

i. investigate how scientists conduct impact analysis of surface change using advanced geospatial technologies,
ii. design a more suitable mapping protocol for process geomorphology in alpine areas,
iii. create a protocol of integrating ANN and this new topographic index for mapping automation, and
iv. create a protocol to combine graph theory and object-oriented analysis to study glacier dynamics.

To achieve these objectives, two study locations were selected for this dissertation, i.e., San Juan Mountains, Colorado, USA, and the Patagonia Ice Field, Argentina. The geomorphologic diversity and human habitation of the San Juan Mountains make it ideal for mapping and studying natural and anthropomorphic landforms (Gamache et al., 2018). More details about the natural and anthropomorphic landforms in this area is discussed in Chapter 4.

The Patagonia Ice Field is the largest ice mass in the Southern Hemisphere excluding Antarctica (Manquehual-Cheuque et al., 2021). The contrasting patterns of glacier dynamics in Patagonia are suitable for mapping and analyzing the underlying reasons for differing glacier movement patterns (Carrasco et al., 2002).

Innovative mapping with ANN can further help in the mapping of basic landforms to show the impact of human activities in alpine environments. This dissertation demonstrates multiple self-designed geospatial algorithms can be used to solve challenging problems in geomorphologic studies today. In addition, graph theory and object-oriented analysis were used to study glacier dynamics. This dissertation suggests that the applicability of topographic shielding is one key component to understand topographic control and local weather circulations.

This dissertation consists of three manuscripts tailored for publication in various geoscience journals. Manuscript One is an analysis of the impact of surface change. Manuscript Two uses object-oriented analysis and graph theory to examine the contrasting patterns on supraglacial surface structure of glacial activity in the Southern Patagonian Icefield. And Manuscript Three integrates a new topographic index and artificial neural networks (ANN) for automated stratification of surface expressions to study geomorphology in the Western San Juan Mountains, Colorado.

REFERENCES CITED

Basu, T. and Pal, S., 2019. RS-GIS based morphometrical and geological multi-criteria approach to the landslide susceptibility mapping in Gish River Basin, West Bengal, India. Advances in Space Research, 63(3), pp.1253-1269.

Bubniak, I.M., Bubniak, A.M. and Gavrilenko, O.D., 2020, May. Digital field geology. In Geoinformatics: Theoretical and Applied Aspects 2020 (Vol. 2020, No. 1, pp. 1-4). European Association of Geoscientists & Engineers.

Carrasco, J.F., Casassa, G. and Rivera, A., 2002. Meteorological and climatological aspects of the Southern Patagonia Icefield. In The Patagonian Icefields (pp. 29-41). Springer, Boston, MA.

Eldrandaly, K.A., Eldin, N., Sui, D.Z., Shouman, M.A. and Nawara, G., 2005. Integrating GIS and MCDM Using COM Technology. Int. Arab J. Inf. Technol., 2(2), pp.162-167.

Evans, I.S., 2019. General geomorphometry, derivatives of altitude, and descriptive statistics. In Spatial analysis in geomorphology (pp. 17-90). Routledge.

Gamache, K., Giardino, J.R., Zhao, P. and Owens, R.H., 2018. Bivouacs of the Anthropocene: Urbanization, landforms, and hazards in mountainous regions. In Urban Geomorphology (pp. 205-230). Elsevier.

Goodchild, M.F., Yuan, M. and Cova, T.J., 2007. Towards a general theory of geographic representation in GIS. International journal of geographical information science, 21(3), pp.239-260.

Manquehual-Cheuque, F. and Somos-Valenzuela, M., 2021. Climate change refugia for glaciers in Patagonia. Anthropocene, 33, p.100277.

Openshaw, S., 1992. Some suggestions concerning the development of artificial intelligence tools for spatial modelling and analysis in GIS. The annals of regional science, 26(1), pp.35-51.

Vitek, J.D., Giardino, J.R. and Fitzgerald, J.W., 1996. Mapping geomorphology: A journey from paper maps, through computer mapping to GIS and Virtual Reality. Geomorphology, 16(3), pp.233-249.

Walsh, S.J., Butler, D.R. and Malanson, G.P., 1998. An overview of scale, pattern, process relationships in geomorphology: a remote sensing and GIS perspective. Geomorphology, 21(3-4), pp.183-205.

Wang, S., 2010. A CyberGIS framework for the synthesis of cyberinfrastructure, GIS, and spatial analysis. Annals of the Association of American Geographers, 100(3), pp.535-557.

Weickert, J., 2000. Applications of nonlinear diffusion in image processing and computer vision.

Whitmeyer, S.J., Nicoletti, J. and De Paor, D.G., 2010. The digital revolution in geologic mapping. Gsa Today, 20(4/5), pp.4-10.

Williams, D.A., Buczkowski, D.L., Mest, S.C., Scully, J.E., Platz, T. and Kneissl, T., 2018. Introduction: the geologic mapping of Ceres. Icarus, 316, pp.1-13.

2. TECHNIQUES FOR STUDYING SURFACE CHANGE

Introduction

This chapter focuses on addressing the fundamental techniques about how geoscientists conduct analysis of the impact of surface change today. Geospatial technology is developing rapidly, however, more often than not, the knowledge domain does not keep up with the technology advancement. This chapter updates the advancement of technology.

More than half of the land surface of Earth has been "plowed, pastured, fertilized, irrigated, drained, fumigated, bulldozed, compacted, eroded, reconstructed, manured, mined, logged, or converted to new uses" (Richter and Mobley, 2009). In less than three centuries, 46 million acres of the virgin landscape in America have been converted to urban uses; and in the next 25 years that number will more than double to 112 million acres (Carbonell and Yaro, 2005). Activities like these have far reaching impacts on life-sustaining processes of the near-surface environment, recently termed the "Critical Zone" (Richter and Mobley, 2009), and if the current rate of land transformation continues, it is unsustainable.

A new geological epoch referred to as the Anthropocene has been proposed (Amundson et al., 2007; Aguilar et al., 2020). The Anthropocene (~250 y BP to present) encompasses some of the most noticeable changes in the history of surface of Earth. (Amundson et al., 2007).

Driven by these myriad global changes caused by human interaction with the natural environment, the Critical Zone concept was conceived in 1998 to represent the

importance of system science in integrating the research of the four scientific spheres (lithosphere, hydrosphere, biosphere, and atmosphere) that interact at the surface of Earth, by studying the linkages, feedbacks, and processes that occurred in the past, are occurring today, and will operate in the future (Dawson et al., 2020).

The Critical Zone is the area of the surface and near-surface systems that extends from bedrock to the atmosphere boundary layer (Anderson et al., 2010). The critical zone lies at the interface of the lithosphere, atmosphere, and hydrosphere (Amundson et al., 2007) and encompasses soils and terrestrial ecosystems. It is a complex mixture of air, water, biota, organic matter, and Earth materials (Brantley et al., 2007). For detailed analysis of the critical zone concept see Giardino and Houser (2015). Thus, the critical zone concept is an appropriate description of the two study locations for the dissertation.

Numerous instruments have been designed and deployed for collecting data related to atmosphere, the surface of Earth, oceans, and the cryosphere (IPCC AR5, 2014). These observational data once retrieved, can be rigorously analyzed with spatial statistics to predict a hazard. The National Oceanic and Atmospheric Administration (NOAA) has been the main driver of state-of-art remote-sensing technology for monitoring precipitation and clouds for long-time periods (Table 1). Radar technology can be used to help measure cloud-water content and microphysical features such as water-droplet size, ice-crystal shape and type (Germann et al., 2006). By using radar observations, hazards resulting from severe storms and tornados can be predicted, identified, and further tracked.

Table 1. NOAA operated Radars adopted for precipitation and cloud observations (NOAA).

NOAA Precipitation and Cloud Radars		
Radar	Wavelength	Application
NOAA/D (Hydro-radar)	3.2 cm	Precipitation, Snow, Storms, Ocean Surface
NOAA/K (Cloud radar)	8.7 mm	Clouds, Boundary Layer, Ocean Surface
NPCO (Cloud radar)	8.7 mm	Long-term Cloud Profiling
MMCR-ARM (Cloud radar)	8.7 mm	Long-term Cloud Monitoring
Ron Brown (Precipitation Radar)	5 cm	Ocean Precipitation Measurement
S-PROF (Precipitation profiler)	10 cm	Precipitation

Artificial Intelligence

Artificial intelligence (AI) is a knowledge-based technique that can serve as an alternative to traditional approaches when modeling environmental complexity is needed. It facilitates insight towards physical process and simulation like a bright brain making its most suitable processing for solving hazard-related problems. To elaborate, 12 AI techniques exist, including: 1) artificial neural networks (ANN), 2) cellular automata (CA), 3) fuzzy cognitive map (FCM), 4) case-based reasoning, 5) rule-based systems, 6) decision tree, 7) genetic algorithms, 8) multi-agent systems, 9) swarm intelligence, 10) reinforcement learning, 11) hybrid systems, and 12) Bayesian networks (Chen et al., 2008). In this section, the focus is on the most popular three, which are ANN, CA, and FCM.

Artificial Neural Network

Artificial neural networks (ANN) are a machine-learning technique, which can learn relationships between specified input and output variables. Neural networks constitute an information processing model that stores empirical knowledge through a learning process and subsequently makes the stored knowledge available for future use. ANN can mimic a human brain to acquire knowledge from the environment through a learning process.

A neuron is the fundamental processing unit in ANNs. A neuron consists of connection links characterized with certain weights (Figure 1). Input is passed from one end of the links, multiplied by the connection weight and transmitted to the summing junction of the neuron (Haykin, 1999). In environmental studies, ANN can facilitate the

modeling of cause-effect relationships such as water-quality forecasting (Palani et al., 2008), and rainfall-runoff modeling (Hsu et al., 1995).

In a classic ANN organization (Figure 1), neurons are simplified by a group of interconnected nodes. The layer of nodes that receive external information is the input layer. The layer that produces the result is the output layer. The layer between them are the hidden layers.

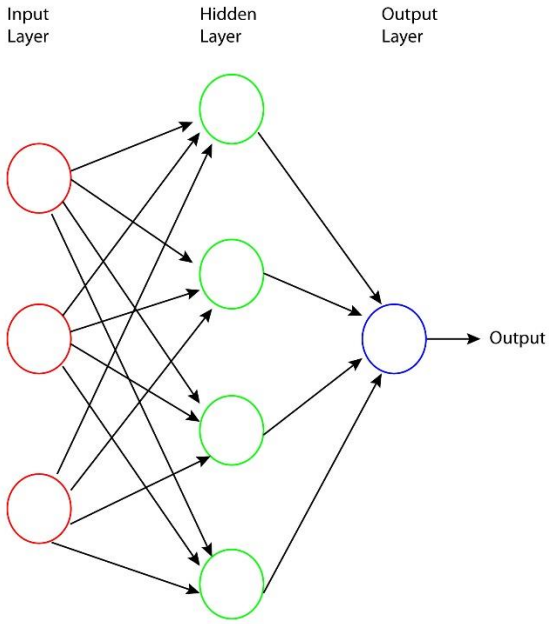

Figure 1. An example of an artificial neural network.

Cellular Automata (CA)

CA is designed for modeling physical processes during which only a local neighborhood interacts (Figure 2). These processes are usually discrete in space and time; however, the state of each neighborhood is synchronously updated according to the preset rules. The spread of wildfire is a good example of such a physical process. When a spot is ignited, the fire propagates along a specific path. Land-cover type, wind speed

and direction, elevation and slope, and meteorologic conditions all are combined to decide the path of fire propagation, which is called the rule in CA. The state of each neighborhood (i.e., burned, burning and unburned) is the result of the rule and the time (Karafyllidis et al., 1997).

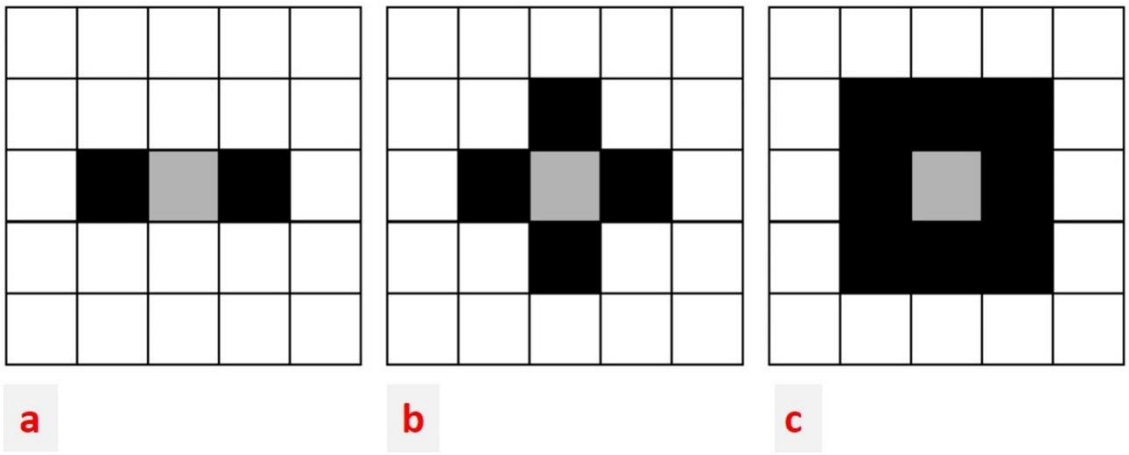

Figure 2. Typical neighborhood: (a) 3-cell neighborhood, (b) 5-cell neighborhood, i.e., ‘von Neumann neighborhood,' and (c) 9-cell neighborhood, i.e., ‘Moore neighborhood'.

Fuzzy Cognitive Mapping

Fuzzy-set theory is designed to exhibit a degree of indeterminate boundaries among target objects that contain members (Sui and Giardino, 1995). Fuzzy-cognitive maps (FCM) are fuzzy-graph structures useful for representing causal reasoning. They represent conceptual nodes that are connected based upon the perceived degree of causality between concepts (Kosko, 1986). Their graph structure allows systematic causal propagation, specifically forward and backward chaining, as used as allowing knowledge representation and analytical reasoning based upon the strength, and

direction of causal connections (Figure 3). FCM is an integration of ANN and Fuzzy-set theory. Thus, it is substantially efficient to adopt FCM to characterize complicated systems such as natural hazards. To date, FCM has been widely used in biomedical, industrial, and engineering fields (Papageorgiou, 2012; Papageorgiou and Salmeron, 2013). In environmental studies, FCM has been applied for predicting cryovolcanism in Titan and evaluating aeolian stability in Texas (Furfaro et al., 2010; Houser et al., 2015).

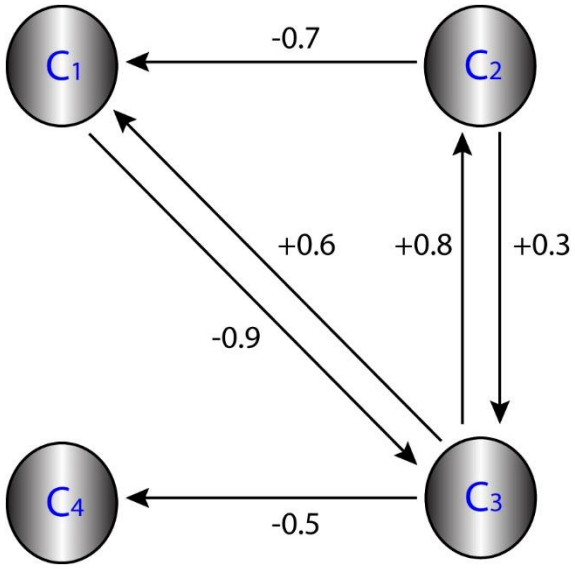

Figure 3. Typical FCM architecture. In this example, there are four nodes, which are connected according to the cause-effect relationship. The initial node of each arrow is the factor that can lead to the result at the end of the arrow. The degree of influence (-1 to 1) can be quantified by human input. The positive sign indicates a direct causal relationship, whereas a negative sign indicates no direct causal relationship.

Mitigation

As mentioned earlier, natural processes are the cause of substantial number of disasters. Hurricanes, earthquakes, tornadoes, floods, landslides and other natural disasters, unfortunately, cannot be foiled. Although these processes cannot be prevented, many opportunities exist to reduce the potential impacts on loss of life, serious injury, damage to the built environment, and curtailment of business operations and negative impact on the environment. Numerous mitigation strategies exist and can be used to reduce damage from hazards. In this section, a Triangular Hazard Mitigation Strategy (THMS; Figure 4) is presented, which is a refined version of risk management theory developed by Greiving et al. (2006).

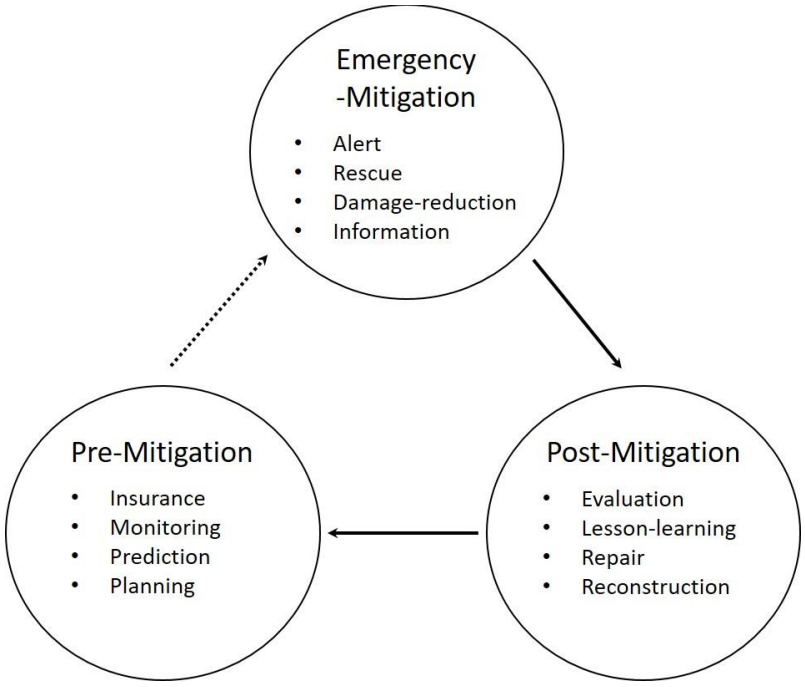

Figure 4. The THMS. Because pre-mitigation does not necessarily prevent a hazard, a dashed line is used to link pre-mitigation and emergence.

In THMS, an occurring hazard is named as an emergency. Emergency-mitigation is the instantaneous action that is needed following an emergency. An efficient emergency-mitigation requires prompt alerts for evacuation, timely and effective rescue, maximized damage-reduction, and transparent information-sharing with the public. Following emergency-mitigation, a short-term, post-mitigation action is applied. Thorough, post-mitigation response includes a full evaluation report of the emergency, explicit summary for lessons learned, applicable repair, and reconstruction, if necessary. The pre-mitigation stage is a long-term preparedness approach to minimize risk at the lowest level. Pre-mitigation activity includes purchase of insurance to cover financial loss, continuous monitoring, prediction modeling, and sustainable planning for infrastructure location, and natural resources usage. A pre-mitigation action does not necessarily prevent the process from becoming a hazard.

Climatology Methods

Overview

Climatologists have long established various approaches for employing current technology for addressing climate-related issues. These approaches, however, are constrained by time and space. All climatology projects begin with data, so in this section, typical climate data are introduced, including observational data and simulation data. Also, statistics such as linear regression, geostatistics, Principal Component Analysis (PCA), Empirical Orthogonal Function (EOF), and wavelet are also addressed in this section.

Weather data

Weather data are essential for climatologists. Acquiring data from appropriate sources requires a cautious approach. Types of data include observational data and modeling data. Observed data include *in situ* data, satellite, and reanalysis data. Climate modeling data are an excellent addition to observed data, such as GCM (general circulation model).

Observational data

In situ data are the most direct way for climate data acquisition. Many weather variables have constantly been measured at meteorological stations, such as precipitation, temperature, wind speed, wind direction, air pressure, air humidity, solar radiance, snow depth etc. Careful selection of instruments is fundamental for collecting useful data. In addition to the instrument itself, data loggers play vital roles for *in situ* data storage at remote locations. New trends for data loggers include an interconnection with digital sensors, real-time data uploading using telemetry with statistics and collecting data via the internet.

Satellite data facilitate *in situ* data collection, because: 1) satellite can collect data for remote locations, such as very rugged, isolated terrain, and 2) satellites offer a large footprint for spatial coverage. Satellites have been used for climate researchers for decades. Examples of mainstream satellites are listed in Table 2.

In essence, the data retrieved from the satellite are digital numbers (DN). Numerous algorithms have been developed to convert the DN into a more complex

biophysical parameter for climatological purposes. Table 3 summarizes some satellite-derived indices that are widely used in climatology.

Table 2. Six examples of satellites, ASTER, AVHRR, Landsat, MERIS, MODIS, and SPOT (Chen, 2015).

Name	Resolution	Orbiting
ASTER	15 m	16 days
AVHRR	1.1 km	Daily
Landsat	30 m	16 days
MERIS	300 m	3 days
MODIS	1 km	Daily
SPOT	6 m	26 days

Table 3. Biophysical indices can be calculated from remote sensing image (Deng and Wu, 2012).

Acronym	Full Name	Field
NDVI	Normalized Difference Vegetation Index	Vegetation
LAI	Leaf Area Index	
SVI	Simple Vegetation Index	
SAVI	Soil Adjusted Vegetation Index	
PVI	Perpendicular Vegetation Index	
NDWI	Normalized Difference Water Index	Water
NDSI	Normalized Difference Snow Index	Snow
SI	Salinity Index	Soil
SINDRI	Shortwave Infrared Normalized Difference Residue Index	
NDTI	Normalized Difference Tillage Index	
LCA	Lignin-Cellulose Absorption Index	

Reanalysis data are a data-assimilation product used in climatological research. It produces climate data sets on a global scale with a time-step of 6-12 hours. During each time-step, approximately 8 million observations are assimilated, including ship reports, weather station records, satellite-data retrieval, buoy information, and radiosonde data. Reanalysis data can be used to produce continuous data back to 1948 (Fan et al., 2008). This technique has been criticized, however, for its lack of reliability, data inaccuracy, and observation discrepancy. Two major climate reanalysis data sources are NCEP/NCAR and ERA-40 (Bromwich and Fogt, 2004).

Modelling data

A simple climatic model can be as basic as a Lapse Rate model, which can be used to build the linear relationship between air temperature and elevation. More complicated models, however, are numerical simulations of Earth to investigate the consequence of the climate system as a response to different forcings, which is also known as a general circulation model (GCM). GCMs can be used to predict future climate at regional and global scales. GCMs can be applied to most climate-related dynamics including the atmosphere, the ocean, sea ice, land surfaces, carbon cycle, hydrology, aerosol, and insolation. For any GCM, three factors need to be considered: 1) spatial resolution, 2) temporal resolution, and 3) level of complexity. These three factors altogether influence the model accuracy and computing cost. Most GCMs facilitate temporal and spatial downscaling capacities for specific research needs (Leung, 2006).

GCMs are numerical modeling of nature, and one must evaluate the existing accuracy of a model to improve them, which is crucial in climatological research.

Scientists have been collectively working to ensure the compatibility of a model. The undergoing Coupled Model Intercomparison Project Phase (CMIP) is a comprehensive collaboration framework for advancing the scientific understanding of climate system (Li et al., 2021). The CMIP has undergone five different phases since 1995, and the current phase is 6 (i.e., CMIP6). The CMIP has focused the research agenda as: 1) investigating climate responses to forcings, 2) evaluating model uncertainties, and 3) assessing future climate change. The progress of CMIP5 has been explicitly documented in the Fifth Assessment Report (AR5) of IPCC (Intergovernmental Panel on Climate Change).

Data Sources and Collaborations

Geoscientists collecting data for climate-change impact analysis need to consider the following factors: 1) grant-writing for financial support, 2) instrument purchase and calibration, 3) making fieldtrip plans, 4) transportation and lodging, 5) sampling strategy, 6) placement of in-field instrumentst, 7) raw-data assessment, 8) data transfer and storage, and 9) field -work safety. High-quality field work can be time consuming, laborious, and expensive. Thus, use of a reliable climate-data sharing platform will substantially reduce individual output. Major online climate-data sources are listed in Table 4. In addition, these sources are free and can be downloaded via the internet.

The analysis of the impact of climate-change requires collaborations at all societal, academic, and governmental levels. Non-profitable organizations exist to help scientists and geoscientists. As addressed previously, IPCC is a good example of global collaboration for solving issues related to climate-change. Additional organizations

include the American Geophysical Union (AGU), the American Meteorological Society (AMS), the American Association of Geographers (AAG), the Geological Society of America (GSA), and the World Meteorological Organization (WMO) to mention a few.

Governmental agencies also play vital roles in building bridges between climate data and user interfaces, such as the National Aeronautics and Space Administration (NASA), the United States Environmental Protection Agency (US EPA), the United States Geological Survey (USGS), the United Nations Development Programme (UNDP), the United Nations Educational, and the Scientific and Cultural Organization (UNESC).

Table 4. Online climate-data sources (Camarillo-Naranjo et al., 2019).

Name	Manager	Data
PRISM	Oregon University	High-resolution climate data
DAYMET	Oak Ridge National Laboratory	Daily climate data
NCEI	NOAA-National Centers for Environmental Information	Historical weather data
ESRL	NOAA-Earth System Research Laboratory	Climate Reanalysis data
CPC	NOAA-Climate Prediction Center	Climate predictions and teleconnections
GES DISC	NASA-Goddard Earth Sciences Data and Information Services Center	Observed climate data from space
TRMM	NASA-Goddard Space Flight Center	Observed precipitation in low latitude
NSIDC	National Snow & Ice Data Center	Snow and Ice data
USGS	U.S. Geological Survey	Runoff, discharge data
NRCS	National Water & Climate Center	Runoff, discharge data
IPCC	Intergovernmental Panel on Climate Change-Data Distribution Centre	GCM data

Missing data

Filling temporal data gaps

Time-series data retrieved from field locations are episodic in nature. Thus, missing data are common encounters in climatic research. For instance, datasets on river discharge retrieved from the United States Geological Survey (USGS) may include data gaps as the result of instrument malfunction or human misoperation. Understanding the missing mechanism is important for handling missing data so that the correct replacement method is used. If the missing data occur randomly, common methods such as multiple regression, expectation maximization, and regression trees can be used in estimating missing values (Kim et al., 2009; Schneider, 2000). If the missing data occurrence is conditioned on a deterministic event that affects the data values, such as a flood, however, the method of estimation of missing values is more complicated (Little et al., 2002).

Filling gaps in spatial data

Biophysical variables, such as surface temperature, exhibit a continuous surface gradient in reality. Field sampling, however, cannot adequately record every location because of limited time and funding. A subset of samples in the form of points can be measured. To fill the spatial gaps or unsampled area, different interpolation methods have been widely adopted in climate research. These methods differ from three perspectives: 1) the mathematic function adopted, 2) the distance and weight being considered, and 3) the number of samples being taken into account. Five typical interpolation approaches are: 1) Nearest Neighborhood interpolation, 2) Fixed Radius (i.e., local averaging), 3)

inverse-distance-weighted (IDW) interpolation, 4) Splines interpolation, and 5) Kriging (Jeffrey et al., 2001). Kriging is also a good geostatistical method for characterizing scale-related issues, which is detailed in following section.

Statistics in Climatology

Weather variables can exhibit collinearity (Carleton, 1999). To employ this type of approach requires specific statistical skills to extract the spatial structure underlying each climate phenomenon. In this section, the basic concepts of linear regression, geostatistics, and data reduction methods (PCA, EOF) and spectral analysis (wavelet) are discussed.

Linear Regression Analysis and Significance Test

In climatology, linear regression is used for modeling the relationship between the dependent variable Y and various independent variable(s) X(s). If only one independent variable exists, it is a simple linear regression. Otherwise, it is multiple-linear regression. One must understand that it is different from multivariate linear regression in which a set of correlated dependent variables (Ys) are predicted. In this section, the focus is placed on simple and multiple linear regressions.

Linear regression has two major applications in climatology: 1) modeling for prediction purpose, and 2) examining correlations among X(s) and Y. For the first application, a fitting function can serve well as a prediction model for linking different climate variables. For instance, the Lapse Rate model is a simple linear regression model for predicting air temperature based upon elevation and altitude. For the second application, Pearson-correlation coefficient is the statistical criteria for the degree of

dependence between X and Y. The coefficient ranges from -1 to +1, where -1 is a totally negative linear relationship, +1 is a totally positive linear relationship, and 0 shows no linear relationship. In climatology, a significance test is typically followed by correlation analysis, because the correlation relationship could be real in nature or could be just a statistical artifact. Over-emphasis on p-values and significant levels, however, could mislead the result of a climate study (Marden, 2000; Ziliak and McCloskey, 2008; Ambaum, 2010; Ling and Mahadevan, 2013).

Geostatistics

Geostatistics are suitable for characterizing spatial variations of weather phenomena. Kriging is one of the geostatistical methods that can quantify the spatial dependence of natural resources. Matheron (1971) first proposed the theory of geostatistics, and Curran (1988) further expanded the theory into remote-sensing studies. As mentioned previously, Kriging is an interpolation method. It is distinct from other interpolation methods, however, because the core of Kriging is a statistical model that adopts spatial autocorrelations, by which spatial structure can be first computed based upon available samples, and new predictions can be made after. Kriging also provides cross-validation capacity to evaluate interpolation accuracy (Krige, 1951).

Spatial autocorrelation is a criterion for examining the statistical relationship among observations. The distance between a pair of sampling points and the direction linking these samples are two major factors that must be considered when computing spatial autocorrelation. A semi-variogram summarizes spatial autocorrelation with the x-

axis as distance and y-axis as semivariance. Semivariance can be calculated with the following function:

$$\gamma(h) = \frac{1}{2n(h)} \sum_{i=1}^{n(h)} [Z(i) - Z(i+h)] \quad (1)$$

where, semi-variance is γ(h), n(h) is the number of paired sampling points at distance h, and Z(i) is the surface value at location i. The complete set of sampling pairs is used to generate a semi-variogram (Longley et al., 2004).

Figure 5. is a classic semi-variogram, in which closer distance exhibits smaller semi-variance whereas longer distance exhibits larger semi-variance. Such a pattern suggests that features closer are more likely to be similar, and that is Tobler's First Law of Geography (Joo et al., 2017). Thus, a semi-variogram can serve as an excellent tool for investigating scale dependence and spatial variability in climatology (Burrough, 1983).

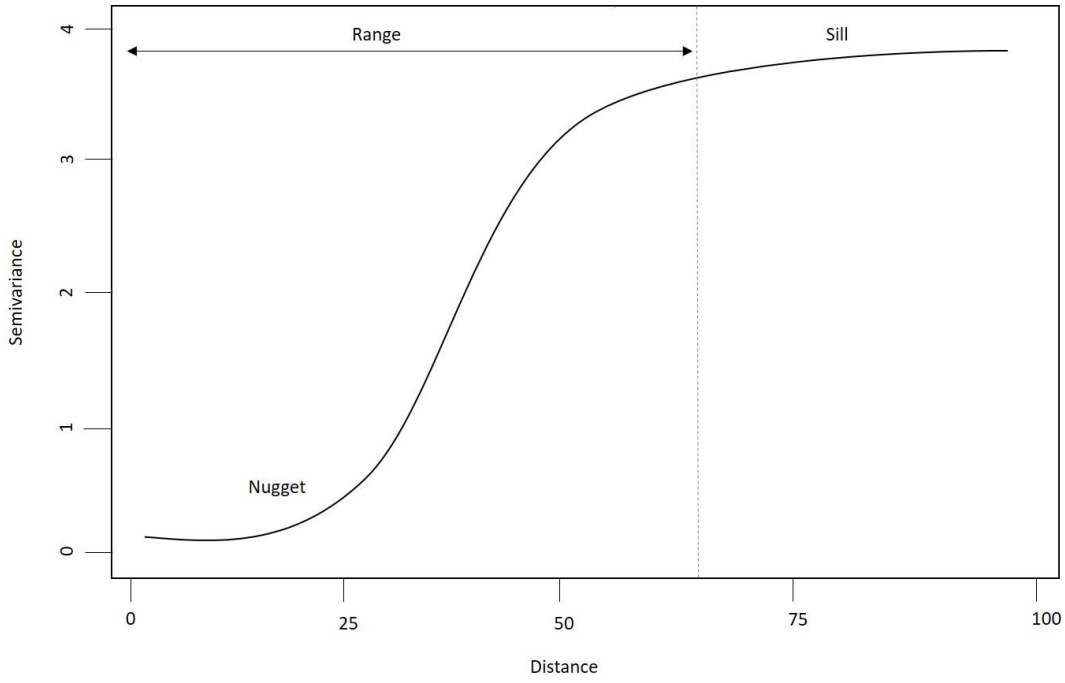

Figure 5. A traditional semi-variogram (Silveira et al., 2018).

Another benefit of the semi-variogram is that it can be used to help determine the best sampling interval when developing strategies for data collection in the field. As shown in Figure 8., a range-distance is a distance where semi-variance approaches flat. It means as distance increases, semi-variance increases; however, spatial autocorrelation decreases until no spatial autocorrelation exists beyond that range. Thus, a range is the maximum distance that a sampling interval can be used in the field to capture every spatial variability because within the range, one point can be representative of every location if they are spatially autocorrelated (Chiles and Delfiner, 1999; Cressie, 1993).

PCA (EOF) and Wavelet Analysis

Principle Component Analysis (PCA) is a data reduction method used in climatology. PCA is a technique that can transform an original dataset with potentially correlated variables into a new dataset with linearly uncorrelated variables (Bretherton et al., 1992). This type of orthogonal transformation can significantly reduce data dimensionality because: 1) the number of new variables is less than or equal to the previous number of variables, 2) the first principal component carries the maximum variance of the original dataset, and 3) all the following principal components carry most variance for the remaining principal components. As a result of the mathematical nature of PCA, it has been widely used for exacting spatial patterns of weather variables at different scales. Empirical Orthogonal Function (EOF) is an extreme case of PCA because EOF is a PCA when applied to time-series data. Thus, EOF is suitable for processing weather data (Lauren, 1956; Thuiller, 2004).

In recent decades, spectral analysis such as wavelet has been used in numerous applications, such as harmonic analysis, numerical analysis, signal and image processing, nonlinear dynamics, fractal analysis, etc. The wavelet transform is very popular in dealing with time-frequency, orthogonality, and scale-space analysis (Foufoula-Georgiou and Kumar, 1994). The essence of wavelet analysis is to transform an array of numbers at a certain dimension from the original digits into an array of wavelet coefficients. A wavelet coefficient informs the correlation between a wavelet function of a certain size and data (Daubechies, 1992). In recent years, wavelet analysis has been employed as a tool for analyzing the power spectra of time-series data in

climatology (Torrence and Compo, 1997). This analysis can help researchers capture regional and overall views of the match between a wavelet function and target data by changing the size of wavelet function and shifting the wavelet, which is called localization (Hubbard, 1998).

The variability of a one-dimensional data array can be represented in the form of a two-dimensional plot showing the variability of amplitude at different scales and how the amplitude is changing at different time frequencies (Lau and Weng, 1995; Torrence and Compo, 1997). For instance, a wavelet analysis can be applied to a precipitation dataset to reveal the periodicity of the high-frequency event such as rain during monsoon seasons.

Geomorphometry: The Best Approach for Impact Analysis

Overview

Geomorphometry is a numerical representation of topography, which integrates various disciplines: i.e., mathematics, Earth science, engineering, and computer science (Pike, 1995). Human beings interact with the surface of Earth every day, so to depict a landform in a qualitative manner is not a big challenge per se. It becomes a major obstacle for individuals, however, who lack the domain knowledge to delineate land surface quantitatively, or even complex when one attempts to characterize a complicated Earth-surface processes, such as erosion and deposition. Geomorphometry is the best approach to overcome such obstacles (Franklin, 2020).

Geomorphometry can help in the understanding of natural processes associated with the surface of Earth, and also it can help support technological needs of society (Pike, 1995). For instance, geomorphometry can help in extracting some underlying information from various fields of study, such as geology, hydrology, and climatology. The extracted information can further be applied in evaluating natural hazards and conserving natural resources. On a societal level, geomorphometry can be used in engineering, transportation, public works, and military operations.

Naturally, the next question is how is a surface categorized in a "GEOMORPHOMETRICAL" manner? Traditionally, six factors that contribute to the topographic existence: 1) elevation, 2) terrain surface-shape, 3) topographic position, 4) topographic context, 5) spatial scale, and 6) landform (object type). The first four factors can be parameterized whereas the last two can be analyzed (Deng, 2007).

As technology advances, especially the advent of GIS and remote sensing, it significantly accelerates the capacities of calculating the aforementioned factors (Goodchild, 1992). Numerous commercial software that can be used in the field of geomorphometry have unique analytical functionality as well as modularity. It is especially common that different software adapts different algorithm even when calculating one single parameter, e.g., slope or aspect. Thus, it is important to first assess the software before using a specific one.

Geomorphometry research and applications

Many applications of geomorphometry exist and include, for example, optimizing crop yields, measuring runway roughness, mapping types of sea-floor terrain,

guiding missiles, assessing soil erosion, analyzing wildfire propagation, mapping ecological regions, and modeling climatic changes. (Pike, 1995). Geomorphometry is especially effective when combined with remote sensing and GIS. Remote sensing can provide raw data to GIS, and various GIS functions have been developed to aid in the interpretation of remote sensing data. Thus, it is difficult to separate remote sensing from GIS in an analytical study (Sofia, 2020).

In geomorphometry, remote sensing normally means collecting information from aerial platforms, such as airplanes, Unmanned Aerial Vehicle (UAV) and satellites. Even though remote sensing cannot replace traditional geomorphic field observations, it has become fundamental to use remote sensing because it offers a synoptic overview of a study area (Eichel et al., 2020).

In the early days of geomorphic research, besides *in situ* study, geomorphologists primarily interpreted phenomena qualitatively from remotely sensed images. Quantitative methods are readily used in geomorphometry today. One significant advantage of using remote sensing in geomorphometry is that it facilitates access to data that are inaccessible via *in situ* observations. A significant advantage of remote sensing is in the recording of information chronologically. Aerial photography records date back to the 1920s. The first Earth Resources Satellite, i.e., Landsat-1 was launched in 1972 (Jensen, 2005).

To conduct successful geomorphometry research using remote-sensing imagery, the spatial, temporal, and spectral resolution need to be carefully scrutinized. The spatial resolution is the smallest cell size of IFOV (instantaneous field of view), which is

closely related to the concept of scale-dependency. Temporal resolution defines the frequency of retrieving images from the same site. Spectral resolution tells the spectral characteristics the channels used by the sensor (Ramsey, 2020).

A 3D view of the landscape can be rendered with the help of remote-sensed images, which significantly enhances the interpretability of land surfaces (Widodo, 2021). Stereoscopic measurements can be used to generate topographic maps or digital representations of topography (i.e., DEM).

Currently Synthetic Aperture Radar (SAR) and Light Detection and Ranging (LiDAR) are two popular technologies used in geomorphometry. SAR is valuable because it can penetrate dry materials, such as sand or dry snow. LiDAR has many merits in delineating land-surface details (Feciskanin and Minár, 2021).

Software Package Evaluation

At present, numerous software packages that can be used to conduct geomorphometric research. In this chapter, thirteen are examined. These software packages can be further classified into four categories, i.e., digital image processing software, GIS systems, hydrology software, and geomorphometry software.

Eighteen criteria were assessed, and the evaluations are summarized in Table 5-9. Each criterion is further ranked as Strong (S), Weak (W), or Null (N). The current url for each software package is listed in Table 10.

In general, ArcGIS®, ENVI®, Erdas Imagine®, GRASS®, and IDRISI® are the top five software packages that are standard for geomorphometric research. Based on evaluation, the ranks for geomorphometric capacity are as follows (from high to low):

GRASS®, Erdas Imagine®, ENVI®, ArcGIS®, IDRISI®. Other software packages have many disadvantages at some point. Some uniqueness of these software packages is listed in Table 11.

Table 5. Evaluation on Lidar input, GPS tracks, Spatial Analysis and Spatial Interpolation. Strong (S), Weak (W), or Null (N).

Software Name	Category	LiDAR Input	GPS Tracks	Spatial Analysis	Spatial Interpolation
ENVI®	Digital Image Processing	S	S	S	W
Erdas Imagine®		S	S	S	S
ER mapper®		N	S	W	N
Arc GIS®	Geographic Information Systems	S	S	S	S
GRASS®		S	S	S	S
SAGA®		S	S	S	S
IDRISI®		W	S	S	S
ILWIS®		S	S	S	S
PC-Raster®		N	W	S	S
TAS®	Hydrology	S	S	S	S
Surfer®	Geomorphometry Systems	N	S	S	N
Landserf®		N	S	S	N
MicroDEM®		S	N	N	N

Table 6. Evaluation on Geostatistics, Image filters, and Image transformation (e.g., PCA). Strong (S), Weak (W), or Null (N).

Software Name	Category	Geo-statisics	Image Filters	Image Transformation (e.g., PCA)	Spatial Modeling
ENVI®	Digital Image Processing	W	S	S	N
Erdas Imagine®		S	S	S	S
ER mapper®		N	S	S	N
Arc GIS®	Geographic Information Systems	S	W	W	S
GRASS®		S	S	S	S
SAGA®		S	S	N	N
IDRISI®		S	S	S	S
ILWIS®		S	W	S	N
PC-Raster®		S	N	N	S
TAS®	Hydrology	S	S	W	W
Surfer®	Geomorphometry Systems	S	N	N	N
Landserf®		S	N	N	N
MicroDEM®		N	N	N	N

Table 7. Evaluation on Image enhancement, Geodatabase, Classification, and Segmentation. Strong (S), Weak (W), or Null (N).

Software Name	Category	Image Enhancement	Geo-database	Classification	Segmentation
ENVI®	Digital Image Processing	S	W	S	S
Erdas Imagine®		S	S	S	S
ER mapper®		S	N	S	N
Arc GIS®	Geographic Information Systems	W	S	W	N
GRASS®		S	S	S	S
SAGA®		N	W	W	N
IDRISI®		S	S	S	S
ILWIS®		S	W	S	N
PC-Raster®		W	W	W	N
TAS®	Hydrology	S	W	W	N
Surfer®	Geomorphometry Systems	N	N	N	N
Landserf®		N	N	W	W
MicroDEM®		N	N	N	N

Table 8. Evaluation on Pattern recognition, Terrain analysis, and Raster analysis. Strong (S), Weak (W), or Null (N).

Software Name	Category	Pattern Recognition	Terrain Analysis	Raster Analysis
ENVI®	Digital Image Processing	W	S	S
Erdas Imagine®		S	W	S
ER mapper®		N	W	W
Arc GIS®	Geographic Information Systems	N	S	W
GRASS®		S	S	S
SAGA®		N	W	S
IDRISI®		W	S	S
ILWIS®		N	S	S
PC-Raster®		N	W	S
TAS®	Hydrology	N	W	S
Surfer®	Geomorphometry Systems	N	S	N
Landserf®		N	S	S
MicroDEM®		N	S	N

Table 9. Evaluation on Vector analysis, 3D visualization, Scripting functionality, and Batch processing. Strong (S), Weak (W), or Null (N).

Software Name	Category	Vector Analysis	3D-visualization	Scripting Functionality	Batch Processing
ENVI®	Digital Image Processing	N	S	S	S
Erdas Imagine®		S	S	S	S
ER mapper®		W	S	W	W
Arc GIS®	Geographic Information Systems	S	S	S	S
GRASS®		S	S	S	S
SAGA®		S	S	S	W
IDRISI®		W	S	N	N
ILWIS®		S	S	W	N
PC-Raster®		N	N	S	N
TAS®	Hydrology	W	W	N	N
Surfer®	Geomorphometry Systems	N	S	S	S
Landserf®		W	S	S	S
MicroDEM®		N	S	N	N

Table 10. Url for each software package.

Software Name	Link
ENVI®	http://www.harrisgeospatial.com/Home.aspx
Erdas Imagine®	http://www.hexagongeospatial.com
ER Mapper®	http://www.hexagongeospatial.com
Arc GIS®	http://www.esri.com/
GRASS®	https://grass.osgeo.org/
SAGA®	http://www.saga-gis.org/en/index.html
IDRISI®	https://clarklabs.org/
ILWIS®	http://www.ilwis.org/
PC-Raster®	http://pcraster.geo.uu.nl/
TAS®	https://www.tradeareasystems.com/products/tas-analyst
Surfer®	http://www.goldensoftware.com/products/surfer
Landserf®	http://www.landserf.org/
MicroDEM®	https://www.usna.edu/Users/oceano/pguth/website/microdem/microdem.htm

Table 11. Uniqueness of some software packages.

Software Name	Uniqueness
SAGA®	This software has fractal dimension analysis module and pattern analysis module.
IDRISI®	It offers a triangular wavelet analysis function and trend analysis of time series images.
TAS®	It is highly dependent upon ArcGIS input.
Surfer®	It is very powerful of 3D visualization.
Landserf®	This is very powerful of generating geomorphometric parameters. Fractal dimensions and multi-scale topographic parameters can be calculated from it.
MicroDEM®	It can offer a way to visual 3D images in time series, and it also provide a dynamic recording of 3D images.

Characterization of Rivers Basins in the San Juan Mountains, Colorado

Background

Alpine streams are a vital source of water for human settlements in mountain terrain, and potential hazards associated with spring melt and intense runoff from summer convective storms. Thus, the identification and characterization of alpine river basins is crucial for the optimization of potable water resources, as well as minimizing floods. Second- and third-order drainage basins are an integral part of the geomorphology of the San Juan Mountains (Figure 6; Strahler, 1952). With an increase in year-round residents and greater influx of tourists to the region, however, a need

exists to improve the management of water resources and to minimize flood hazards in the San Juan Mountains (Nardini et al., 2020).

Global change can dramatically impact alpine water resources by changing precipitation patterns and amount of precipitation as wells as warmer winter and summer temperatures. Temperature changes can promote higher rates of evaporation in summer months and changes in the type of precipitation from snow to rain. Seasonal change can also occur. The beginning of the winter precipitation season can be pushed to late fall or even mid-winter. And the beginning of spring melt season can be delayed by several weeks to a month.

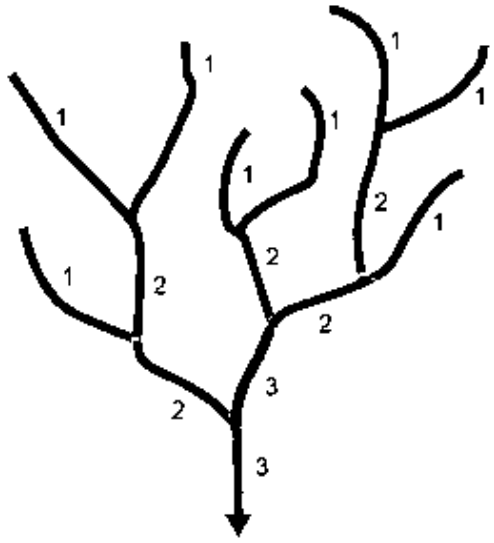

Figure 6. The Strahler stream order system. Second- and third-order drainage basins are an integral part of the geomorphology of the San Juan Mountains.

All the previously mentioned changes impact surface in groundwater resources. To analyze and understand the surface change on water resource requires study of the linkage between atmospheric processes and geomorphology of a drainage basin. Thus, this section demonstrates the use of a new time and cost of time and cost-effective technique to determine surface roughness. Surface roughness is a major basin-wide threshold, which serves as an indicator of precipitation as well as a controller of drainage pattern development and rate of runoff.

In the San Juan Mountains, streams represent regional topography and local surface roughness. The study area encompasses the Ironton, Ophir, Ouray, Silverton, and Telluride USGS Quadrangles in Southwestern Colorado, covering an area of 805 Km^2 (Figure 7).

I have developed a geospatial approach that implements a geomorphometric index to efficiently delineate river basins in mountain terrains. To accomplish this Fast Fourier Transformation (FFT) analysis is employed to confirm that no scale dependence for the regional topography exists. And, to supplement the FFT, a new topographical-classification approach that addresses surface roughness to better understand hydrological controls in the study area, was created. Lithology was coupled with the topographical-classification map. Additionally, divergence and convergence indices were developed based on water flow to improve the existing river-channel extraction algorithm. This new method is cost-effective and speeds up delineating river basins in mountain terrains to better manage water resources and prepare hazard mitigation plans.

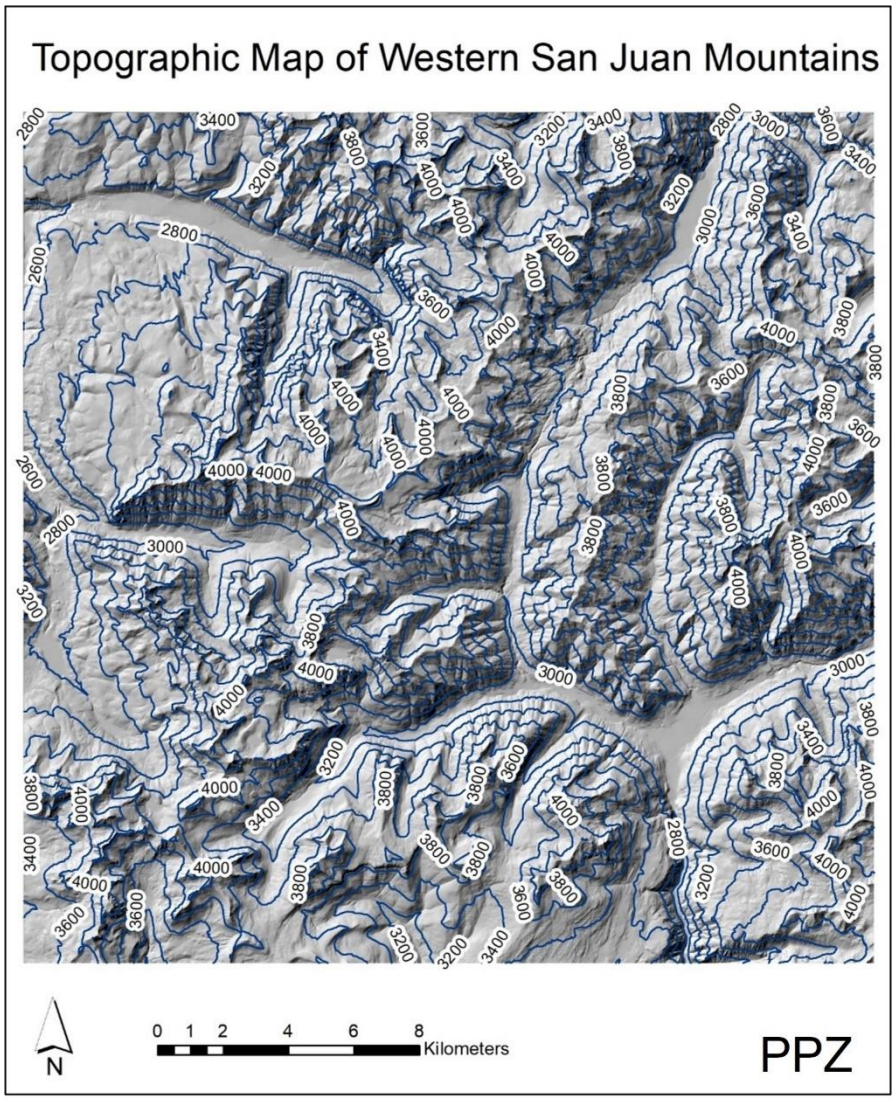

Figure 7. The topographic map the study area in San Juan Mountains. The San Juan has rugged topography dominated by ridges and valleys.

Scale Characterization

The 2-D Discrete Fourier Transformation (DFT) can benefit the field of digital image processing with respect to image enhancement, image restoration, data compression, data fusion, and other applications (Cooley et al., 1969; Anuta, 1970). DFT

transforms the information from an original image with spatial domain to frequency domain. Thus, it can aid in revealing information hidden in frequency domains, such as periodicity, orientation, and scale (Gonzalez et al., 2009). A Fast Fourier Transformation (FFT) algorithm is the implementation of DFT in reality and can be applied by a couple of software packages (e.g., ENVI) and several programing languages (e.g., MATLAB®, IDL® and Python®).

To examine the scale-dependence issues in the San Juan Mountains, I developed a protocol to adopt FFT techniques and image filter technique. The steps in the protocol are as follows: a DEM of 10-meter spatial resolution of the study area (Figure 8a) is first converted into Fourier spectrum then centered and enhanced by a log transformation (Figure 8b). To check the scale regarding orientation, a wedge-based filter with 5-degree interval (Figure 8c) is applied to the FFT image. To check scale regarding distance, a ring-based filter with a 5-pixel interval (i.e., 50 m; Figure 8d) is also applied to the FFT image.

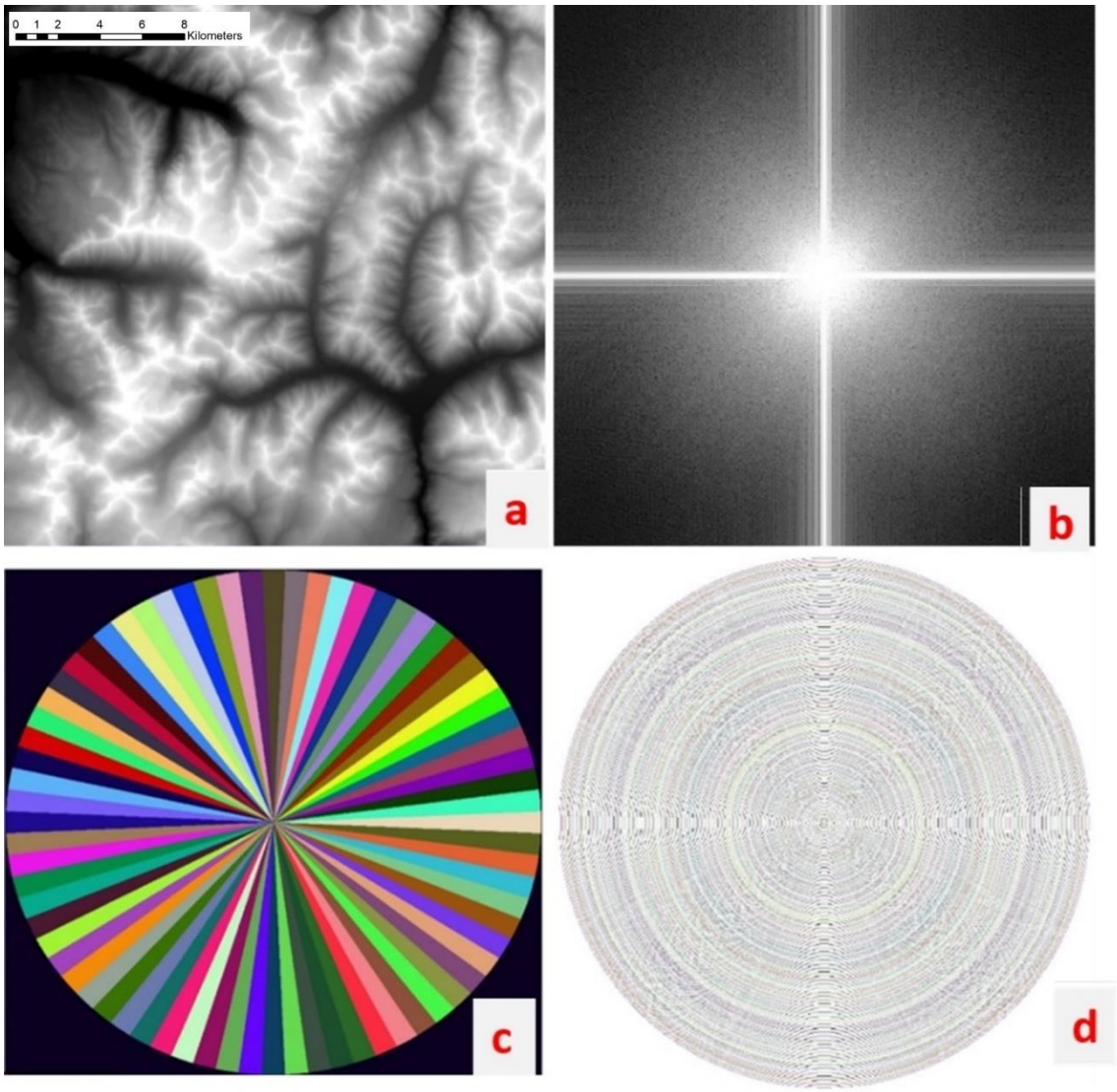

Figure 8. a) The DEM of the study area with 10-meter spatial resolution. b) The FFT image based on the DEM. A log transformation is applied for image enhancement. c) A wedge-based filter is applied to the FFT image. The interval is every 5 degrees. d) A ring-based filter is applied to the FFT image. The interval is every fifth pixels.

Within each filter segment (i.e., wedge and ring), FFT intensity is first summed and then averaged by a count of pixels in each segment. The final statistics are plotted as

shown in Figure 9. Figure 9a illustrates no strong dependence based on surface orientation. Figure 9b illustrates that a strong scale dependence of 70 meters is evident.

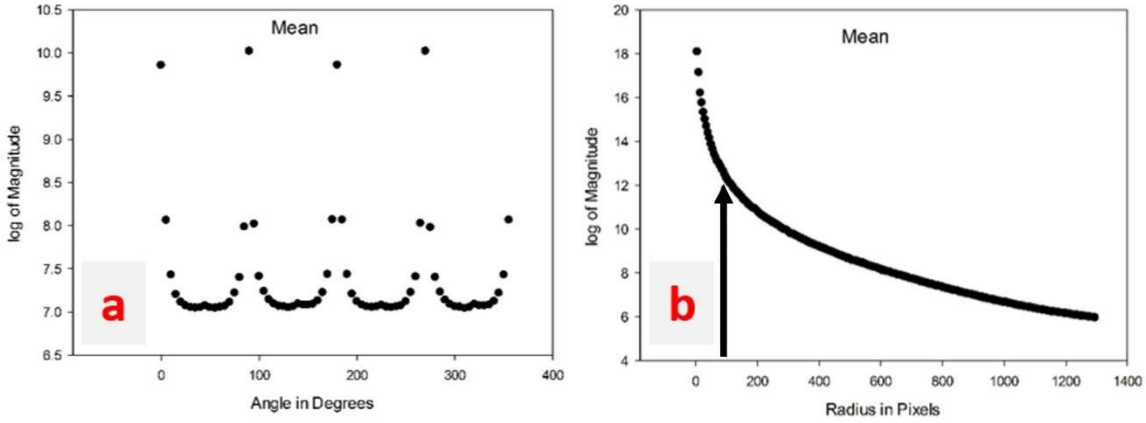

Figure 9. a) The average magnitude within each wedge segment. b) The average magnitude within each ring segment.

Terrain Analysis

Pennock et al. (1987) and Pennock (2003) have proposed a classification regime based on landform shapes, which Giardino (1971) developed, including divergent shoulder, convergent shoulder, divergent backslope, convergent backslope, divergent footslope, convergent footslope, and level (Figure 10). In Figure 10, A shows a slope that is flat and straight; B represents a slope that is convex in plain view and convex in elevation; C shows a slope that is convex in plain view and concave in elevation; D shows a slope that is convex in plain view and concave in elevation; E shows a slope that is concave in plain view and concave in elevation; F shows a slope that is concave in plain view and straight in elevation; and G shows a slope that is concave in plain view

and convex in elevation. The arrows on each diagram show potential flow pathways for water down the slopes.

I adopted this algorithm to reclassify the DEM of the San Juan Mountains. The result shows a unique spatial pattern of different landforms in the San Juan Mountains, which has not been applied in other research (Figure 11). Surface roughness can facilitate evaluating rates of surface erosion, understanding drainage development and runoff pathways, and extracting geomorphic features (Hengl and Reauter, 2009; Florinsky, 2012). Hobson (1972) introduced the surface roughness factor (SRF) by incorporating slope and aspect of a local terrain. Hobson method was used to compute the surface roughness ratio over the San Juan Mountains (Figure 12). I then integrated landform, surface roughness, geomorphology, terrain convexity/concavity and lithology to assess the rate of erosion across the western San Juan Mountains.

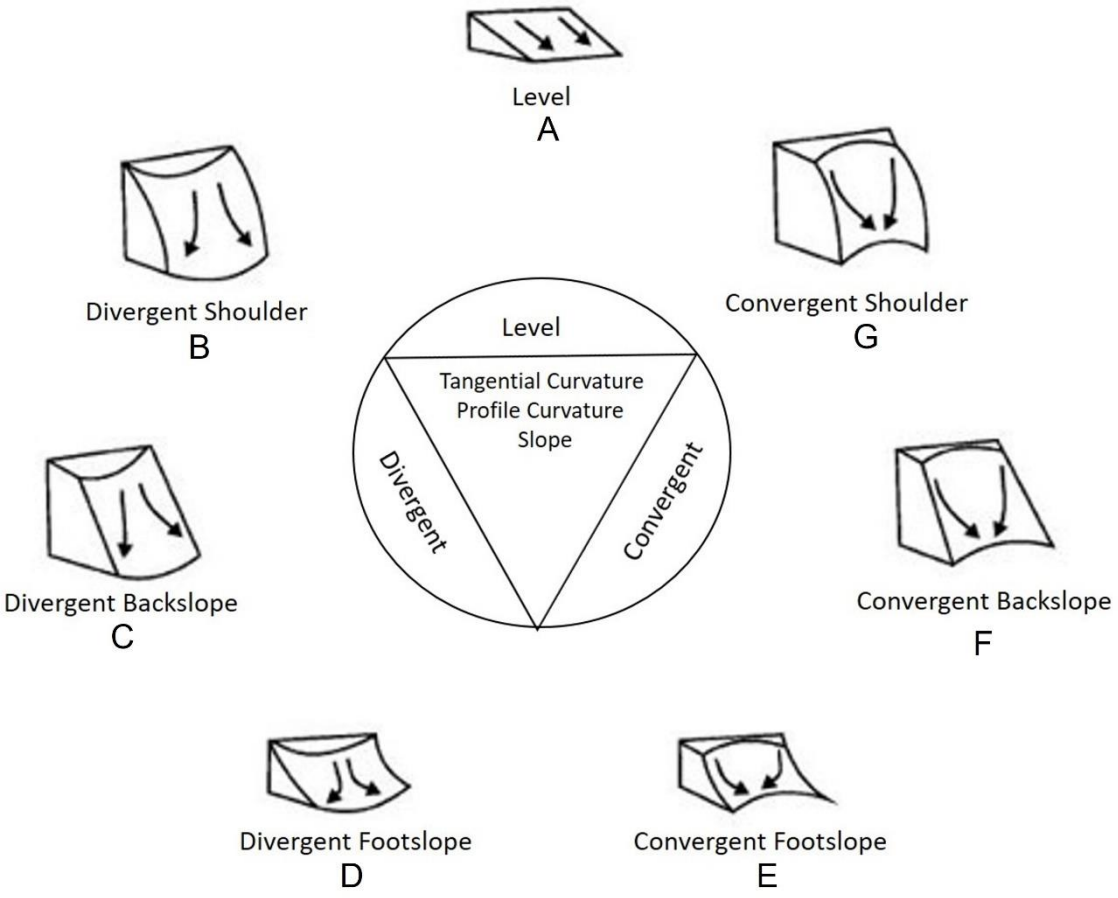

Figure 10. Illustration of original classification based on landform (Giardino, 1971).

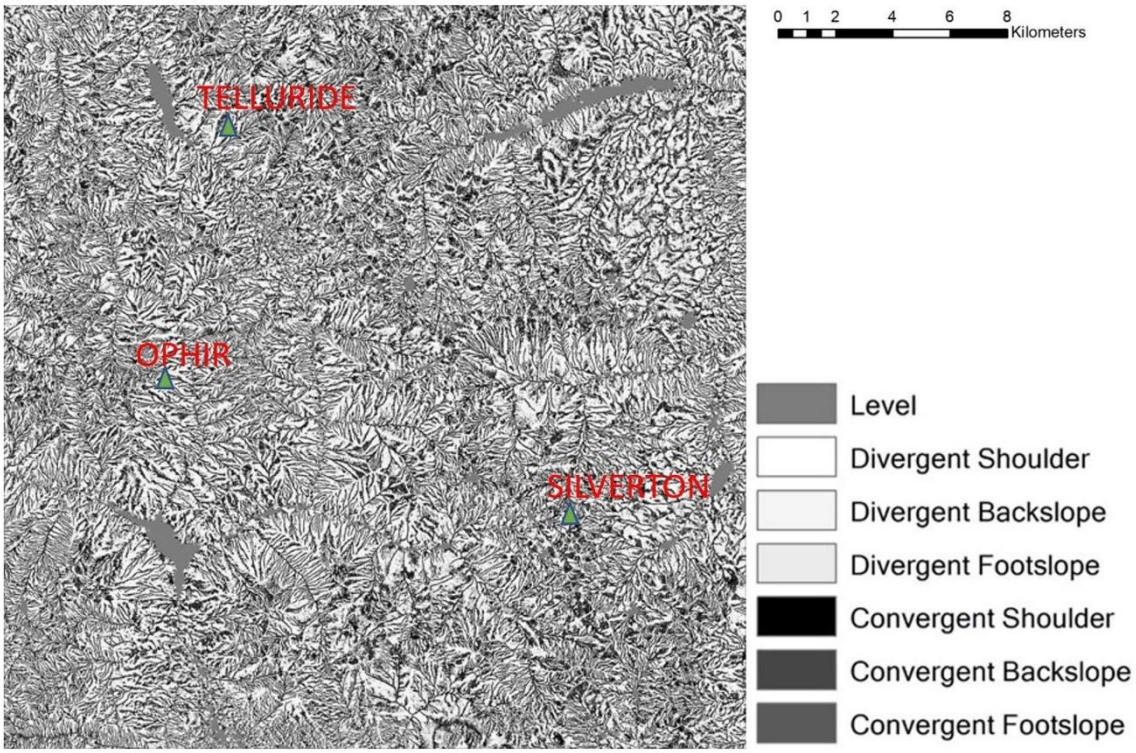

Figure 11. It shows the six slope categories (A-G) used to classify slopes in the San Juan Mountains.

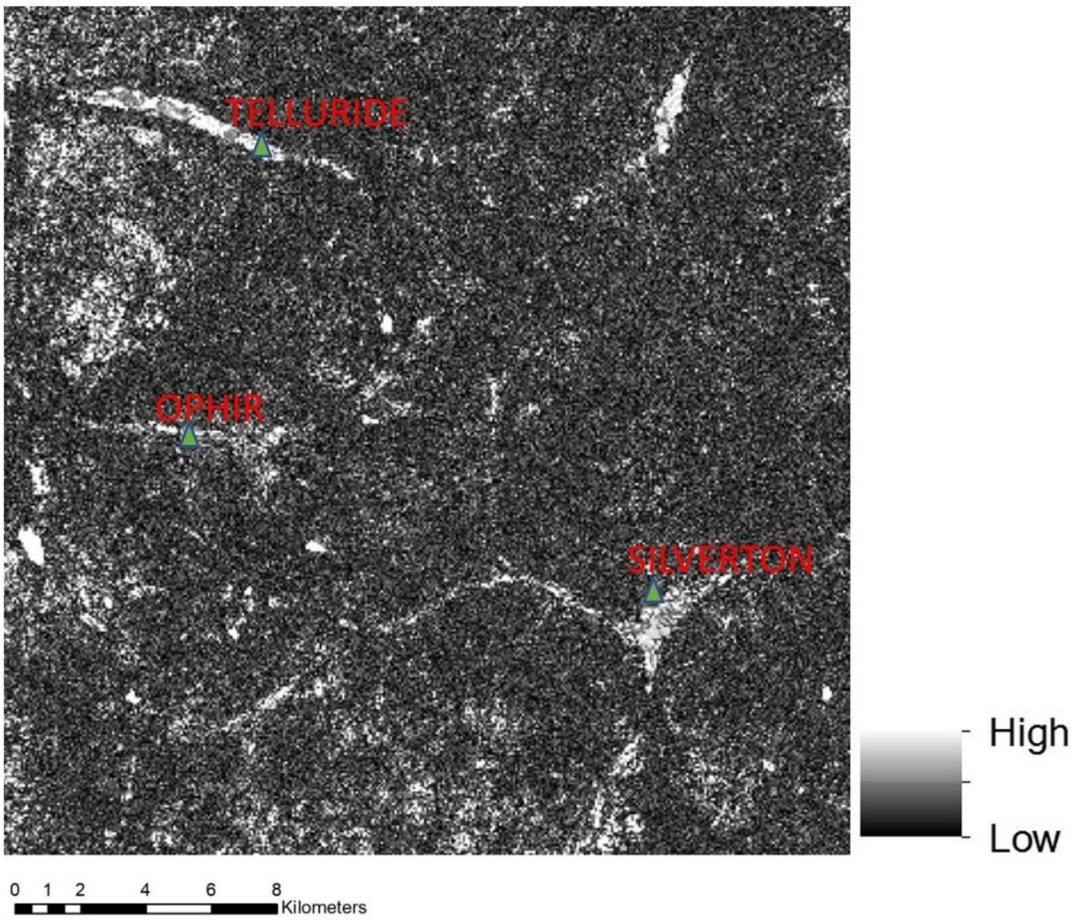

Figure 12. Surface roughness in the San Juan Mountains based on the Hobson (1972) method.

Extraction of River channels based on new topographic index

Geomorphometry offers the efficiency and flexibility for developing new algorithms for impact analysis. This case study illustrates how I developed the topographic index for delineating the directions of river flow. This algorithm can be seen in Figure 13. Figure 13 shows the potential pathway for water flow from one pixel to an adjacent pixel. For each pixel, if water flows towards all eight neighboring pixels, this

pixel is classified as divergent. In contrast, if water flows into the center pixel from all eight neighboring pixels, this pixel is classified as convergent (Claps et al., 1994). Divergence and convergence images are computed based on this theory (Figure 14.) Divergent features, such as mountain ridges, are highlighted in the divergent image (Figure 14a). Convergent features, such as a river channel, are highlighted in the convergent image (Figure 14b).

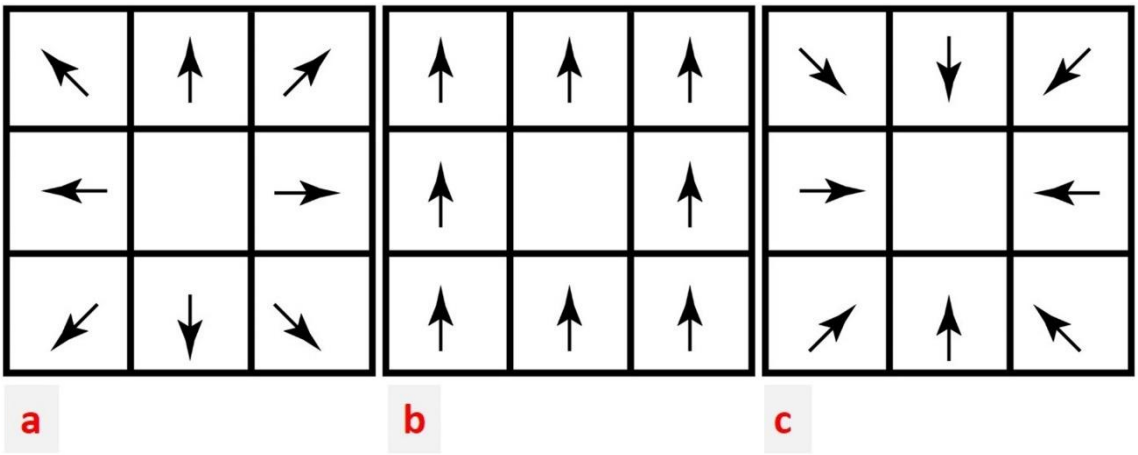

Figure 13. Illustration of the convergence and divergence concepts. a) Divergence, b) Level, c) Convergence.

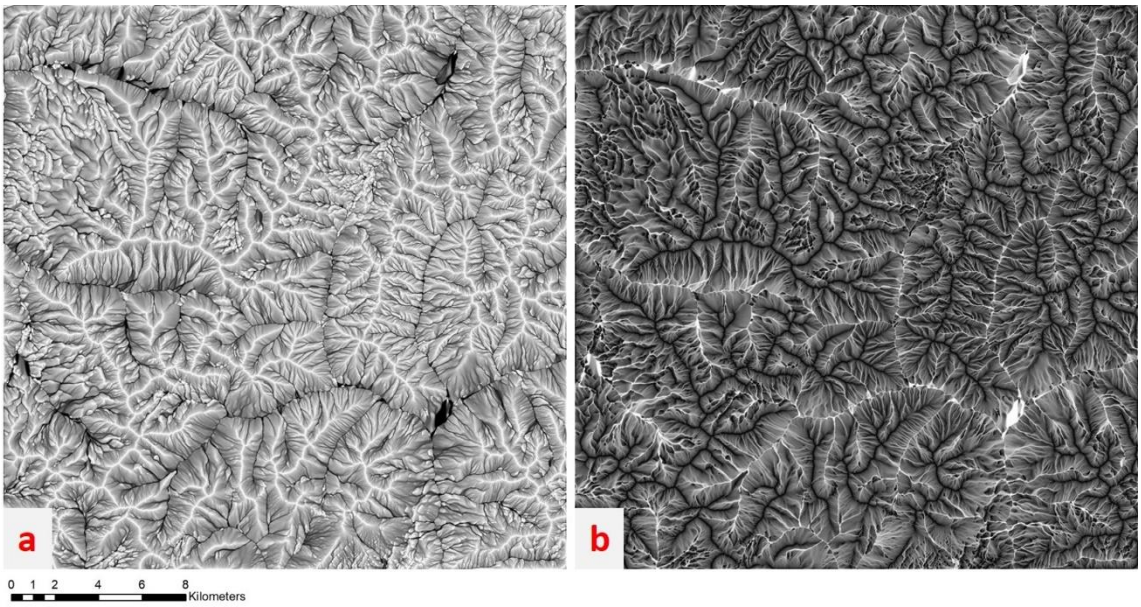

Figure 14. a) The divergence index image, showing mountain ridges as highlighted. b) The convergent index image, showing drainage channels, as highlighted.

To extract river channels from convergence images, two methods are tested and compared in this study, including a thresholding method and a fuzzy classification method. Because a divergence image is normalized between 0 to 1 (Figure 14b), based on the histogram, it is reasonable to establish several thresholds, which can separate a river channel from other low-intensity features. In this research, values at 0.8, 0.7, 0.6, 0.5, and 0.4 were established.

The thresholding method is a typical hard-classification rule to discriminate different classes. This rule omits that in reality only one transition exists between one class and another (Jensen, 2005). Fuzzy-set theory, however, can compensate the omission because of its strong capacity of dealing with imprecise data (Zadeh, 1965;

Wang, 1990). To apply a fuzzy classification, a fuzzy-membership function needs to be selected first. In this research, I adopted an exponential decay function for fuzzy classification (Figure 15). The classification results are shown in Figure 16 and Figure 17. By comparison, fuzzy classification approach is more reliable than the thresholding approach.

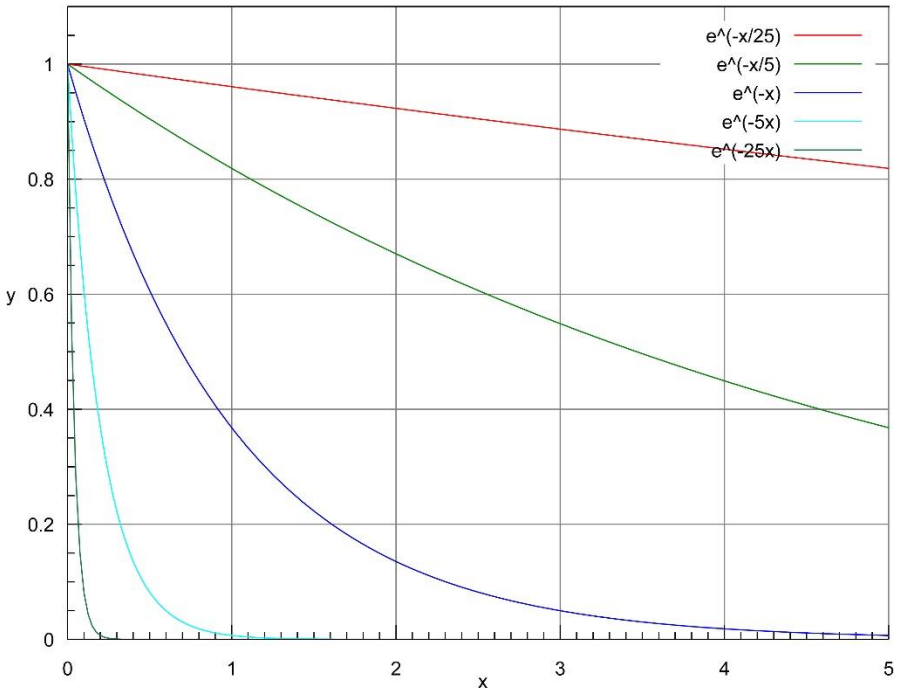

Figure 15. The exponential decay function used in fuzzy classification. Note the power of the function can dramatically alter the results of the classification.

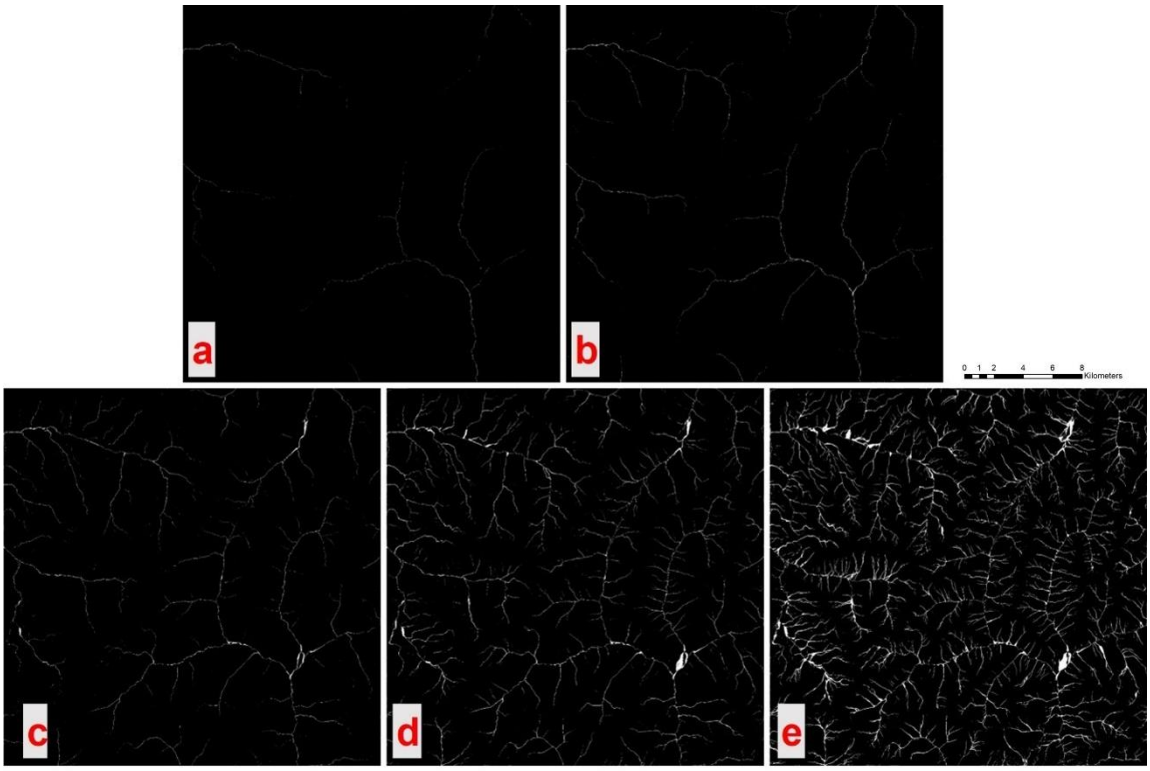

Figure 16. The results from the thresholding method at values of a) 0.8. b) 0.7. c) 0.6. d) 0.5. e) 0.4, respectively.

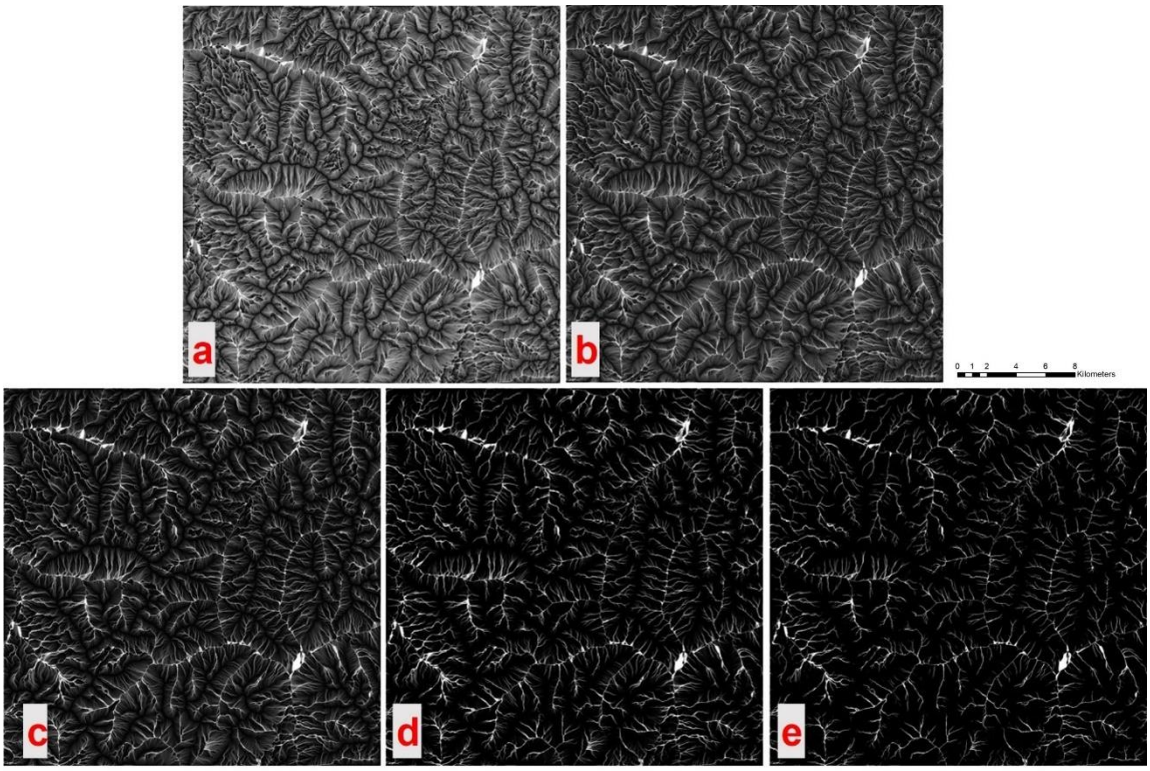

Figure 17. The results from the fuzzy classification at powers of a) 50. b) 25. c) 10. d) 5. e) 1, respectively.

Discussion

FFT is effective tools for characterizing scale dependence issues in mountainous settings. This case study shows the dominate scale in the San Juan Mountains is 70 m, and no strong scale associated with orientation exists. Landform classification and surface roughness can help better understand the geomorphology. Convergence index is a valuable resource for delineate drainage channels, and ongoing research is using rigorous statistics analysis can be used to validate the erosion rate in the San Juan Mountains. Drainage channel stratification can be implemented using topology and automation.

Comparison of the images in Figure 17 with Google Earth image at a scale of 1:2400 shows that it is possible to detect second order and larger streams. Unfortunately, with a DEM resolution of 10 m the detection of first order is not doable.

REFERENCES CITED

Aguilar, R.G., Owens, R. and Giardino, J.R., 2020. The expanding role of anthropogeomorphology in critical zone studies in the Anthropocene. *Geomorphology*, *366*, p.107165.

Amundson, R., Richter, D.D., Humphreys, G.S., Jobbágy, E.G. and Gaillardet, J., 2007. Coupling between biota and earth materials in the critical zone. *Elements*, *3*(5), pp.327-332.

Ambaum, M.H., 2010. Significance tests in climate science. *Journal of Climate*, *23*(22), pp.5927-5932.

Anderson, R.S., Anderson, S., Aufdenkampe, A.K., Bales, R., Brantley, S., Chorover, J., Duffy, C.J., Scatena, F.N., Sparks, D.L., Troch, P.A. and Yoo, K., 2010. Future directions for critical zone observatory (CZO) science. *CZO Community*, *29*.

Anuta, P.E., 1970. Spatial registration of multispectral and multitemporal digital imagery using fast Fourier transform techniques. *IEEE transactions on Geoscience Electronics*, *8*(4), pp.353-368.

Brantley, S.L., Goldhaber, M.B. and Ragnarsdottir, K.V., 2007. Crossing disciplines and scales to understand the critical zone. *Elements*, *3*(5), pp.307-314.

Bretherton, C.S., Smith, C. and Wallace, J.M., 1992. An intercomparison of methods for finding coupled patterns in climate data. *Journal of climate*, *5*(6), pp.541-560.

Bromwich, D.H. and Fogt, R.L., 2004. Strong trends in the skill of the ERA-40 and NCEP–NCAR reanalyses in the high and midlatitudes of the Southern Hemisphere, 1958–2001. *Journal of Climate*, *17*(23), pp.4603-4619.

Burrough, P.A., 1996. Opportunities and limitations of GIS-based modeling of solute transport at the regional scale. *Applications of GIS to the Modeling of Non-point Source Pollutants in the Vadose Zone*, *48*, pp.19-38.

Camarillo-Naranjo, J.M., Álvarez-Francoso, J.I., Limones-Rodríguez, N., Pita-López, M.F. and Aguilar-Alba, M., 2019. The global climate monitor system: from climate data-handling to knowledge dissemination. *International Journal of Digital Earth*, *12*(4), pp.394-414.

Carbonell, A. and Yaro, R.D., 2005. American spatial development and the new megalopolis. *Land Lines*, *17*(2), pp.1-4.

Carleton, A.M., 1999. Methodology in climatology.

Chen, S.H., Jakeman, A.J. and Norton, J.P., 2008. Artificial intelligence techniques: an introduction to their use for modelling environmental systems. *Mathematics and computers in simulation*, *78*(2-3), pp.379-400.

Chen, B., Huang, B. and Xu, B., 2015. Comparison of spatiotemporal fusion models: A review. *Remote Sensing*, *7*(2), pp.1798-1835.

Chiles, J.P. and Delfiner, P., 1999. Modeling spatial uncertainty. *Geostatistics, Wiley series in probability and statistics*.

Claps, P., Fiorentino, M. and Oliveto, G., 1996. Informational entropy of fractal river networks. *Journal of Hydrology*, *187*(1-2), pp.145-156.

Cooley, J.W., Lewis, P.A. and Welch, P.D., 1969. The fast Fourier transform and its applications. *IEEE Transactions on Education*, *12*(1), pp.27-34.
Cressie, N., 1993. *Statistics for spatial data*. New York.

Curran, P.J., 1988. The semivariogram in remote sensing: an introduction. *Remote sensing of Environment*, *24*(3), pp.493-507.

Daubechies, I., 1992. *Ten lectures on wavelets*. Society for industrial and applied mathematics.

Dawson, T.E., Hahm, W.J. and Crutchfield-Peters, K., 2020. Digging deeper: what the critical zone perspective adds to the study of plant ecophysiology. *New Phytologist*, *226*(3), pp.666-671.

Deng, C. and Wu, C., 2012. BCI: A biophysical composition index for remote sensing of urban environments. *Remote Sensing of Environment*, *127*, pp.247-259.

Eichel, J., Draebing, D., Kattenborn, T., Senn, J.A., Klingbeil, L., Wieland, M. and Heinz, E., 2020. Unmanned aerial vehicle-based mapping of turf-banked solifluction lobe movement and its relation to material, geomorphometric, thermal and vegetation properties. *Permafrost and Periglacial Processes*, *31*(1), pp.97-109.

Fan, Y. and Van den Dool, H., 2008. A global monthly land surface air temperature analysis for 1948–present. *Journal of Geophysical Research: Atmospheres*, *113*(D1).

Feciskanin, R. and Minár, J., 2021. Polygonal simplification and its use in DEM generalization for land surface segmentation. *Transactions in GIS*.

Florinsky, I., 2016. *Digital terrain analysis in soil science and geology*. Academic Press.

Franklin, S.E., 2020. Interpretation and use of geomorphometry in remote sensing: a guide and review of integrated applications. *International Journal of Remote Sensing*, *41*(19), pp.7700-7733.

Furfaro, R., Kargel, J.S., Lunine, J.I., Fink, W. and Bishop, M.P., 2010. Identification of cryovolcanism on Titan using fuzzy cognitive maps. *Planetary and Space Science*, *58*(5), pp.761-779.

Germann, U., Galli, G., Boscacci, M. and Bolliger, M., 2006. Radar precipitation measurement in a mountainous region. *Quarterly Journal of the Royal Meteorological Society: A journal of the atmospheric sciences, applied meteorology and physical oceanography*, *132*(618), pp.1669-1692.

Giardino, J.R., 1971. *A comparative analysis of slope characteristics for the Colorado Plateau* (Master thesis, Arizona State University).

Goodchild, M.F., 1992. Geographical information science. *International journal of geographical information systems*, *6*(1), pp.31-45.

Greiving, S., Fleischhauer, M. and Wanczura, S., 2006. Management of natural hazards in Europe: The role of spatial planning in selected EU member states. *Journal of environmental planning and management*, *49*(5), pp.739-757.

Haykin, S., 1999. Self-organizing maps. *Neural networks-A comprehensive foundation, 2nd edition, Prentice-Hall*.

Hengl, T. and Reuter, H.I. eds., 2008. *Geomorphometry: concepts, software, applications*. Newnes.

Hobson, R.D., 1972. surface roughness in topography: quantitative approach. Pages 221-245 in RJ Chorley, editor. Spatial analysis in geomorphology. Harper & Row, New York, New York, USA.

Houser, C., Bishop, M.P. and Barrineau, P., 2015. Characterizing instability of aeolian environments using analytical reasoning. *Earth Surface Processes and Landforms*, *40*(5), pp.696-705.

Hsu, K.L., Gupta, H.V. and Sorooshian, S., 1995. Artificial neural network modeling of the rainfall-runoff process. *Water resources research*, *31*(10), pp.2517-2530.

Hubbard, B.B., 1998. *The world according to wavelets: the story of a mathematical technique in the making*. AK Peters/CRC Press.

Jeffrey, S.J., Carter, J.O., Moodie, K.B. and Beswick, A.R., 2001. Using spatial interpolation to construct a comprehensive archive of Australian climate data. *Environmental Modelling & Software*, *16*(4), pp.309-330.

Jensen, J. R., 2007. *Remote Sensing of the Environment.* New Jersey: Pearson Prentice Hall.

Jensen, J. R., 2005. *Introductory Digital Image Processing.* New Jersey: Pearson Prentice Hall.

Joo, D., Woosnam, K.M., Shafer, C.S., Scott, D. and An, S., 2017. Considering Tobler's first law of geography in a tourism context. *Tourism Management*, *62*, pp.350-359.

Karafyllidis, I. and Thanailakis, A., 1997. A model for predicting forest fire spreading using cellular automata. *Ecological Modelling*, *99*(1), pp.87-97.

Kim, T.W. and Ahn, H., 2009. Spatial rainfall model using a pattern classifier for estimating missing daily rainfall data. *Stochastic Environmental Research and Risk Assessment*, *23*(3), pp.367-376.

Kosko, B., 1986. Fuzzy cognitive maps. *International journal of man-machine studies*, *24*(1), pp.65-75.

Krige, D.G., 1951. *A statistical approach to some mine valuation and allied problems on the Witwatersrand: By DG Krige* (Doctoral dissertation, University of the Witwatersrand).
Kumar, P., 1994. Wavelet analysis in geophysics: An introduction. *Wavelets in geophysics*, pp.1-43.

Lau, K.M. and Weng, H., 1995. Climate signal detection using wavelet transform: How to make a time series sing. *Bulletin of the American meteorological society*, *76*(12), pp.2391-2402.

Leung, L.R., Kuo, Y.H. and Tribbia, J., 2006. Research needs and directions of regional climate modeling using WRF and CCSM. *Bulletin of the American Meteorological Society*, *87*(12), pp.1747-1751.

Li, X., Liu, Y., Wang, M., Jiang, Y. and Dong, X., 2021. Assessment of the Coupled Model Intercomparison Project phase 6 (CMIP6) Model performance in simulating the spatial-temporal variation of aerosol optical depth over Eastern Central China. *Atmospheric Research*, *261*, p.105747.

Ling, Y. and Mahadevan, S., 2013. Quantitative model validation techniques: New insights. *Reliability Engineering & System Safety*, *111*, pp.217-231.

Little, R.J. and Rubin, D.B., 2019. *Statistical analysis with missing data* (Vol. 793). John Wiley & Sons.

Longley, P.A., Goodchild, M.F., Maguire, D.J. and Rhind, D.W., 2005. *Geographic information systems and science*. John Wiley & Sons.

Marden, J.I., 2000. Hypothesis testing: from p values to Bayes factors. *Journal of the American Statistical Association*, *95*(452), pp.1316-1320.

Matheron, G., 1971. *The Theory of Regionalized Variables and Its Applications.* Paris: Mines Paris Tech.

Nardini, A., Yepez, S., Zuniga, L., Gualtieri, C. and Bejarano, M.D., 2020. A Computer Aided Approach for River Styles—Inspired Characterization of Large Basins: The Magdalena River (Colombia). *Water*, 12(4), p.1147.

Papageorgiou, E.I., 2011. Learning algorithms for fuzzy cognitive maps—a review study. *IEEE Transactions on Systems, Man, and Cybernetics, Part C (Applications and Reviews)*, *42*(2), pp.150-163.

Papageorgiou, E.I. and Salmeron, J.L., 2012. A review of fuzzy cognitive maps research during the last decade. *IEEE Transactions on Fuzzy Systems*, *21*(1), pp.66-79.

Pennock, D.J., 2003. Terrain attributes, landform segmentation, and soil redistribution. *Soil and Tillage Research*, *69*(1-2), pp.15-26.

Pennock, D.J., Zebarth, B.J. and De Jong, E., 1987. Landform classification and soil distribution in hummocky terrain, Saskatchewan, Canada. *Geoderma*, *40*(3-4), pp.297-315.

PIKE, R.J., 1995. Geomorphometry-progress, practice, and prospect. *Zeitschrift für Geomorphologie. Supplementband*, (101), pp.221-238.

Ramsey, M.S. and Flynn, I.T., 2020. The spatial and spectral resolution of ASTER infrared image data: A paradigm shift in volcanological remote sensing. *Remote Sensing*, *12*(4), p.738.

Richter, D.D. and Mobley, M.L., 2009. Monitoring Earth's critical zone. *Science*, *326*(5956), pp.1067-1068.

Schneider, T., 2001. Analysis of incomplete climate data: Estimation of mean values and covariance matrices and imputation of missing values. *Journal of climate*, *14*(5), pp.853-871.

Silveira, E.M.D.O., Mello, J.M.D., Acerbi Júnior, F.W. and Carvalho, L.M.T.D., 2018. Object-based land-cover change detection applied to Brazilian seasonal savannahs using geostatistical features. *International Journal of Remote Sensing*, *39*(8), pp.2597-2619.

Sofia, G., 2020. Combining geomorphometry, feature extraction techniques and Earth-surface processes research: The way forward. *Geomorphology*, *355*, p.107055.

Strahler, A.N., 1952. Dynamic basis of geomorphology. *Geological society of america bulletin*, *63*(9), pp.923-938.

Stocker, T.F., 2013. Close Climate Change 2013: The Physical Science Basis. Contribution of Working Group I to the Fifth Assessment Report of the Intergovernmental Panel on Climate Change.

Sui, D.Z. and Giardino, J.R., 1995. Applications of GIS in Environment Equity Analysis. In *GIS LIS-INTERNATIONAL CONFERENCE-* (Vol. 2, pp. 950-959). AMERICAN SOCIETY FOR PHOTOGRAMMETRY AND REMOTE SENSING.

Thuiller, W., 2004. Patterns and uncertainties of species' range shifts under climate change. *Global change biology*, *10*(12), pp.2020-2027.

Torrence, C. and Compo, G.P., 1998. A practical guide to wavelet analysis. *Bulletin of the American Meteorological society*, *79*(1), pp.61-78.

Wang, F., 1990. Fuzzy supervised classification of remote sensing images. *IEEE Transactions on geoscience and remote sensing*, *28*(2), pp.194-201.

Widodo, B., Edy, I., Suroso, J.S., Andry, C., Heri, N. and Santoso, G.A.A., 2021. Mapping and 3D modelling using quadrotor drone and GIS software. *Journal of Big Data*, *8*(1).

Woods, R.E., Eddins, S.L. and Gonzalez, R.C., 2009. Digital image processing using MATLAB.

Zadeh, L.A., 1965. Fuzzy Sets, Information and Control, 8: 338-353. *MathSciNet zbMATH*.

Ziliak, S. and McCloskey, D.N., 2008. *The cult of statistical significance: How the standard error costs us jobs, justice, and lives*. University of Michigan Press.

3. CONTRASTING PATTERNS OF GLACIER ACTIVITIES IN THE SOUTH PATAGONIAN ICEFIELD

Introduction

This chapter focus on explaining the contrasting patterns of glacier activities in the Southern Patagonia Icefield. To have a better understanding of the confusing phenomenon, this chapter first develops a new technique to quantify the change of the glacial-surficial structure as a substitute to the traditional approach by using the fluctuation of glacier terminus and mass balance change. This chapter further evaluates the findings of this new method and explains the underlying reason by evaluating multiple factors.

The Patagonian Icefield (PI) is intimately related to the livelihood of millions of people in Chile and Argentina (Courdrain et al., 2005; Bradley et al., 2006). Figuratively, the Patagonian Icefield functions as the water tower for this whole region (Figure 18), as it contains a large proportion of available fresh water and plays a significant role in the water circulation regime (Carey, 2010; Viviroli et al., 2011; Black, 2016; Berthier et al., 2020).

The down-wasting and accelerating glacial melt in the Patagonian Icefield is of concern because of its influence on downstream livelihood, social-economical related activities, such as power generation, irrigation, and tourism (Anacona et al., 2014; Carrivick and Tweed, 2016). Furthermore, the largest river, the Chile-Baker River, flows from the glaciers in Northern Patagonia Icefield (NPI), and glacial lakes in Southern

Patagonia Icefield (SPI) yield the last and largest free-flowing river, the Argentina-Santa Cruz River (Casassa et al., 2002; Tagliaferro et al., 2013).

Figure 18. The Patagonia Icefields in the high altitude of South America. Northern Patagonia Icefield (NPI) and Southern Patagonia Icefield (SPI) together influence millions of livelihoods in Chile and Argentina. Figure 18 adapted from Antarctic.Org.

The Patagonian Icefield is also globally significant because the glacier melt in this close-sea region can impact the rise of local sea-level (Rignot et al., 2003; Gardner et al., 2013). Ample geomorphic evidence of glacial melting, including down-wasting since the Little Ice Age, exists in this region (Aniya, 1995; Glasser et al., 2005). Simulations of climate change are useful for factors that facilitate accelerated glacial melting, including increasing temperature and shifting precipitation patterns (Bamber and Rivera, 2007; Schaefer et al., 2013; Natalia et al., 2020). Unfortunately, *in situ* records that could be useful for documenting glacier activities in the Patagonian Icefield are sparse (Pellikka and Rees, 2010). Glacier variations, however, can be archived using remote sensing. Nevertheless, a lack of systematic examinations of glacier fluctuations in the Patagonian Icefield still exists throughout recent decades (Raup et al., 2007; Ohmura, 2009; Malz et al., 2018).

Excluding the Antarctic ice mass, the Patagonian Icefield is the largest ice mass in the Southern Hemisphere (Skvarca et al., 2010; Naruse et al., 1997; Rivera et al., 2007; Masiokas et al., 2009). Compared to other maritime glacial regions (e.g., Alaskan, or Northern European glaciers) the Patagonian Icefield is situated at a much lower latitude (46.5^{o} and 51.5^{o}). And despite location, the Patagonian Icefield glaciers are more vulnerable to climate change compared to various counterparts (Meier, 1984; Marzeion et al., 2017). As a result of melting, the Patagonia Icefield contributed 0.042 ± 0.002 mm per year to sea-level rise during the period 1968-2000, accounting for 9% of the sea-level rise from mountain glaciers, whereas Alaskan glaciers contributed 30% to sea-level rise with a five-times larger area (90,000 Km^2; Rignot et al., 2003). The Southern

Patagonian Icefield accounts for 73% of the amount in the Patagonian Icefield. Thus, this research focuses on Southern Patagonian glaciers (Casassa, 1987; Schaefer et al., 2013).

Of 69 major outlet glaciers in the Patagonian Icefield, 62 are calving glaciers (Aniya 1999). These calving glaciers, however, do not exhibit uniform variations in response to similar micro-climatic conditions (Sakakibara and Sugiyama, 2014). For instance, Glacier Perito Moreno (GPM) and Glacier Ameghino (GA) are two glaciers with connected accumulation zones and a separation of 8 km at the lower reaches (Figure 19). GPM has been stable since the 1920s, but GA has been retreating rapidly (Minowa et al., 2015). Greater rates of retreat have also been found in Glacier Upsala and Glacier Jorge Montt (Sakakibara and Sugiyama, 2014; Rivera et al., 2012). Other observations suggest that calving variations of the glaciers in the Patagonian Icefield are not controlled by micro-climate alone (Meier and Post, 1987; Benn and others, 2007; Post et al., 2011). Uncertainties still exist because limited research has been undertaken regarding rates of change in the glacier terminus, change in the absolute mass balance, and driving factors for each glacier in the Patagonian Icefield (Rivera et al., 2005; Raymond et al., 2005; Cassass et al., 2006; Schaefer et al., 2015; Mernild et al., 2017).

Minowa et. al (2015) mapped two glaciers, Glaciar Perito Moreno (GPM) and Glaciar Ameghino (GA) in the SPI. SRTM DEM, ALSO DEM, Landsat ETM+/TM were used in their study, revealing that GPM has had a very stable terminus since 1920s, whereas GA is a fast-retreating glacier with 334m/yr before 1976 and 20m/yr after 1976.

Their study concluded that this contrasting pattern is the result of different AARs (Accumulation Area Ratio).

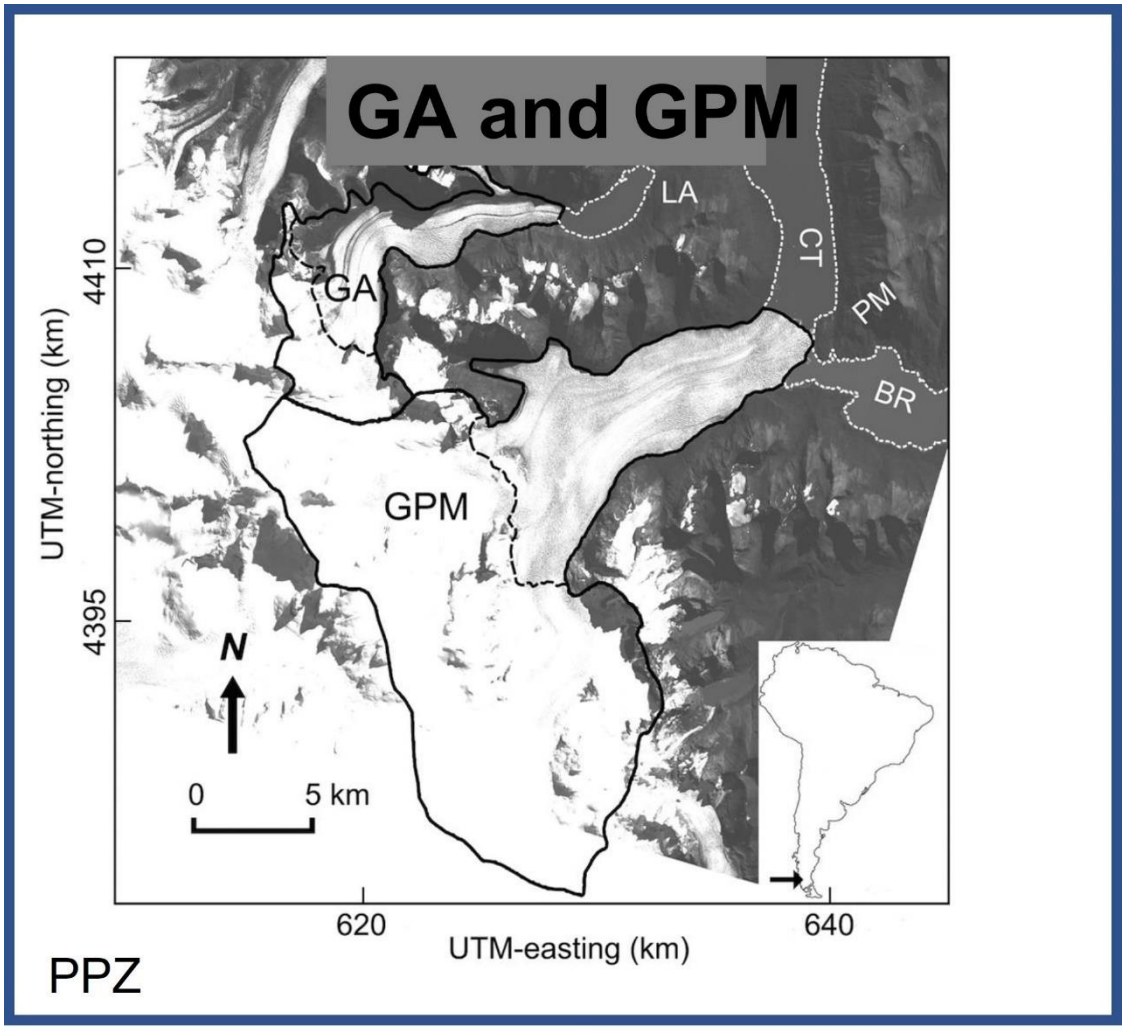

Figure 19. GPM and GA glaciers. Both glaciers are adjacent to each other but exhibit totally contrasting responses to the environment. Figure 19 is adopted from Minowa et al. (2015).

Glacier fluctuations are governed by climate forcing, solar radiation, topographic exposure, and tectonic force (Lodolo et al., 2020). These four factors function together from daily scale to millennial scale to regulate glacier mechanics and further influence the rate of glacier fluctuation (Strecker et al., 2007). To what spatial scale each factor can influence glacier activity, however, has still not been addressed in existing research (Benn, 2014). GA and GPM have connected accumulation zones, both located on the eastern side of the PI (Figure 19). In addition, GA and GPM calve into Lake Argentino, which indicates that these two glaciers have similar sensitivity to climate forcing (Masiokas et al., 2020). My research proposes a new conceptual model (Figure 20) to carefully examine how the glacier-surface structure changes over time in response to these four factors with an emphasis on topographic control.

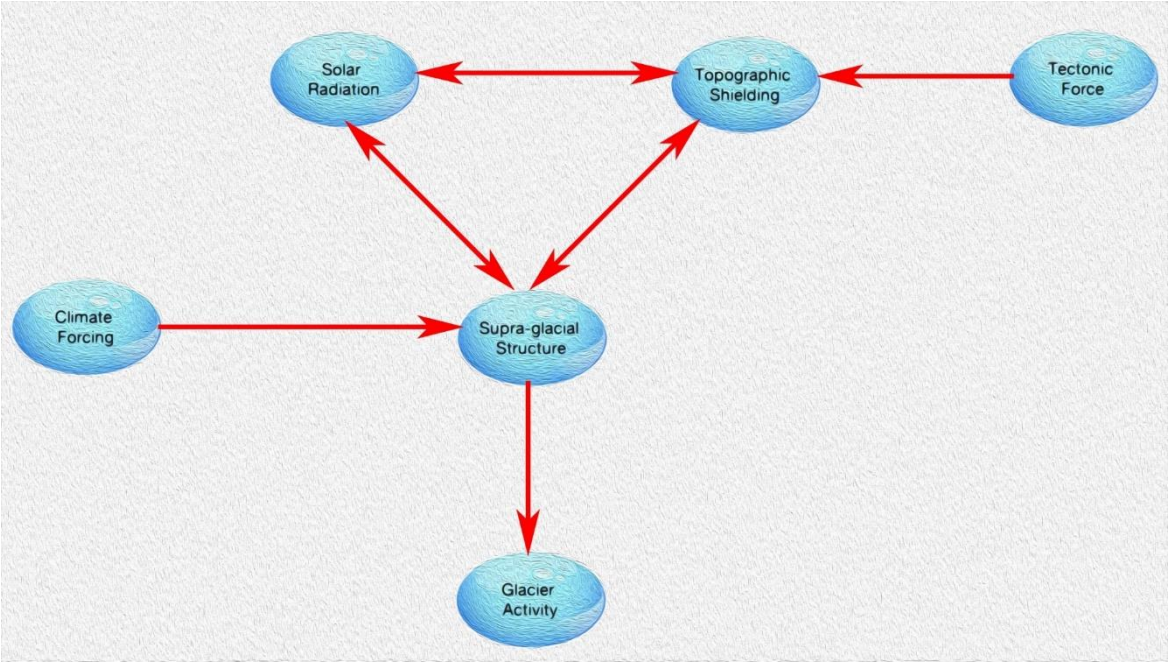

Figure 20. The conceptual model. The change in glacier surface-structure as an intermedia state instead of glacier fluctuation as the only measure of glacier dynamics is highlighted.

Pixel-based mapping approaches have numerous limitations, and do not account for spatial information of glacier-surface structure. Object-based mapping methods using topographic information can be more suitable for characterizing the glacier surface because of supra-glacial complexity. In my research, I first developed a new land-surface parameter (convergence index) to facilitate the characterization of the glacier-surface. Then I examined the potential of object-oriented analysis to characterize glacier surfaces, and I evaluated the suitability of network analysis of graph theory to assess glacier topography and change over time. Finally, I carefully checked the topographic exposure in the vicinity to evaluate the conclusion that Minowa et al. (2015) proposed.

Study Area

Patagonian Icefields

Patagonia is a climatically diverse region of South America extending from about 40°S to the southern tip of the continent at 56 °S (Figure 18; Minowa et al., 2021; Garreaud et al., 2002). In the western regions, extending from the Pacific coast to the crest of the Andes Mountains, cold temperatures and high rates of precipitation support rainforests, rivers, and the largest mid-latitude ice masses on Earth, the Hielo Patagónico or Patagonian Ice Fields (Warren and Sugden, 1993; Garreaud et al., 2002). Covering an area of 17,200 km^2, the Patagonian Ice Fields are divided into two separate ice fields: Hielo Patagónico Norte (Northern Patagonian Icefield) and Hielo Patagónico Sur (Southern Patagonian Icefield) by a fjord (Aniya, 2013). The elevation of the total icefield ranges from 0 m on the west, to 3910 m at Monte San Valentin, located on the northeastern corner of the Northern Patagonian Icefield (Figure 18).

Southern Patagonian Icefield

The Southern Patagonian Icefield (SPI) is the larger of the two Patagonian ice fields and estimated to be the third largest on Earth, just after Greenland and Antarctica (Naruse and Anya, 1992; Warren and Sugden, 1993; Carrasco et al., 2002; Aniya, 2013). It is also the closest single body of permanent ice closest to the equator (Carrasco et al., 2002), extending from 49.5° S to 51.5° S along the 73.5° W meridian, the icefield covers over 13,000 Km^2 (Aniya et al., 2000). Elongated in a north-south direction with a length of ~360

km (Aniya and Skvarca, 1992), the width of SPI gradually narrows from North to South, with an average width of 30-40 km (Lopez et al., 2010).

Climate

The SPI has a high frequency of cloud-cover and precipitation events resulting from the mid-latitude westerlies regime and frontal systems (Figure 21), which dominate the region (Carrasco et al., 2002). The SPI is further influenced by annual weather cycles during which weak winds blow to the southwest during the winter followed by stronger, north-northwesterly winds in the summer. The elements of the weather system contribute to high levels of cloud cover and annual precipitation (Carrasco et al., 2002). The topography of the region causes higher precipitation to the west, exceeding 7,000 mm on the coast and 10,000 mm on the SPI. Precipitation on the eastern side of the Argentine Patagonia is often below 400 mm. Seasonal temperature oscillations are more pronounced on the eastern side of Patagonia than on the western side (Carrasco et al., 2002).

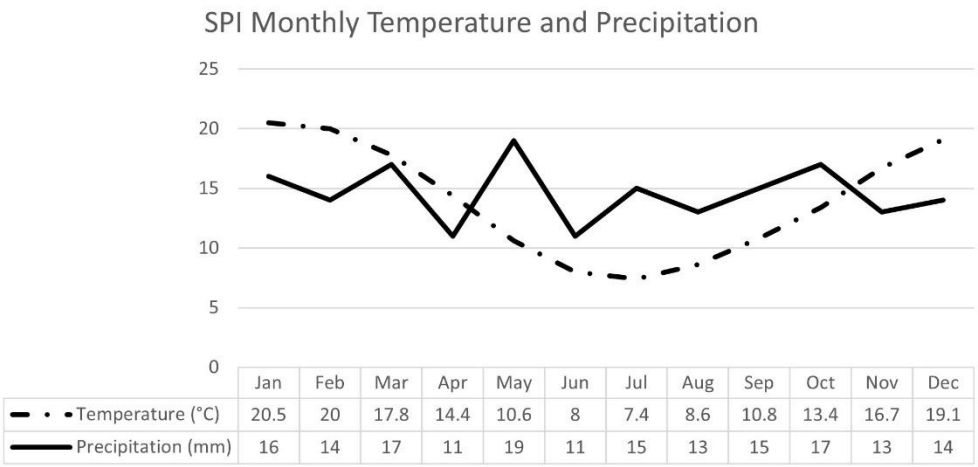

	Jan	Feb	Mar	Apr	May	Jun	Jul	Aug	Sep	Oct	Nov	Dec
Temperature (°C)	20.5	20	17.8	14.4	10.6	8	7.4	8.6	10.8	13.4	16.7	19.1
Precipitation (mm)	16	14	17	11	19	11	15	13	15	17	13	14

Figure 21. The average monthly precipitation and temperature of the Southern Patagonia Ice Field.

Geomorphology

Elevation of glacial ice ranges from 0 to 2,000 m and is punctuated by nunataks ranging in height from 2,000-3,500 m (Warren and Sugden, 1993). In the southern portions of the SPI, the ice field retains contiguous ice cover, but its dynamics are regarded as a series of small individual icecaps (Warrne and Sugden, 1993). With 48 major outlet glaciers, the SPI is the most severely glaciated region of the Andes. The glaciers on the eastern side calve into proglacial lakes, and the glaciers on the western side calve into fjords of the Pacific Ocean (Aniya et al., 1997, 2013; Carrasco et al., 2002).

The largest river in Chile, the Baker River, originates from the glaciers in NPI, and glacial lakes in SPI yield the last and largest free-flowing river in Argentina, the Santa Cruz River (Figure 18; Casassa et al., 2012; Tagliaferro, et al., 2013). The mountains of

the southern Chilean Pacific coast are prominent water towers for the region because of the large ice reserves and high rates of orographic precipitation (Immerzeel et al., 2020).

Tectonic Setting

Tectonics of southern Patagonia play a fundamental role in the topography and geomorphic processes, which dominate the region. The Nazca, South American, and Antarctic plates form a triple junction called the Chile Triple Junction (CTJ) in the fore-arc basin of the southern Patagonia Icefields which causes an abrupt and major increase in elevation and relief (Figure 21; Georgieva et al., 2016). The presence of an extensive slab window beneath southern Patagonia may be the cause of the abrupt and dramatic elevation increase in the region because it supports the high topography (Guillaume et al., 2010; Georgieva et al., 2016). Thomson et al. (2010) linked elevated summits in southern Patagonia with latitudinal climate gradients and alterations to the efficiency of glacial erosion, which further allows for slowed erosion and protection of high-relief topography.

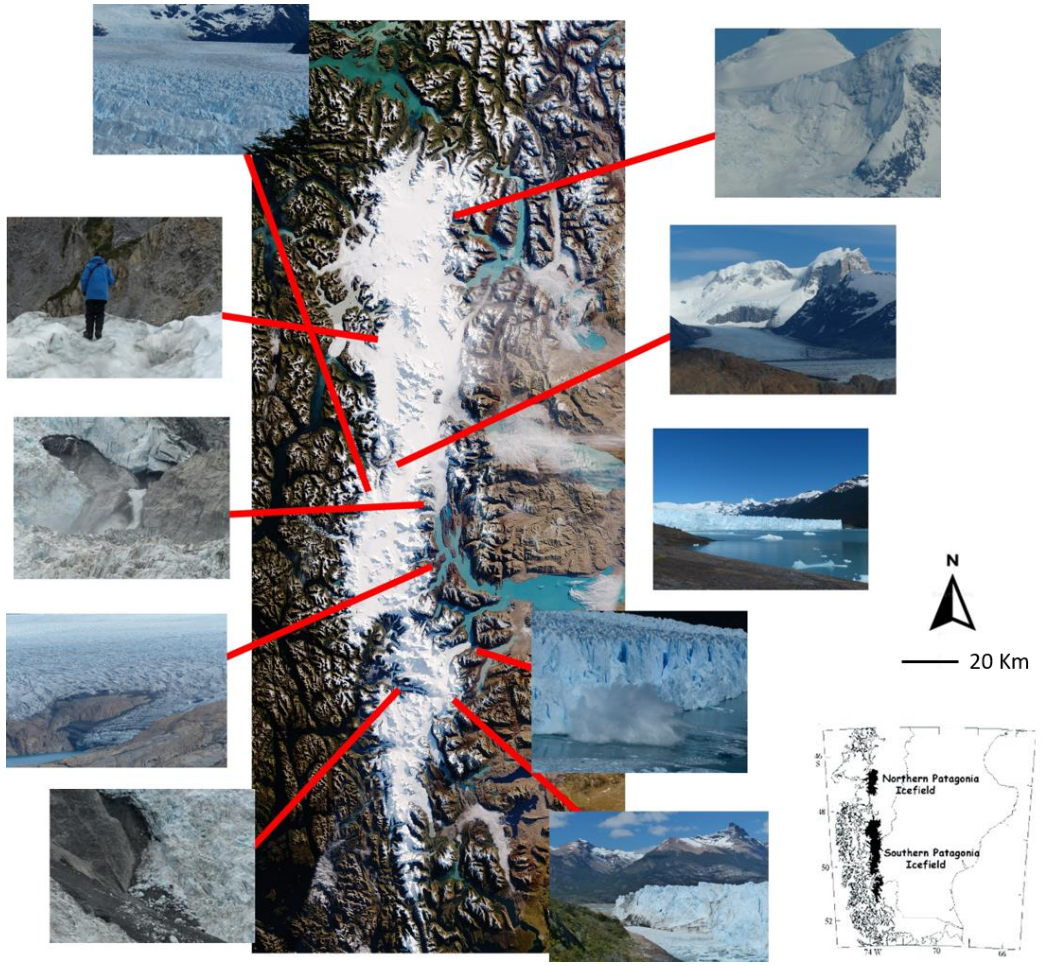

Figure 22. The inset map shows the location of the study site in South America. The base satellite image is a mosaic of cloud-free images acquired by Landsat 8 on April 29, May 1, and May 24, 2016 (NASA Landsat Image Gallery). Ten onsite photos illustrate the surface complexity of glacier surface and extreme neighboring terrain. A calving activity was also well documented during the field work.

Field work in Southern Patagonian Icefield was conducted in 2017 by a group of geologists including Dr. John R. Giardino. Ten classic field photos are selected in Figure 22 to illustrate the diverse surface structure of glaciers and the extreme neighboring terrains. The

complexity of glacier surface is the result of the mixed component of different geomorphological features, including terminal moraines, lateral moraines, crevasses, supra-glacial streams, and debris. A calving event was also captured during this trip.

Methodology

In this research I only focuses on the year from 2000 to 2011 to examine the change in the surface-structure on the GPM and GA. My research is only limited to the 11-year span is because of the following two reasons:

i. SRTM DEM of 2000 has been widely used for multiple glacier studies, which commonly servers as a bassline DEM to conduct change analysis.

ii. Southern Patagonia is notoriously known for the continuous cloud-cover, which makes it extremely difficult for generating DEM from multi-spectral sensors, e.g., Landsat and ASTER. Thus, only imageries from 2000-2011 were the only cloud-free images available.

DEM analysis

This research has adopted two DEMs, including Shuttle Radar Topography Mission (SRTM) DEM V4 and Advanced Spaceborne Thermal Emission and Reflection Radiometer (ASTER) GDEM V2. SRTM was generated in 2000 and ASTER DEM was generated in 2011. Both DEMs are first reprojected by using UTM18S coordinate system, and then DEM artifacts, including no-data pixels and stripes, are filled using cubic convolution. The spatial resolution of SRTM is 75 meters in mid-latitude and the spatial resolution of ASTER is 25 meters. ASTER DEM is then resampled into 75 meters using bilinear interpolation to align with SRTM DEM-grids, suggesting that both centroids of each cell are 100% overlapped.

The elevation changes of the glacier surface from 2000 to 2011 was measured by differencing ASTER GDEM and SRTM DEM. Figure 23 illustrates the elevation difference with a span of 10 years where both GPM and GA glaciers are highlighted.

For further spatial analysis, I digitized centerlines for these two glaciers starting from the terminus and ending at estimated equilibrium line altitude (ELA). The path length for GA is about 12 kilometers and GP is 13 kilometers. Along these centerlines, elevational differences are shown in Figure 24. The average of GPM is -4.3m whereas the average of GA is -20.3m.

The correlation ecoefficiency of the two DEMs is 0.995 with an average difference of ±2.9m. A hypsometry analysis also suggests these two DEMs match closely with each other (Figure 25). Some small mismatch in high elevation areas do occur, especially in the accumulation zones because of low contrast of fresh snow when generating the DEM using stereoscopic techniques. Because this research mainly focuses on the structure change of the glacier surface in the ablation zone and the topographic control by the neighboring terrains, this small mismatch in the accumulation zone has minimal impact of the results of my study.

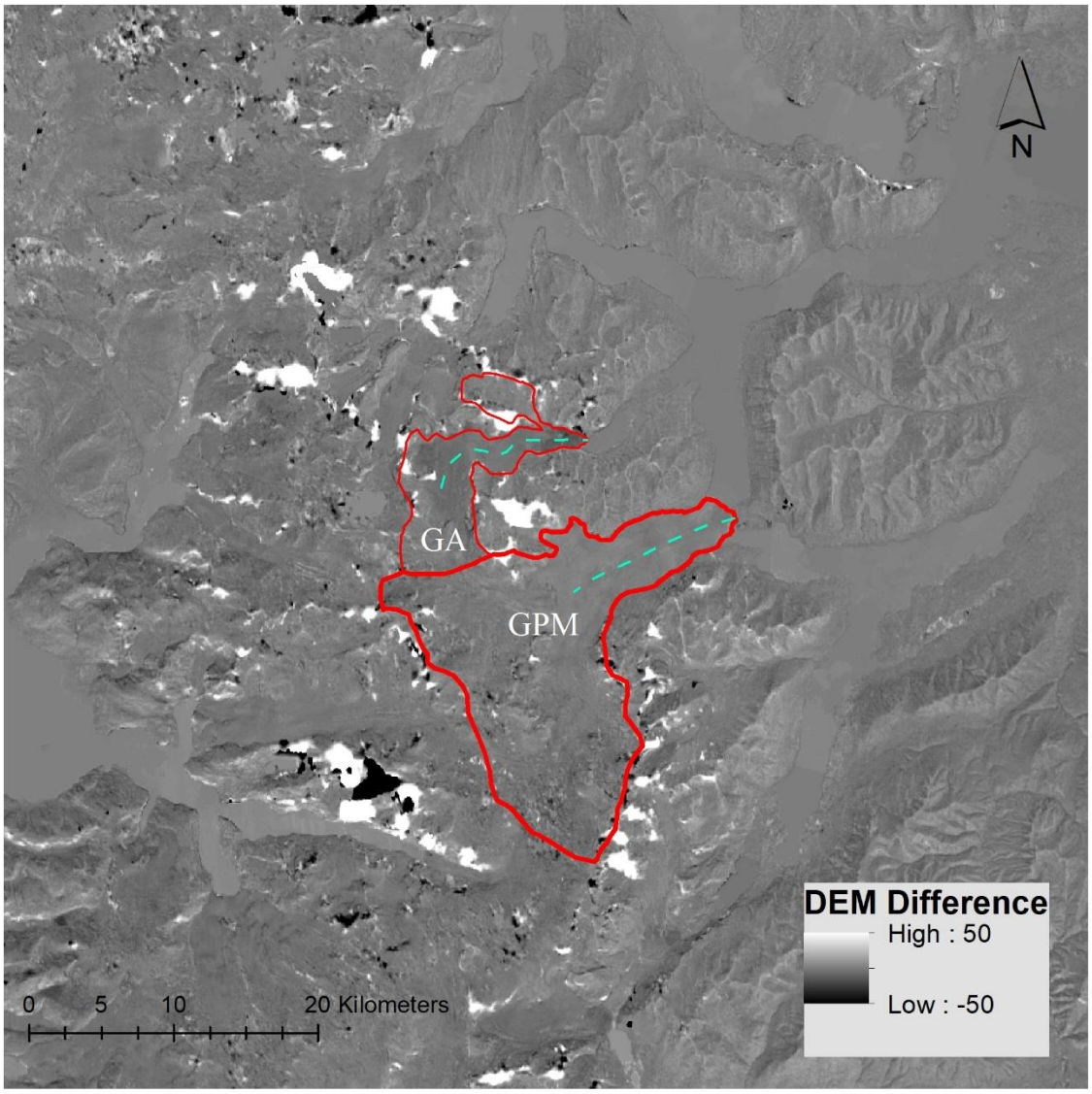

Figure 23. Surface-elevation changes over GPM and GA from 2000 to 2011. Glacier boundaries (in red) are retrieved from Global Land Ice Measurements from Space (GLIMS) database. The dashed curves represent the central flowlines from terminus to estimated ELA that was used in Minowa et al., 2015. Note the detectable area of high elevation of difference (i.e., >50m) only exist in either accumulation zones or mountain ridges because of clouds and shadow.

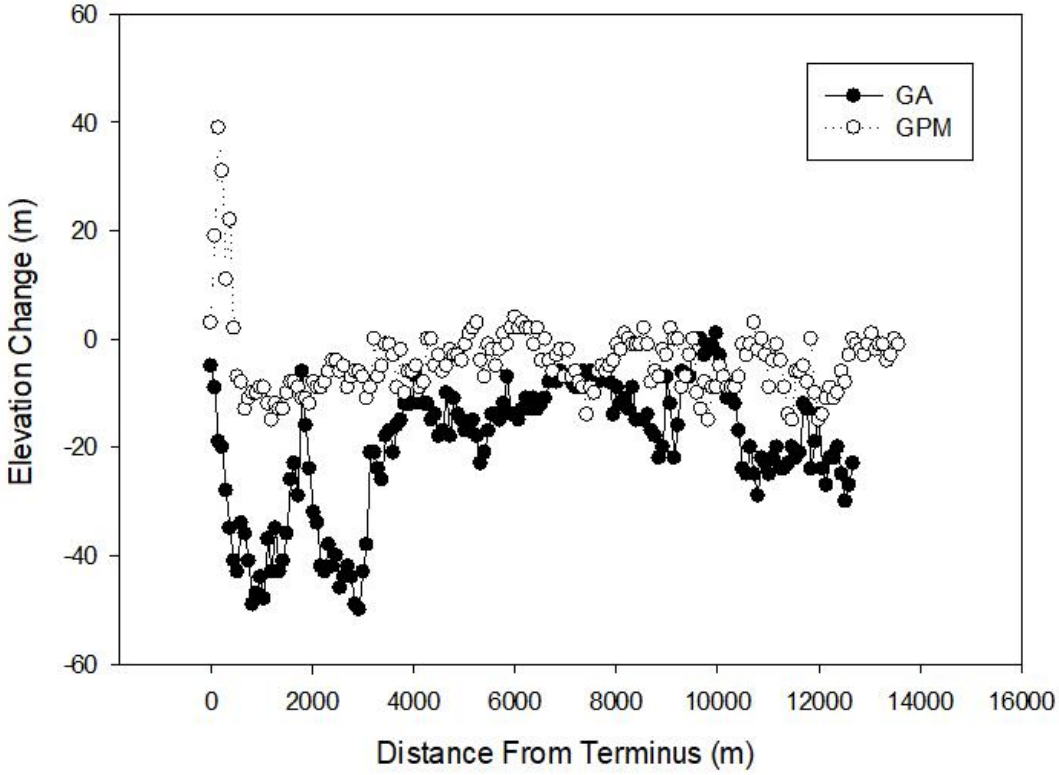

Figure 24. Change in surface elevation in GA and GPM along the central flowlines shown in Figure 23. GPM elevation change is very consistent, but GA elevation change varies significantly.

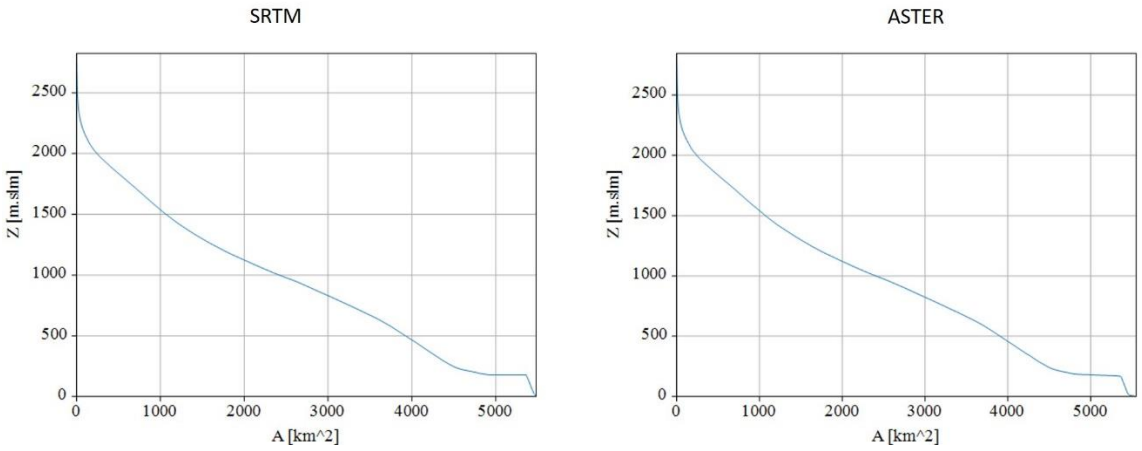

Figure 25. The hypsometry curves for SRTM and ASTER DEMs. With 0.995 correlation ecoefficiency, these two curves match.

Convergence Index and Segmentation

In this study, I designed a protocol of using a new topographic index for segmentation to characterize the structure of the glacier-surface (Figure 26). This index can be used as a terrain parameter to show the local relief as a set of convergent features (e.g., supraglacial ponds) and divergent features (e.g., ogives and medial moraines) on the glacial surface. Thus, the index is the most optimal parameter to measure the convexity and complexity of the glacial surface as a response to glacial mass movement and down-wasting cascade.

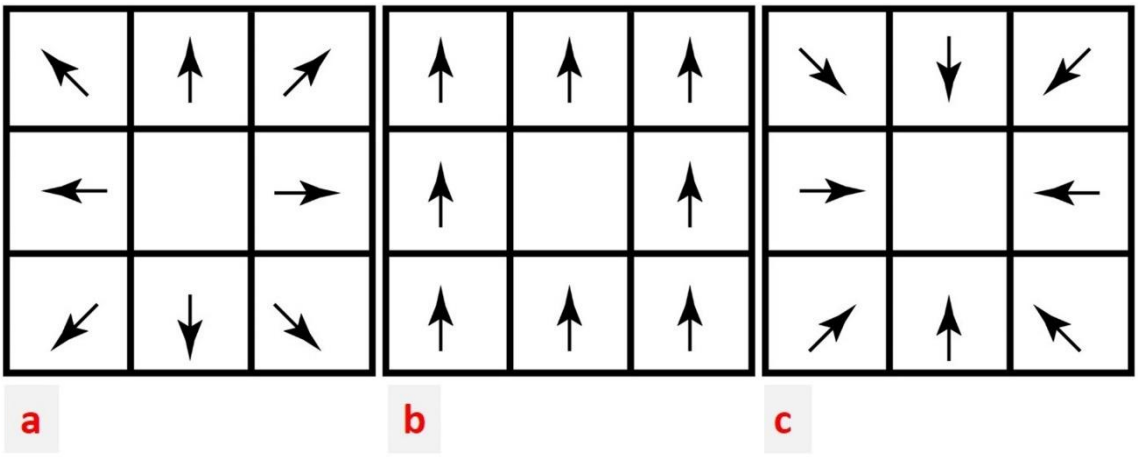

Figure 26. Schematic figure for this index. Illustration of the convergence and divergence concepts. a) Divergence, b) Level, c) Convergence.

For each pixel, if water flows towards all eight neighboring pixels, this specific pixel is classified as divergent. In contrast, if water flows into the center pixel from all eight neighboring pixels, this specific pixel is then classified as convergent (Claps et al., 1994). Mathematically speaking, convergence indices can be computed with a 3x3 moving window using the following equation:

$$Convergence = \sum_{i=0}^{n} \frac{|\cos\emptyset_i - \cos\emptyset_{\varepsilon,i}| + |\sin\emptyset_i - \sin\emptyset_{\varepsilon,i}|}{4n} \qquad (2)$$

Where, n is the number of neighboring pixels, $\emptyset_i$ is the aspect of pixel i towards the center of the moving window, and the $\emptyset_{\varepsilon,i}$ is the aspect from the center towards the pixel i. The convergence index ranges from 0 to 1, and a higher value refers to a higher degree of convergence. For instance, a perfect pit pixel will equal 1 and a perfect peak will equal 0.

Specifically, the convergence index represents the agreement of flow direction of surrounding pixels within a local scale, which makes the convergence index perform better at delineating boundary changes than other first-order and second-order derivatives, including slope, aspect, profile curvature, tangential curvature, and surface roughness. The unique morphology of supraglacial features, thus, can be clearly characterized using such an index. In GA and GPM, glacier boundaries (terminus and lateral moraines) are relevantly convergent (Figure 27). In the ablation zone, glacier-flow directions are also well delineated, and the glacier surface exhibits a much more complex spatial pattern compared to the accumulation zone and mountain terrains. Each glacier exhibits different spatial patterns, and the spatial frequencies of patterns are significantly enhanced on the glacier surface.

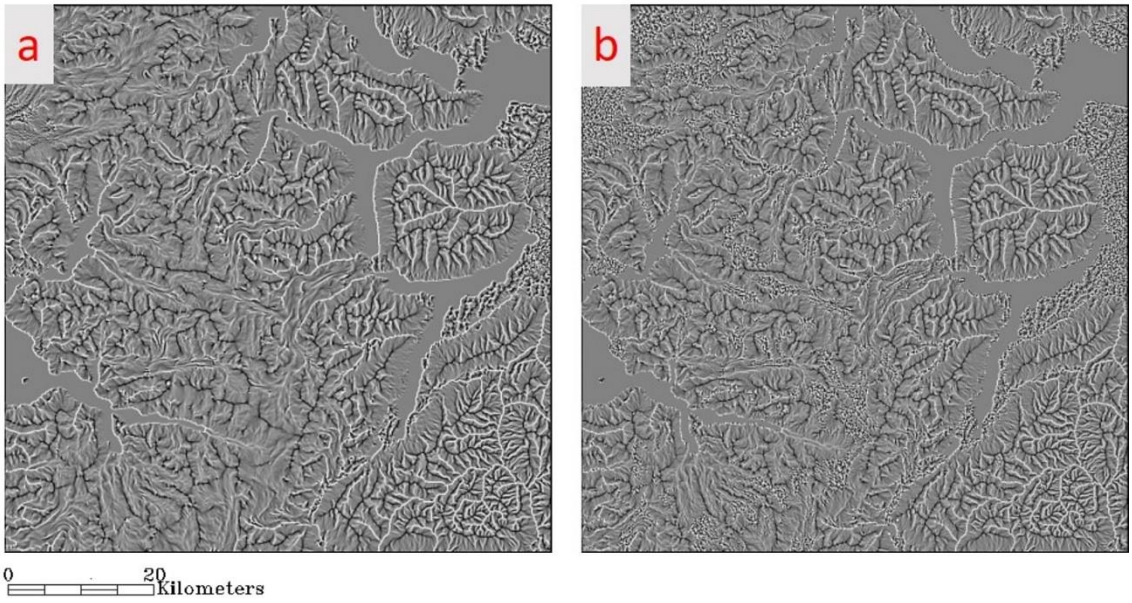

Figure 27. Convergence index computed based on Equation (1). The left image shows the SRTM convergence index, and the right image shows the ASTER convergence index.

Furthermore, different glaciers demonstrate varying degrees of glacial activity from advancing to retreating as well as stagnating. Although these activities depict the status of the glacier-terminus, unfortunately, they neglect the dynamics of the glacier. For a given period, each glacier shows unique spatial complexity in its ablation zone, and the degree of complexity is determined by the spatial distribution of various features including ridging features (moraines), concave features (streams and ponds), and more complicated features (crevasses). Using such micro-topography can be a better alternative approach to investigate glacier dynamics and mass balance.

In addition, pixel-based convergence still cannot fully satisfy the need to understand glacial-surface change at a meaningful scale. To accomplish this, I used a segmentation approach to aggregate pixels showing similar convexity into one object, which carries certain feature information about the glacier surface. After numerous substantiation tests, I found using a threshold of 0.55 returns the best result for this study area (Figure 28). In Figure 28, the white color represents convergent features whereas the black color represents the divergent features. The GA and GPM glacier surface remains distinguished compared to other locations in the map because the flow direction of glaciers can be easily detected. In addition, each glacier maintains its own spatial signature.

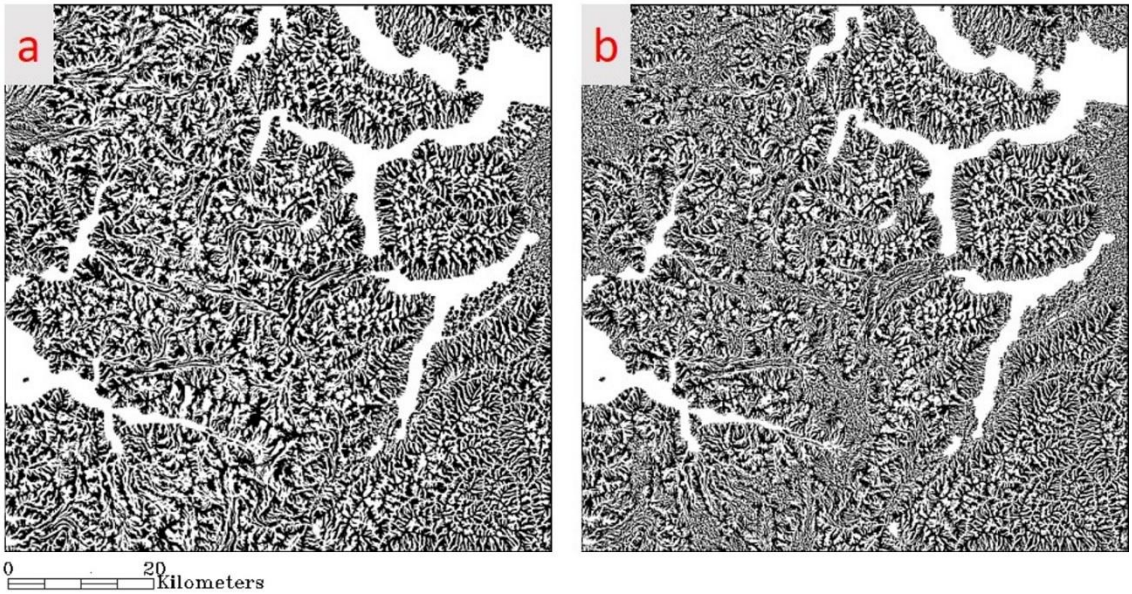

Figure 28. Segmentation results based on convergence index from Figure 27. I selected 0.55 as the best threshold to generate the object. The white color shows convergent object and black color means divergent objects. The left is the SRTM convergence segmentation, and the right is the ASTER convergence segmentation.

Object-oriented network analysis (Graph Theory)

Graph theory has been broadly used in the fields of hydrology, landscape ecology, debris-flow, and geomorphology (Dehmer et al., 2014; Heckmann, 2015). The common applications of graph theory in geoscience focus on analyzing the connectivity and network structure of meaningful spatial features within a specific system. Thus, the method has great potential to facilitate the study of complexity and dynamics of the structure of the glacial surface. In previous section, convergent and divergent objects are collectively highlighted on the glacier surface and represent specific glacial-geomorphological features, which makes a strong case for using graph theory to connect the features and further quantify the network complexity, as a parameter to measure the surface down-wasting and movement dynamics.

In this dissertation, I designed a glacier-specific graph theory protocol (Figure 29) to quantitatively configure the linkages between convergent and divergent objects within certain search radii so supraglacial flux can be measured. In detail, from any pixel of a study area image, I calculated the number of convergent objects around the center pixel; and from each surrounding convergent object for that pixel, I calculated how many divergent objects are around the centroid of each convergent object. The sum of convergent and divergent objects clearly delineates the complexity of glacier surface. In Figure 29, the green star represents a specific gird location; the red dot represents centroid of convergent network; the yellow link represents the link from grid location to the convergent network; the blue triangle represents the divergent network; and the blue link represents the link from convergent network to divergent network.

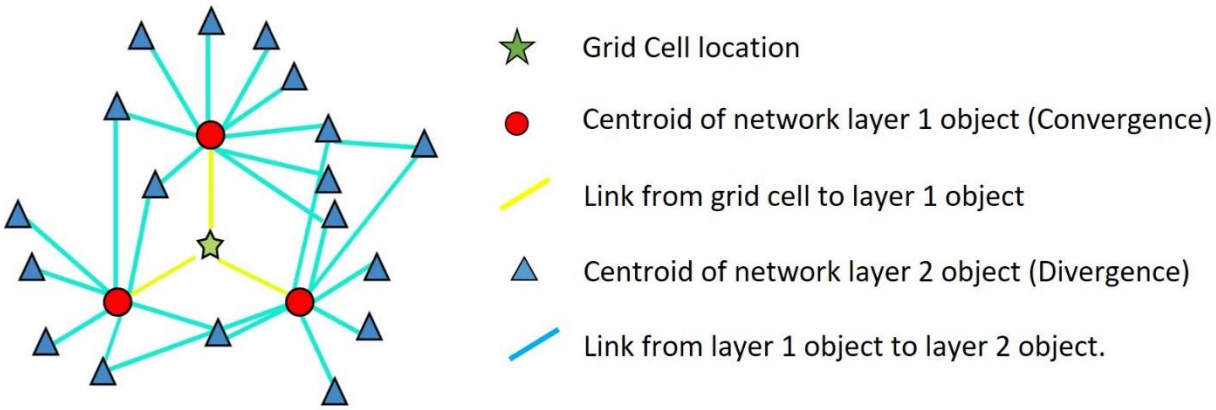

Figure 29. Conceptual diagram of network analysis.

Technically speaking, I first had to perform a centroid analysis (Figure 30) for and ASTER segmentation images. The distance analysis of centroids is based on nearest pair of centroid points. For each point, whether it is convergent or divergent, I searched for its nearest point and calculated the distance. Relative scale size of each object had to be also considered. The result suggests a mean distance for the nearest pair for SRTM is 526 meters and 389 meters for ASTER. Because both images are resampled into 75 meter-resolution, 526 meters on the SRTM is equal to 7 pixel-sizes whereas 389 meters on the ASTER is equal to 5.1 pixel-sizes. This information helps to determine the proper search radius needed for graph theory. In this study, I used two-cascade search radius (Figure 29). For each pixel, I searched for a convergent object. The radius is 5 pixels. From convergent to divergent, the radius is 3. Both radii are comparable to the averaged pixel distance.

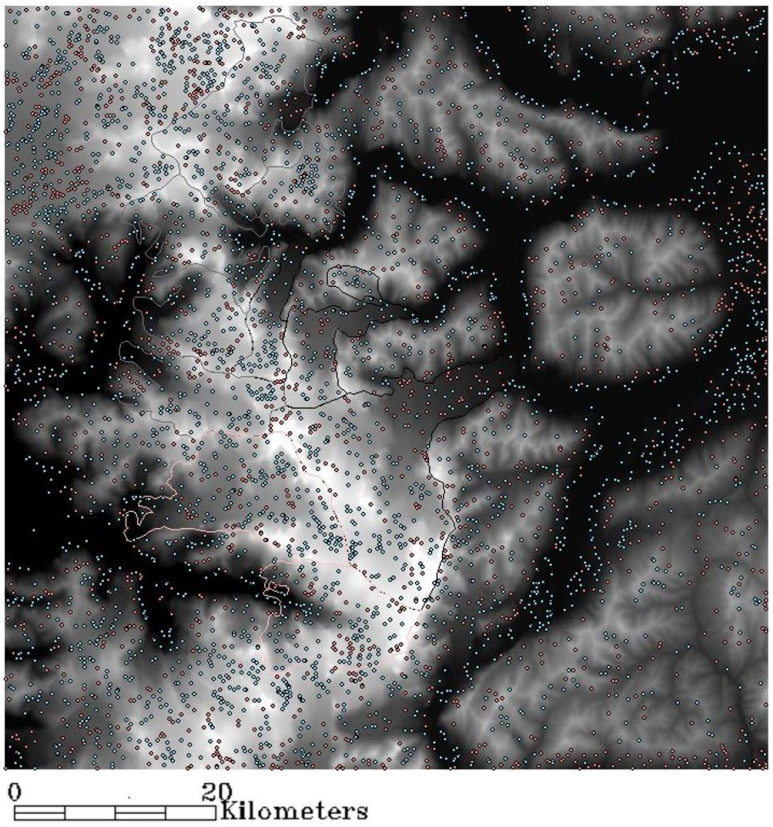

Figure 30. Overall object, divergent object, and convergent object images with centroids. SRTM centroids overlayed on convergent and divergent objects. Blue is divergent. Red is convergent. SRTM centroid-distance analysis is based on divergent and convergent objects. The mean distance of nearest pair of points for SRTM is ~500 meters. ASTER centroid-distance analysis is also based on divergent and convergent objects. The mean distance of nearest pair of points for ASTER is ~400 meters.

Topographic Exposure

Topographic exposure, also known as TOPEX (Ruel et al., 2002), is a quantitative measurement of neighboring topography that constrains the local flux exchange, which is very important in glacial settings, including incoming direct solar radiation which provides the major energy source, wind-flow exposure which regulates the convection and evaporation, snowfall amount which contributes to accumulation on the glacier, and regional temperature which controls the ablation. Unfortunately, existing commercial software does not provide a feasible solution for generating accurate TOPEX, so I had to develop a protocol to effectively calculate TOPEX.

For the algorithm, the inputs are height of the elevation and distance to the focal pixel. The combination of these two variables creates the angle of inflection, which is the angle used to quantify the shielding parameter. Figure 31 well demonstrates the relationship between elevation and distance for a certain location in a complex terrain setting. Semantically within a predetermined search radius in a specific direction, I calculated the inflection angles α of Point A, B and C, s. Point B yields the highest inflection angle whereas Point C yields the lowest inflection angle α_c. The higher the inflection angle equates to a higher topographic shielding effect but lower exposure. As a result, within a search radius, zero minus the maximum inflection angle, $0-\alpha_b$, is the TOPEX.

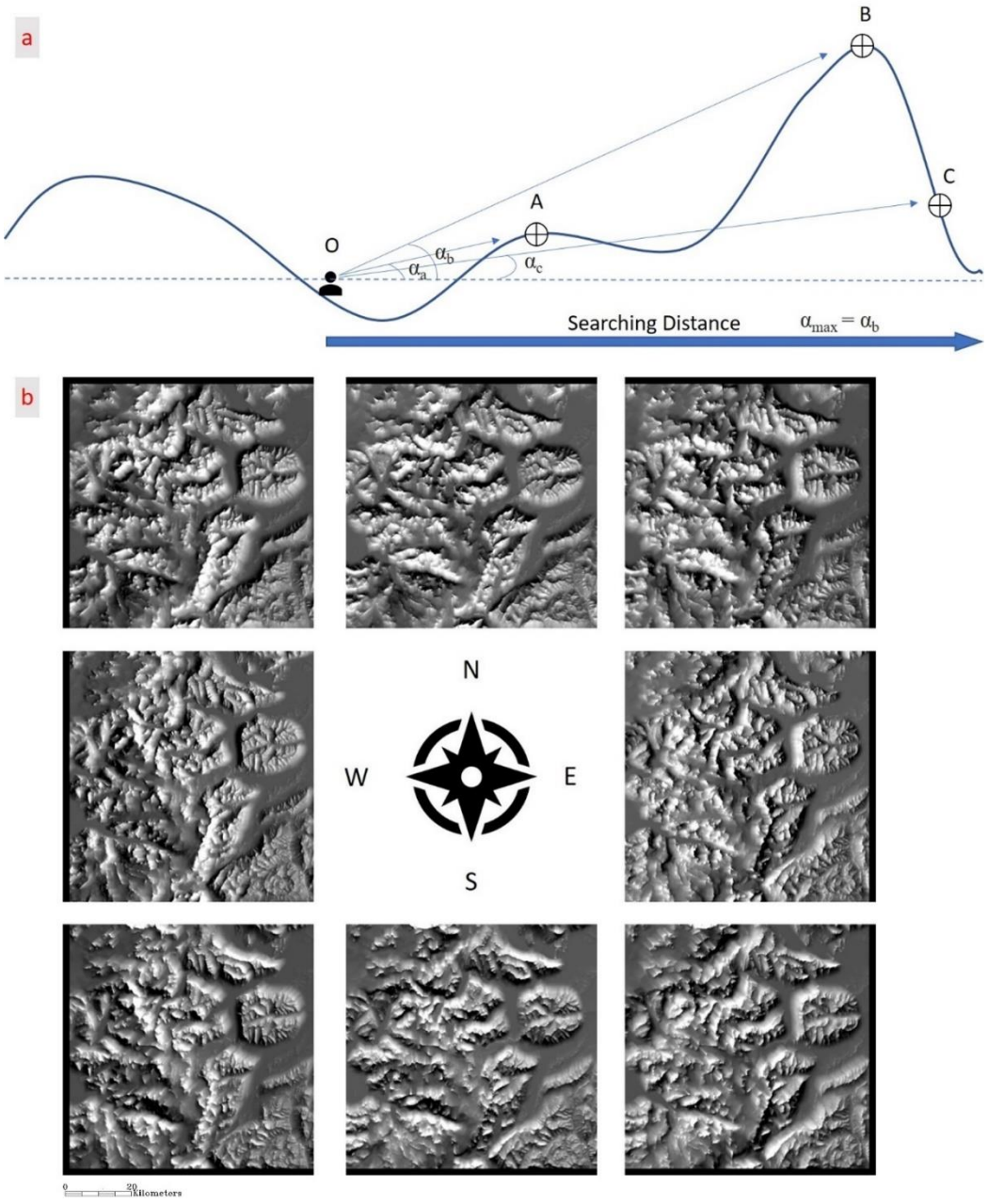

Figure 31. The semantics of how to calculate Topographic Exposure Index (a). Figure 31b is the intermediate results of all inspection angles in eight directions. The dark border for each image is the padding zone of image processing within the search distance.

In the Patagonia Icefields, the surrounding mountains significantly influence the flux exchange of glacier mass, so it is essential to examine the topographic shielding of all aspects to assess the role and impact. This research adopts the semantics shown in Figure 31a to calculate the inspection angle in 8 different directions (i.e., north, northeast, northwest, south, southeast, southwest, west, and east) using a search radius from 225 meters (3 pixels) to 2025 meters (27 pixels). Figure 31b shows the intermediate results of all inspection angles in the eight directions, respectively. Zero minus the integrated inflection angles from 8 directions produces the final TOPEX for the study area.

Results

Object-oriented characterization of glacier surface

Object-oriented analysis provides an innovative way to investigate glaciers from meaningful scale. Unlike traditional pixel-based approach, object-oriented analysis treated pixels sharing similar attribute as one feature, i.e., object. Thus, it is suitable to use this approach to examine the change in glacier-surface structure.

The SRTM Segmentation works perfectly in separating the glacier terminus from proglacial lakes in GA and GPM (Figure 32). The convergent-divergence index and segmentation results set the tone of this research. Thus, it is very important to evaluate the accuracy of segmentation results. In glacial environments, the glacier terminus normally exhibits the sharpest transition from ice-snow mass to either a proglacial lake or the terminal moraine (Glasser et al., 2005); and this is especially the case for the

Southern Patagonia Icefield, because large amounts of the glaciers are calving into the ocean or continental lakes. In my study I found GA and GPM are calving into Argentino Lake, and the termini (Location 2 and 3 in Figure 32) can be clearly detected by segmentation images (Figure 34a, 34b) when comparing to the same locations of Landsat image retrieved in 2000 (Figure 32c).

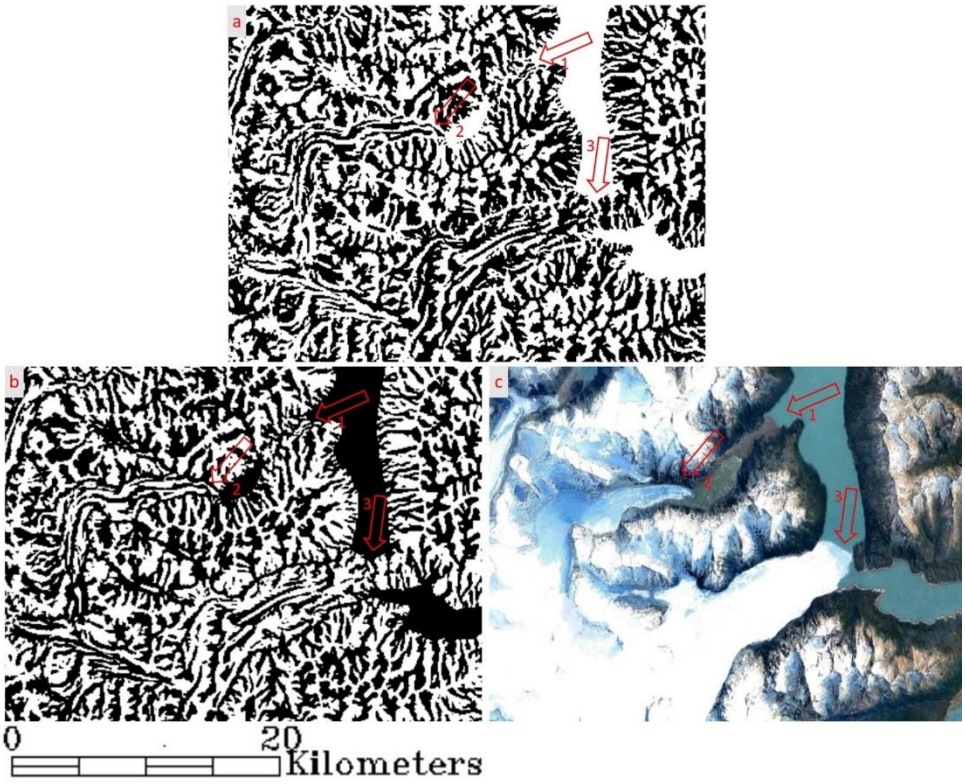

Figure 32. The SRTM convergence segmentation image (a); the SRTM divergence segmentation image (b); and the Landsat image retrieved in 2000 (c). Red arrow of Location 1 is the prehistorical glacial deposit. Red arrows of Location 2 and 3 are termini for GA and GPM respectively.

The segmentation image facilitates the study of glacier dynamics in South Patagonia. Figure 39a is the convergent segmentation image whereas Figure 39b is the

divergent segmentation image, which is simply a binary-offset image to Figure 39a. The convergent segmentation (Figure 32a) highlights the features exhibiting convergent characteristics (e.g., crevasse and supra-glacial streams), which are the result of down-wasting and glacier mass movement. On the contrary, the divergent segmentation (Figure 32b) highlights the features with divergent characteristics (e.g., lateral moraines), which can be used as an indicator for dominant glacier flow directions and surface structure complexity. In Figure 32, the termini of GA and GPM show divergent characteristics, and the flow direction can also be detected in the images.

Additionally, location 1 in Figure 32 is a prehistorical glacial deposit that now functions as a glacier dam between the current GA and Argentino Lake. By examining the segmentation images, the structure of this glacial dam is well characterized, and the adjacent mountain terrain in the study area exhibit a totally different pattern from the glacial surface, which further suggests the accuracy of the segmentation protocol is of an acceptable level to be very useful for geomorphological mapping and glacial studies.

Graph theory for the change in surface structure

As discussed in the previous paragraph, in a supra-glacier system, the convergent objects and the divergent objects interact with each other to transport flux and energy, and the current morphologies and structures are the result of such a mechanism. In addition, these objects operate together in response to glacial processes to form a complete complex supra-glacial system (Heckmann et al., 2015). The innovative adoption of graph theory into glacial research creates a new path to evaluate the dynamics of the glacier-surface and quantify the complexity of the glacier-surface

structure. The link maps (Figure 33), which are the results from the accurate input of object parameters that are generated from the segmentation protocol, illustrate the number of links that are around each pixel in the study area utilizing a two-cascade network model (Figure 29). The relationship links, quantitatively shows the complexity of the relationship within the network and this parameter can be visualized in Figure 33 as a measure of how complicated the surface structure is. In Figure 33, the SRTM-link image and the ASTER-link image have considerable agreement with each other in non-glacial areas; however, on glacier surfaces, the difference is evident. Additional details from the centerline extraction analysis for GA and GPM are shown in Figure 34. The detailed information is summarized in Table 12.

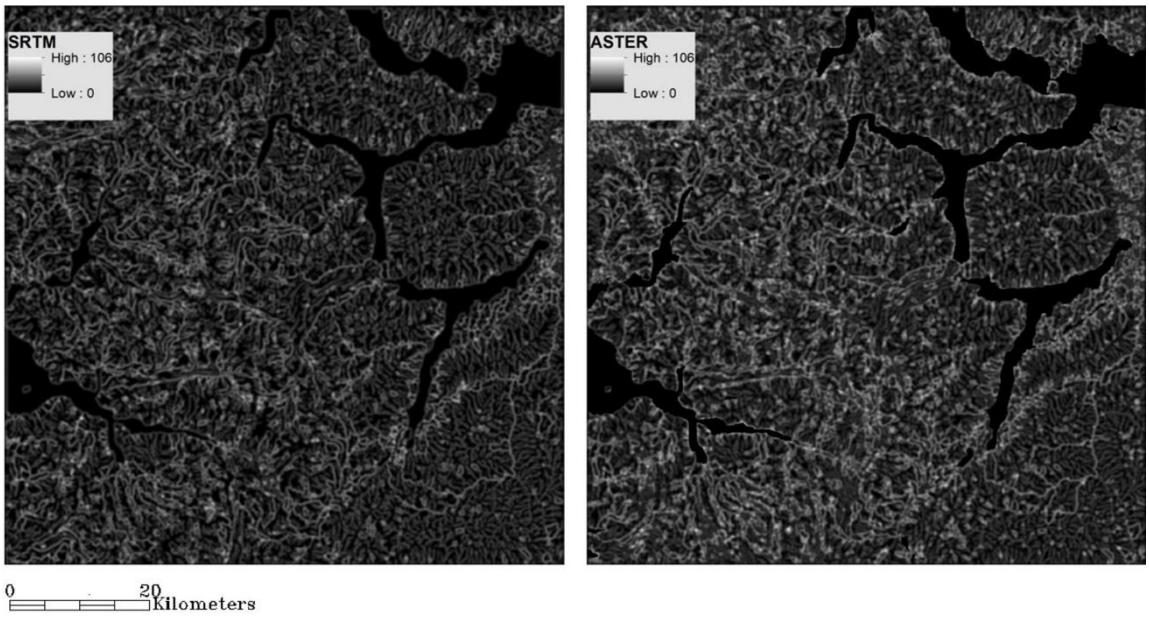

Figure 33. Network analysis results for SRTM and ASTER imageries. Both images show considerable agreement for nonglacial areas such as non-snow-covered mountains and low-elevation islands.

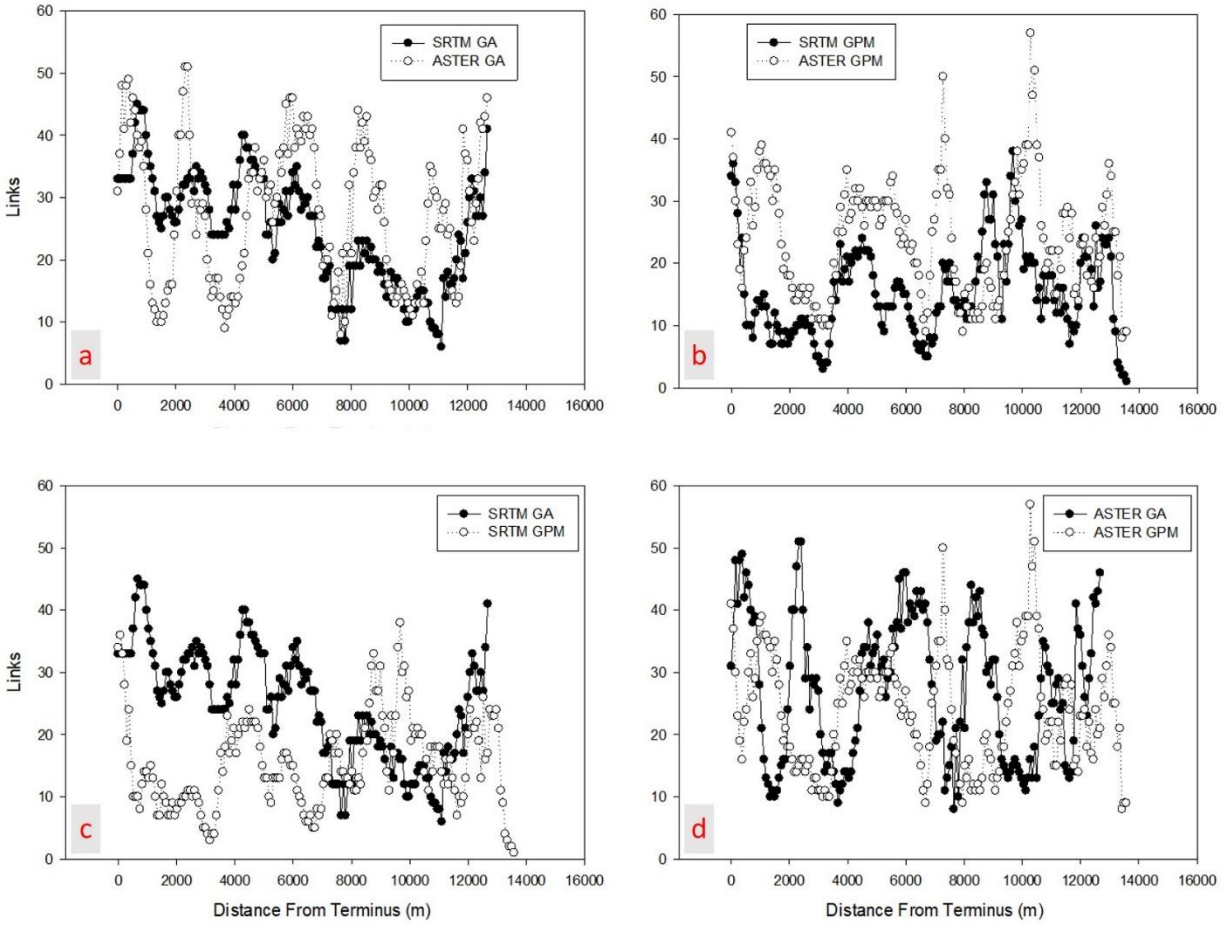

Figure 34. Cross-comparisons of center-line profiles extracted from network analysis over GA and GPM using SRTM and ASTER DEMs.

Topographic Exposure

Topographic features surrounding glaciers exert a profound influence on glacier activities via exposure that is shielding or lack of shielding. In my research I accurately calculated topographic exposure based on a distance-limited topographic exposure

model that was illustrated in Figure 31, and the results are shown in Figure 35. My topographic exposure index image (Figure 35a) addresses the nature of topographic control in the Southern Patagonian Icefields, and it provides a new approach to quantitatively evaluate the topographic constraints imposed by surrounding terrain.

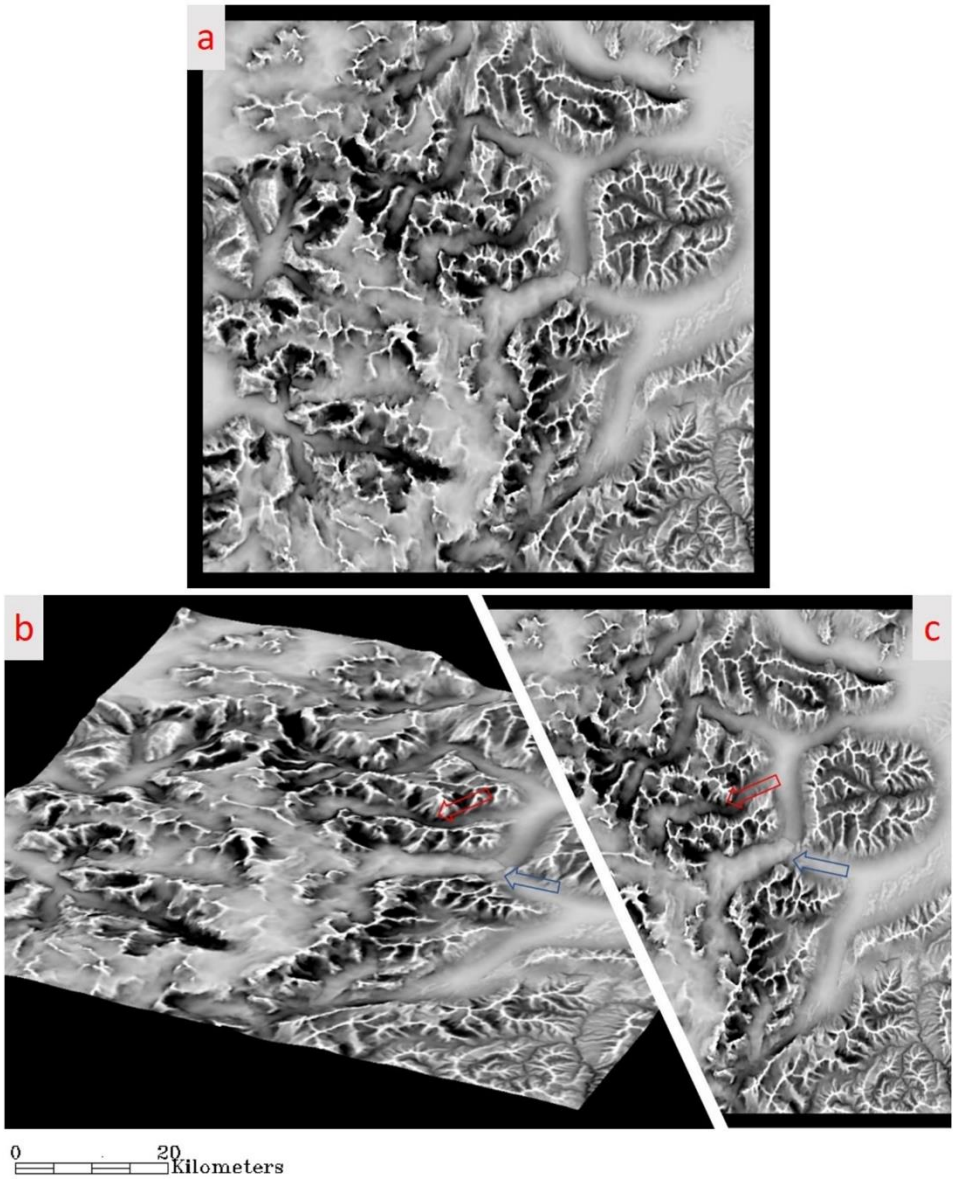

Figure 35. The topographic exposure results. Figure 35a shows the TOPEX for the complete study area. Figure 35b is the 3D visualization of Figure 35a. Figure 35c helps to evaluate the potential of using TOPEX to map geomorphological features, such as glacier terminus, cirque, and mountain ridges.

In my results, all glacier valleys exhibit a relatively dark shade because (a) in a typical glacier system snow-ice mass is constrained by solid valley walls from neighboring terrains and (b) continuous glacial erosion further deepens the bedrock and enhances the shielding effects in the glacier valleys. Contrary to the glacier valleys, Figure 35a shows all mountain ridges are highlighted by the brightest shades because they are the most exposed geomorphic features in the study area. In addition, because this study adapts a search distance between 3 pixels to 27 pixels in eight compass directions, the ability to locate major topographic features is significantly enhanced. Figure 35b is the 3D visualization of the topographic exposure index overlaid with the SRTM elevation. Figure 35c is the planimetric view of GA and GPM, which helps to see the mapping potential of using the topographic-exposure index. In Figure 35b and 35c, GA (red arrow) and GPM (blue arrow) termini exhibit a distinguished shade change and the lateral boundaries are also well delineated. Some other glacial features, including cirques, horns, aretes, and truncated spurs, can also be clearly discriminated in the GA and GPM valley-glacier area.

Figure 36 show additional analysis of topographic exposure in GA and GPM. Figure 36a is the extraction image of TOPEX only on glacier surfaces. Figure 36b is the center-line analysis for TOPEX in GA and GPM. Figure 36a provides a closer look of how topographic exposure differs on glacier surfaces. I suggest that overall GA exhibits a much lower exposure than GPM; and this is especially distinct in the GA terminus area, upper ablation zone, lateral boundary areas adjacent to glacier valley, and even in

some accumulation areas. Figure 36b further supports this observation by demonstrating (a) GPM has a higher exposure than GA from the terminus to the ELA, (b) GPM exposure curve remains stable, (c) GA exposure curve shows an increasing trend from the terminus to the upper ablation zone. A sharp decreasing trend also occurs when GA approaches the ELA, (d) the close-to-zero stale curve from GPM suggests the surface of GPM is relatively flat, and (e) GA has a well shielded terminus area and accumulation zone.

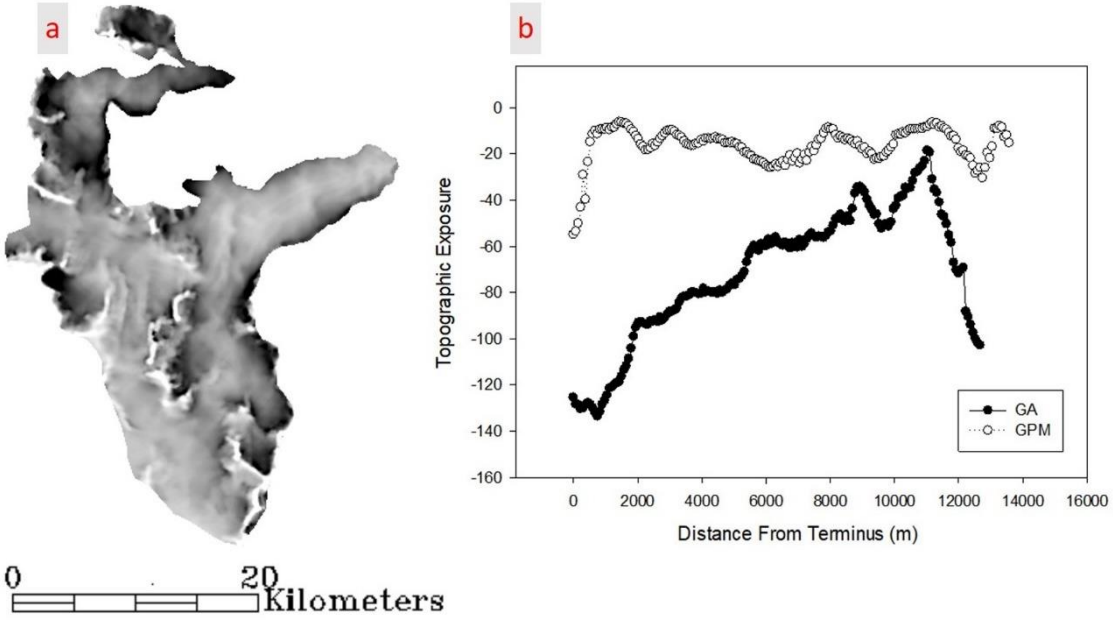

Figure 36. TOPEX analysis for GA and GPM. Figure 36a is the glacier surface extraction for TOPEX. Figure 36b shows the center-line analysis for TOPEX.

Table 12. Detailed information shown in Figure 36.

Subject	Topic	Findings
GA (Figure 36a)	**SRTM**	**Terminus Area (0-1000m)** SRTM GA increases from 30 to nearly 50 but then start dropping to below 30. **Tongue (0-6000m)** SRTM GA shows a relative stable structure in glacier tongue (0-6000m) with an average of 30 links. **Upper Ablation Zone (6000-12000m)** SRTM GA suddenly drops to below 10 with a small fluctuation between 8000m to 12000m. **Close to ELA (12000m-13000m)** SRTM GA starts climbing from 5 links around 12000m to above 40 links when approaching ELA (13000m). **Overall Trend** Overall SRTM GA shows a stable glacier tongue but gradual decreasing trend till it's getting close to ELA.
	ASTER	**Terminus Area (0-1000m)** ASTER GA increases from 30 to 50 but then start dropping to 10. **Tongue (0-6000m)** ASTER GA shows a very unstable structure in glacier tongue (0-6000m). It swings 5 times between 50 and 10 with an average of 30 links. **Upper Ablation Zone (6000-12000m)** ASTER GA continues the highly swinging pattern 4 times between 6000-1000m and then starts to climb up with a much smaller fluctuation range. **Close to ELA (12000m-13000m)** ASTER GA reaches 50 links again when approaching ELA. **Overall Trend** Overall ASTER GA shows a very unstable glacier tongue and upper ablation zone. It swings 10 times from terminus to ELA.
GPM (Figure 36b)	**SRTM**	**Terminus Area (0-1000m)** SRTM GPM's terminus drops sharply from nearly 40 to 10 with first 400 meters and then comes back to 15 at around 1000m. **Tongue (0-7000m)** From 1000m, SRTM GPM shows a decreasing pattern, and it drops to 3 at about 3600m. Then SRTM GPM starts coming back to 20 but again drops under 10 at 7000m. **Upper Ablation Zone (7000-12000m)** From 7000m, SRTM GPM starts increasing from under 10 to 40 at 10000m. It drops gradually under 10 again at 12000m **Close to ELA (12000m-14000m)** SRTM GPM starts climbing above 20 at 13500m but suddenly drops under 10 when approaching ELA. **Overall Trend** Overall SRTM GPM shows a very unstable terminus area structure, but the remaining glacier tongue and upper ablation keep stable with moderate fluctuation. It is noted link number drops when approaching ELA for SRTM GPM.
	ASTER	**Terminus Area (0-1000m)** ASTER GPM's terminus also drops sharply from nearly 40 to 15 with first 400 meters but restores to 40 at around 1000m. **Tongue (0-7000m)** From 1000m, ASTER GPM drops sharply from 40 to 10 at 3600m. It's combing back above 30 but also drops under 10 again at 7000m. **Upper Ablation Zone (7000-12000m)** From 7000m, ASTER GPM shows a high-amplitude vibration between 10 and above 50. It swings 5 times from 7000m to 12000m. **Close to ELA (12000m-14000m)** ASTER GPM has over lapping pattern with SRTM GPM. It starts climbing above 30 at 13500m but also suddenly drops under 10 when approaching ELA. **Overall Trend** Overall ASTER GPM shows an extreme unstable terminus area and glacier tongue area. The upper vibrates with high amplitude. The pattern close ELA agrees with SRTM GPM.

Table 13 Continued.

Subject	Topic	Findings
SRTM (Figure 36c)	**GA VS. GPM**	**Terminus Area** Both SRTM GA and SRTM GPM starts at around 35 in terminus position. GA increased from 35 to nearly 50 but GPM drops sharply in terminus area. **Tongue** SRTM GA shows a gradual decreasing pattern in glacier tongue, but SRTM GPM shows a relative stable pattern of fluctuation pattern in glacier tongue. SRTM GA is always above SRTM GPM in tongue area. **Upper Ablation Zone** SRTM GA keeps decreasing in upper ablation zone, but SRTM GPM starts increasing in the first half of upper ablation zone but decrease in the second half. **Close to ELA** SRTM GA keeps increasing to above 40 when approaching ELA. SRTM GPM increases to above 20 but then drops dramatically under 10 at ELA **Overall Trend** SRTM GA has much higher value in both glacier terminus region and glacier tongue. It shows a gradual decreasing pattern till 10000m approximately. The link number increases when approaching ELA. SRTM GPM has very unstable terminus but relatively glacier tongue. Its upper ablation zone has higher values than SRTM GA, but it drops to nearly 1 in ELA.
ASTER (Figure 36d)	**GA VS. GPM**	**Terminus Area** ASTER GA starts at 30 and increases to 50 within first 400m. ASTER GPM starts at 40 but decrease to 15 with first 400m. **Tongue** Both ASTER GA and ASTER GPM show fluctuation patterns in glacier tongues. ASTER GA exhibits higher amplitude in this area. **Upper Ablation Zone** Both ASTER GA and ASTER GPM still show fluctuation patterns in upper ablation zones. ASTER GPM exhibits slightly higher amplitude. From 10000m, ASTER GA starts climbing. **Close to ELA** ASTER GA keeps increasing when approaching ELA, but ASTER GPM dramatically decreases towards ELA. **Overall Trend** Overall, both ASTER GA and ASTER GPM exhibit very contrasting link patterns in every part of its own glacier body. It is worth to note 10000m is a watershed for GA.

Discussion:

The existing approaches to mapping glaciers do not accurately map glacier boundaries in the Patagonia Icefields. In this section I first evaluated the current mapping protocols and assessed if my study can facilitate glacier mapping. This section also addressed the adaptability of integrating graph theory into glacier studies to understand glacier dynamics. The underlying reasons of the contrasting patterns of the GA and the GPM was also discussed in this section.

Glacier mapping

Existing glacier study frontiers and limitations

In general, two major ways for evaluating sensitivity of a glacier to the impact of surface change: analysis of terminus fluctuation and measurement of mass balance. To note, each method has its individual merits over temporal and spatial scales; however, each method also entails disadvantages related with sampling accuracy and uncertainty (Malz et al., 2018; Casassa et al., 2014).

The advent and wide adoption of remote sensing (rs) technology and its application with Geographic Information Science (GIS) have favored studying glacier system dynamics (Raup et al., 2007). New avenues of research, such as ground/aerial/satellite photography of surface characterization, digital terrain modeling, geomorphometry, geomorphological mapping, geo-computation, and geo-visualization (Giardino and Harbor, 2013), that used remote sensing and GIS began to augment traditional glacier studies around 1970s (Ye et al., 2006). Furthermore, these studies

allowed researchers to better conceptualize and to study the complexity of the glacier system (Figure 20).

Before the International Geophysical Year (IGY) in 1957/1958, remote sensing was only used for the purpose of mapping the extent of glaciers. The advent of new remote sensing sensors and technologies after the IGY, however, enabled researchers to quantify many glacial parameters that were previously unattainable from in-situ measurement (Jensen, 2007). Some of these parameters include surface reflectance and albedo, surface temperature, gravity field and moisture content, glacier zones and mass balance, glacier area and topography, lithology, glacier volume, and surface velocity (Rees, 2005; Pellikka and Rees, 2010).

The change in glacier terminus can be classified as retreat, advance, or stagnation; and it can serve as a good proxy for the change in the mass-balance of the glacier and can help to determine types of glaciers (Wilson et al., 2016). Sparse *in situ* data exists for documenting variations in glacier terminuses in SPI. Therefore, remote sensing and GIS can provide an alternative methodology for monitoring and analyzing glacier fluctuations as well as further assessing glacier sensitivity to climate change (Racoviteanu et al., 2008; Racoviteanu et al., 2009; Hock and Huss, 2021). The existing glacier inventory (e.g., WGI, RGI) is inadequate to meet scientific needs today, because the boundaries of glaciers are not accurate and need to be updated with more precision and accuracy. GLIMS is a big improvement for the global glacier inventory (Raup et al., 2007), especially for glaciers in SPI. The semi-automated terminus-mapping algorithm in GLIMS needs more rigorous scrutiny of terminus detection aided by digital image

processing techniques and the incorporation of the direction of surface-flow into a transect approach for calculating changes in terminuses over time (Kargel et al., 2014). Room still exists to improve the research conducted using GLIMS, including automating the whole process of glacier terminus detection, enhancing the accuracy of mapping debris-covered glaciers, addressing, and correcting the errors associated with image processing, and designing a robust workflow for calculating terminus distance.

To date, the major glacier inventories in SPI are based on manual digitization from satellite images; however, these methods are extremely time-consuming for large areas and errors can be easily introduced by varying spatial resolutions and human error introduced by the cartographer (Paul et al., 2013; Minowa et al., 2015). Other existing mapping methods in optical remote sensing can be grouped in four categories: (1) pixel-based mapping to extract differences in the domain of spectral feature space, including supervised classification and artificial neural networks (ANNs; Keshri et al., 2009; Shukla et al., 2009; Bjambri and Bolch, 2009; Bhambri et al., 2011); (2) morphological variables derived from DEM, such as profile-plan-tangential curvatures, local relief, slope, and aspect (Bolch and Kamp, 2006). (3) multi-criteria approach to incorporate surface classification, spatial analysis, morphometric parameters, and thermal contrasting (Paul et al., 2004; Shukla et al., 2010); (4) objected-oriented mapping approach based on spectral information (Benz et al., 2004; Rastner et al., 2014). Unfortunately, these methods are all region specific and have not been thoroughly tested for SPI glaciers. Thus, it is timely and important to develop a new glacier mapping algorithm that is suitable for SPI glaciers.

Increasing debris load in several PI glaciers has been observed in recent decades (Glasser et al., 2016； Aniya et al., 1993; Harrison and Winchester, 1997; Janke et al., 2015; Bravo et al., 2021). The existence of debris in PI glaciers make it notoriously difficult to map the terminus and to characterize glacial-surface structure (Bolch et al., 2007; Pratap et al., 2015). This debris is transported to the glacier tongues by mass movement such as snow avalanches or ice/rock-falls from extremely steep adjacent terrain and the incorporation of bedrock movement from glacier bed into the glacier, and eventually at the surface (Fischer et al., 2006; Fischer et al., 2010). Thick debris acts as an insolation blanket and can retard glacier response to long-term changes in weather patterns (Pelto, 2000; Benn and Evans, 2014) and facilitate supraglacial lake formation (Benn et al., 2000; Benn et al., 2001; Sakai and Fujita, 2010). The thick debris, however, often hampers detection of the glacier boundary either in the field or by remote sensing because of the similar spectral signature of the debris to the surrounding terrain (Bhambri and Bolch, 2009; Bhambri et al., 2011). Traditional mapping methods on clean-ice glaciers adopt the spectral features of snow and ice in the visible and near-infrared (VNIR) spectrum compared to short-wave infrared (SWIR), including Normalized Difference Snow Index (NDSI) and band ratioing (Kaab et al., 2002; Paul et al., 2002; Andreassen et al., 2008; Racoviteanu et al., 2008; Racoviteanu et al., 2009). Neither are suitable for mapping debris-covered glaciers (Quincey et al., 2005; Raup et al., 2007).

Can this study facilitate glacier mapping?

My study proposes a stepwise approach to evaluate change in the structure of the glacier-surface, including convergence-index image (Figure 27), segmentation image (Figure 28), and link image (Figure 33); and each of which is very distinct from existing glacier mapping protocols as mentioned previously, because any of these parameters individually can facilitate glacier mapping at certain perspective. To elaborate, the convergence-divergence index can highlight the glacier terminus because of the calving nature of the dominant glaciers in SPI (Hata and Sugiyama, 2021.). Segmentation image can aggregate the pixels with similar topographic attribute (i.e., degree of convergence) into one object; thus, glacier mapping focuses on concrete geomorphologic features instead of individual pixels. Link images, based on graph theory, further quantify the structure complexity of the glacier surface and termini and lateral boundaries are well delineated.

A photo taken by J. R. Giardino at Location 3 of Figure 32 can be used to validate the mapping protocol (Figure 37). In this photo, the calving front of the GMP shows a clear divergent characteristic, and this divergent nature is well reflected in Figures 27, 28 and 33. Note the sufficient gap between the GMP glacier terminus and the viewing station in this photo. This gap can be clearly detected in Figure 32b but not identifiable by Landsat image (Figure 32c), which further suggests the stepwise mapping protocol is more robust than traditional spectral information-based glacier mapping.

Figure 37. Photo of GPM terminus. The calving front of the glacier is well captured (Photo by J. R. Giardino, 2017).

I admit a challenge exists when undertaking this research with respect to DEM noise from ASTER. Resampling a 25-meter ASTER DEM into the same size (75 meter) as a SRTM DEM, produces instrumental noise from ASTER DEM that is inherently downscaled to the new ASTER DEM. This noise is especially pronounced on water bodies because of the close to zero value, which results in a very sensitive response to any small noise and elevation change. This noise creates very tiny regional puddles in the fjords and Argentino Lake, which significantly hampers generating meaningful intermediate results that can be evaluated using graph theory. Thus, a cost-effective

noise removal method had to be developed. Figure 38a shows that before noise removal, dramatic elevation noise occurs in the ASTER DEM that hampers segmentation results.

To minimize the ASTER DEM noise, I developed a cost-effective mask approach. First, I used a SRTM DEM as a reference because SRTM is well known for its high quality and noise-free reputation. Based on the SRTM DEM, I generated a waterbody mask, which covers the fjords and Argentino Lake. Second, I used this mask to extract the ASTER DEM to obtain all the waterbody elevation pixels. I statistically assessed the elevations within the mask and choose the most frequently occurring value to represent the new elevation for the entire waterbody. Third, I used the new value as a substitute value for the ASTER DEM waterbody pixels. The new segmentation result is shown Figure 38b.

Five reasons support why this approach is well suitable for this study: (1) the research is investigating how the structure of the glacier-surface changes over time by use of object-oriented analysis and graph theory. Thus, this approach does not influence glacier-surface elevation. (2) Because of the calving nature of GA and GPM, this approach reduces pro-glacial waterbody noise and produces “cleaner” glacier termini. (3) The GPM glacier has been stagnant for decades, so substituting waterbody elevation around the glacier terminus will not influence terminus-structure change. (4) Even though the GA glacier has been retreating, the mask will still enhance data quality because considerable noise exists between the GA terminus and the prehistorical glacier dam (Figure 32). (5) If the waterbody noise is not removed, the surface structure from

both termini will be much more complex based on the two-cascade network analysis model (Figure 29).

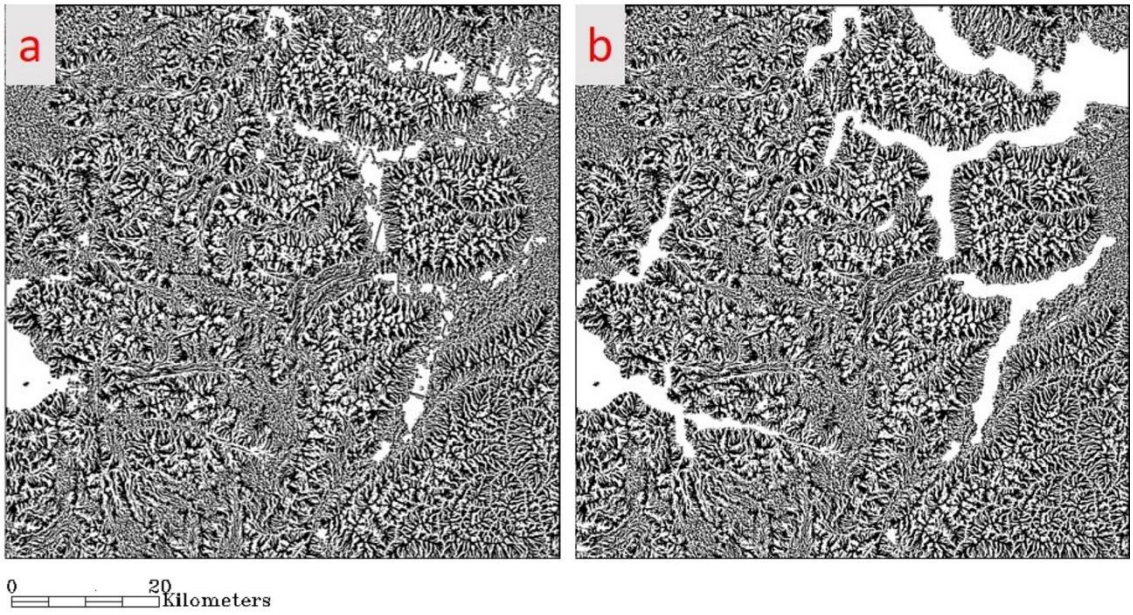

Figure 38. Segmentation results from the ASTER DEM before and after noise removal. Figure 40a is before noise removal, and Figure 40b is after noise removal.

Change in the structure of the glacier surface

Limitations of using mass balance and velocity field

In the Patagonian Icefields, glacier mass balance can be remotely retrieved using four approaches: (1) extrapolation of limited field mass balance records (Rivera et al., 2007; Bamber and Rivera, 2007; Quincey et al., 2014); (2) gravity field based on remote sensing images (Chen et al., 2007; Jacob et al., 2012; Wouters et al., 2014); (3) laser altimetry (Kaab, 2008; Moholdt and Kaab, 2012; Winsvold et al., 2018); and (4)

differencing between digital elevation models (Willis et al., 2012; Dussaillant et al., 2018). *In situ* methods that are the foundation of numerous approaches, such as, repeated annual measurements of snow density by using snow stakes on the glacier surface are very labor-intensive, and the results of sampled glaciers used for extrapolating a whole region are generally unevenly distributed, which can easily introduce errors (Hubbard and Glasser, 2005). Gravity retrieved from the GRACE (Gravity Recovery and Climate Experiment) satellite can be used to estimate glacier mass balance, but its low resolution of 300 m and its high sensitivity mass-balance signal is biased towards supraglacial/englacial water content and significantly limit its accuracy in ice extent areas located in rugged terrain, such as the SPI glaciers (Gardner et al., 2013). The laser altimetry method—using sensors such as ICESAT (Ice, Cloud and Land Elevation Satellite)—can be used to calculate the change in glacier-volume, but the accuracy of ICESAT is highly dependent on three factors: trends within the acquisition footprints, types of land-cover (including snow, ice, water, debris, and glacier boundary), and surface density. Thus, major uncertainty exists (Zwally et al., 2003; Jaber et al., 2012; Neckel et al., 2014). The DEM differencing approach requires a prior correction of artifacts, which can be the result of a combination of sensor error, altitude error produces by curvature, penetration error if using c-band of SRTM, and systematic errors introduced by stereographic techniques (Mölg et al., 2017; Dall et al., 2001; Kervyn et al., 2008; Paul, 2008; Bolch et al., 2011; Nuth and Kaab, 2011; Gardelle et al., 2012).

To aggravate matters, even adopting the same method of calculating glacier-mass balance for the SPI, may yield different results by different research groups (Malz et al.,

2018; Dussaillant et al., 2018). One could assume that these estimates are as much art-based as they are science-based, and significant inconsistencies will remain. The existing knowledge gaps associated with mass-balance calculation can be somehow mediated by increasing the accuracy of the stratification and glacier-boundary delineation of the glacier surface, especially at the terminus (Paul et al., 2017).

In addition to mas balance and its byproducts, the glacier-velocity field has also been used for understanding glacier dynamics even though it is extremely computational time-consuming from a regional scale perspective for mountain glaciers (Burgess et al., 2013). Quality estimates of glacier-surface velocity can aid in the understanding of processes related to glacier dynamics, including supra-glacial mass transport, ice-flow instability, identification of surging type glaciers, supra-glacier lake development, ice-flow direction, and glacier boundary (Paul et al., 2015). For the Patagonian Icefield, on most remote sensing platforms the dominant cloud cover across the year impedes the satellite acquisition for useful spectral signature of the Earth surface; the maritime environments and westerlies components of the upper circulation compound the difficulty of retrieving clear imagery. Even though synthetic aperture radar (SAR) has exceptional penetration of cloud and can serve as an alternative to optical remote sensing, it is oversensitive to moisture, which makes it more suitable for icesheets than for valley glaciers. Besides, most velocity fields are generated by two approaches: normalized cross-correlation in the spatial domain, and orientation correlation in the frequency domain (Heid and Kaab, 2012). The first approach is extremely labor intensive, and the second approach requires a computation region of high visual contrast

(Leprince et al., 2007; Lewis, 1995; Paul, 2015). Thus, both approaches are not ideal for the study of the SPI.

Can this study help to understand glacier dynamics?

The integration of object-oriented analysis with graph theory enables a new, innovative approach as an alternative to evaluating the dynamics of glacier-surfaces when compared to traditional methods. To better visualize the structure change over time and to verify the legitimacy of using this stepwise protocol as a substitute to mass balance and velocity field in the Southern Patagonian Icefield, I used the boundaries of GA and GPM to extract three major parameters, including convergence-index images, segmentation images, and link-number images (Figure 39). Figure 39 illustrates how this protocol is developed.

In this study, the spatial pattern of chronical-surface structures demonstrates the influence of flow dynamics and glacier down-wasting that cannot be easily captured by optical remote sensing. As the glacier moves, either by bedrock sliding or internal deformation, other processes occur simultaneously on the glacier surface: (1) transportation; (2) deposition; (3) energy transfer; (4) weathering; (5) hydraulic process; and (6) topographic controlling. These processes work together to form distinctive glacial landforms. This new protocol is especially suitable for evaluating glacier dynamics from a process perspective because the degree of convergence reveals the uneven topographic nature of the glacier surface, which is the outcome of the above six processes.

Figure 39a and Figure 39b illustrate how the spatial unevenness is distributed over the surfaces. ASTER convergence retains some of the convergence from SRTM but still does exhibit more convergence features in the ablation zone and the upper accumulation zone of GA and GPM. After the convergence is aggregated into accurate geomorphic features, it is easier to detect the change in surface structure as shown by comparing Figure 39c and Figure 39d. Some agreement between SRTM and ASTER segmentation images exists. It is interesting that the ASTER segmentation image shows more details in approaching terminus. The link-image based on graph theory can further quantify the structure change occurring on glacier surface (Figure 39e and Figure 39f). The link image change from SRTM to ASTER for both glaciers has been explicitly examined. They are shown in Table 12.

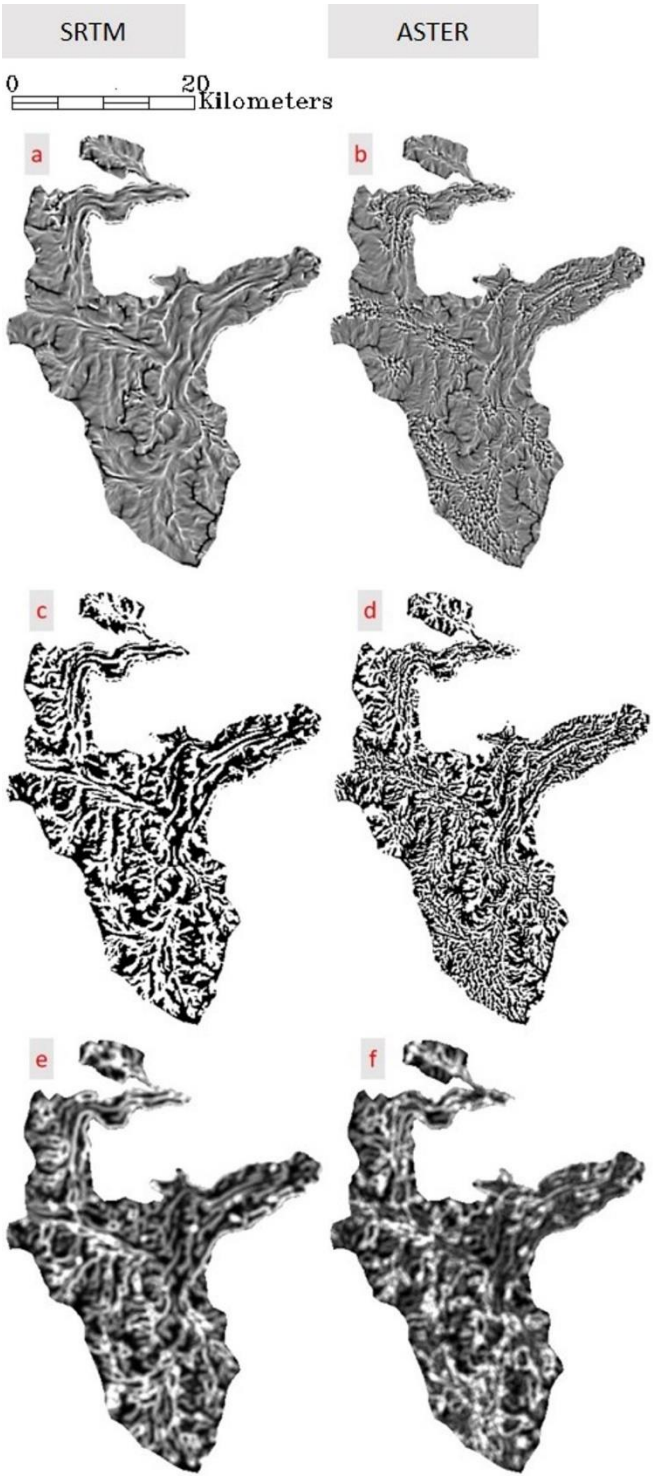

Figure 39. Convergence images (a and b), segmentation images (c and d) and link images (e and f).

To further evaluate the change of the structure of the glacier-surface, I conducted a post analysis to calculate the difference between the SRTM-link image and the ASTER-link image (Figure 40a). This difference image (Figure 40a) is the first existing image that can quantitatively evaluate how the structure of the glacier-surface changes over time. A centerline analysis from this difference image (Figure 40b) also suggests this change is across the whole glacier-ablation zone. Based on Figure 40, additional interpretations regarding glacier dynamics are summarized in Table 13. The terminus of the retreating glacier GA has considerably less structure complexity, but the terminus of the stagnant glacier GPM has notable increasing surface complexity. The GA appears to have more active upper-ablation zone as well as on ELA, however, the GPM has an inactive upper-ablation zone and ELA. These findings further demonstrate that the contrasting patterns show in the rates of terminus fluctuation (Minowa et al., 2015) and extend to the change in the glacier -surface structure.

Table 14. Details about how GA and GPM surface structure changes over time.

	GA	GPM
Terminus Region	Extreme decreasing structure complexity	Extreme Increasing structure complexity
Glacier Tongue	Negative or small changes for most areas	Positive changes for most areas and very stable
Upper Ablation Zone	Significant increasing structure complexity and oscillate	Decreasing and less structure complexity
Close to ELA	Close to zero	Close to zero

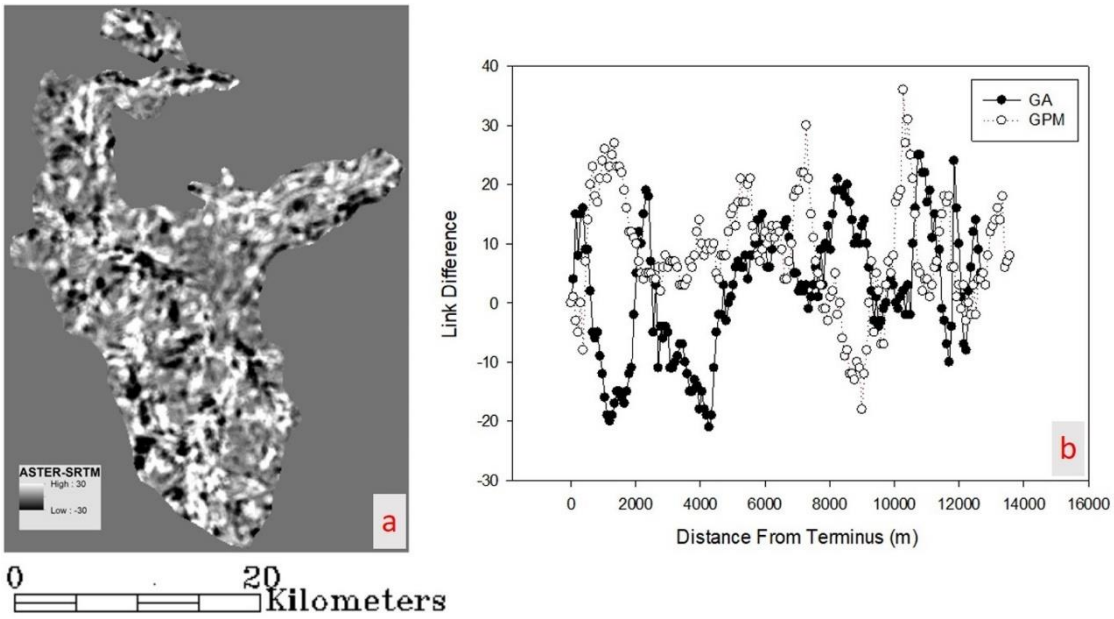

Figure 40. Post analysis of link images. Figure 40a is the difference between ASTER-link and SRTM-link images. Figure 40b is the centerline analysis of Figure 40a.

Do contrasting patterns exist for GA and GPM?

Topographic control

Only TOPEX

In a glacial environment, topographic control plays a vital role in regulating direct solar radiation input, diffuse radiation scattering, snow avalanche origin, wind-fetch path, and supraglacial microclimate. Explaining glacier activities by omitting topographic control can lead to inaccurate conclusions regarding glacier dynamics. Unfortunately, most existing glacier studies do not take topographic factor into consideration. My study uses TOPEX as a proxy for topographic control to evaluate if the TOPEX is the major reason for the contrasting patterns of the GA and the GPM respectively, and the findings (Figure 35 and Figure 36) are important because:

I. It demonstrates the GA has a much lower topographic exposure than the GPM. Because the GA still exhibits a retreating pattern, a lower TOPEX normally means the glacier is more shielded by local terrain. It further demonstrates that TOPEX alone may not explain well the contrasting patterns of these two glaciers, especially for the GA.

II. The TOPEX of the GPM surface remains relatively stable. It demonstrates that the GPM terminus has been stable for decades. Topographic control, at least for the GPM, might help to form a substantially stagnant front because the glacier surface exhibits a balanced distribution of topographic exposure, which suggests the microclimate on the GPM is relatively consistent.

Solar panel effect

TOPEX alone cannot fully address the driving mechanism of contrasting patterns between the GA and the GPM. Nevertheless, the intermediate result for TOPEX, i.e., the maximum inspection angle (Figure 31b) can assist in explaining how much topographic conditions can influence glacier activity. Because the Patagonia Ice Field is in the mid-high latitude of the Southern Hemisphere, the solar geometry allows north-facing slopes to receive much higher solar radiation in an alpine setting. Based on this fundamental knowledge base, I further developed an enhanced semantic model for topographic control (Figure 41). In this model, within the same search distance as shown in Figure 31a, a location with higher inspection angle will receive more direct solar radiation than a location with a lower inspection angle, because like a roof-mounted solar panel, a

power unit of higher inspection angel normally means a broader interface occurs within a unit planimetric area. Thus, it will gain more solar energy than the lower one.

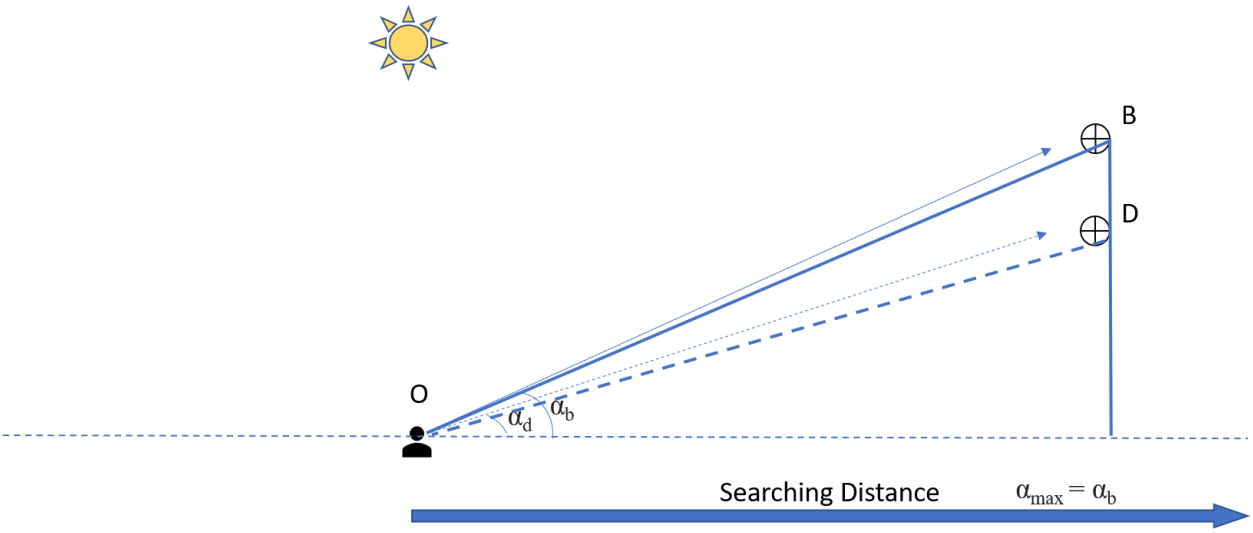

Figure 41. The semantic diagram to show the "Solar Effect" in Patagonian Icefield. In the diagram, B and D are two semantic locations of different height but with the same search distance. α_b and α_b are the inspection angle for B and D.

Figure 42 shows the North-facing inspection angle, and it clearly illustrates that the GA-adjacent North-facing slope (red arrow) has a much higher inspection angle than the GPM-adjacent North-facing slope (green arrow). If these North-facing slopes are viewed as solar panels, they will reserve solar energy in the daytime and release energy to adjacent objects with lower temperatures that is, glaciers. The energy transfer mechanism is beyond the scope of this study, and the solar panel effect is only one possible assumption.

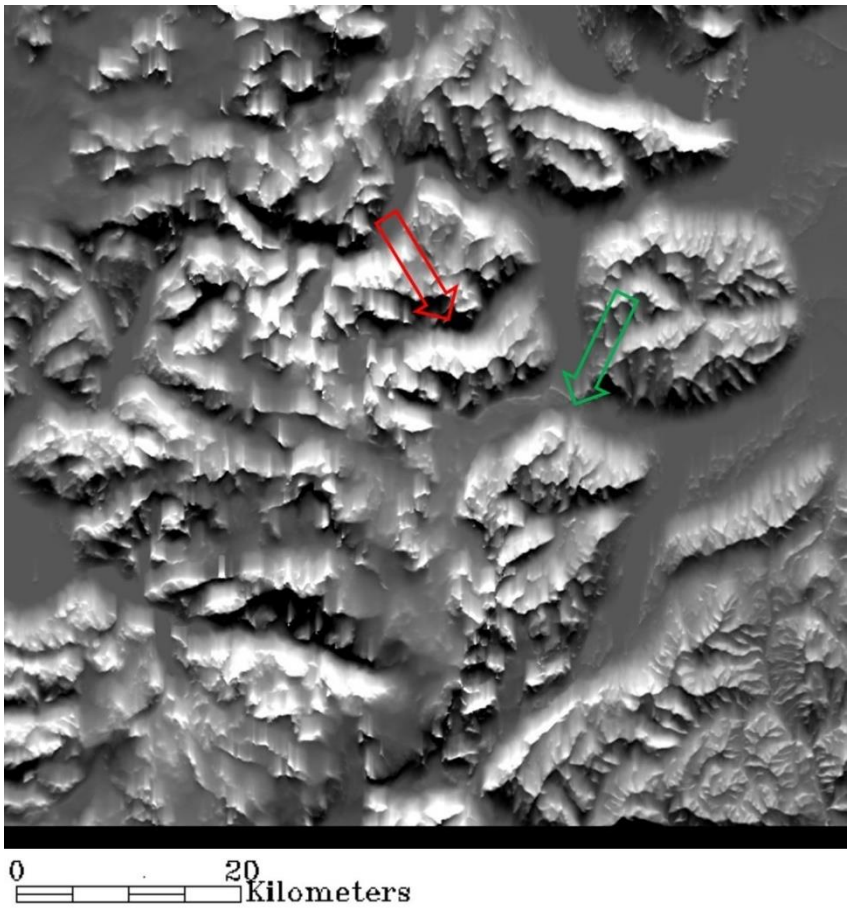

Figure 42. The North-facing inspection angle image. The red arrow is pointing to the GA-adjacent North-facing slope and the green arrow is pointing to the GPM-adjacent North-facing slope. A brighter value means a larger Max Viewing angle in the search radius. Because these are north-facing slopes, which means brighter pixels will result in relatively larger interface to receive solar radiation. By comparing the GPM and the GA glacier valleys, one can see the large difference. The GA has much brighter north-facing slopes when compared with the GPM.

Landslide relic in the GA

The *Solar-Panel Effect* provides a partial explanation of the contrasting patterns between the GA and the GPM, so a more detailed scrutiny of the geomorphological constraints is needed. Examination of multi-temporal satellite images from 1969 to 2011 confirmed that a large rock-mass (Figure 43a) extrudes into the glacier tongue in the GA. This seemingly landslide relic significantly alters the GA glacier-flow dynamics because (1) the GA glacier valley has a narrowing trend; (2) the width of this landslide relic is more than one third of the glacier-valley width; (3) ring-shape ogives radiate around this rock mass (Figure 43b, red arrow) but no such pattern exists in the upper glacier tongue (Figure 43b, blue arrow).

The third example, the magnitude of how the landslide relic influences the dynamics of glacier-flow of the GA is the ring-shape ogives, which are the result of Bernoulli's principle. In fluid dynamics, Bernoulli's principle states that an increase (decrease) in the speed of the fluid occurs simultaneously with a fall (rise) in "static" pressure. The glacier valley narrowed by landslide relict caused an increase of movement for glacier close to the rock mass (Figure 43). This speed increase further resulted in a fall of "static" pressure. The pressure difference perpendicular to the flow direction is the major cause of the ring-shaped ogives. The maximum radius reaches all the way to the medial moraine, which is half the width of the GA surface. In addition, this landslide relic is also on the North-facing slope of the GA, which further contributes to the *Solar Panel Effect* by increasing the energy convection from rock to ice.

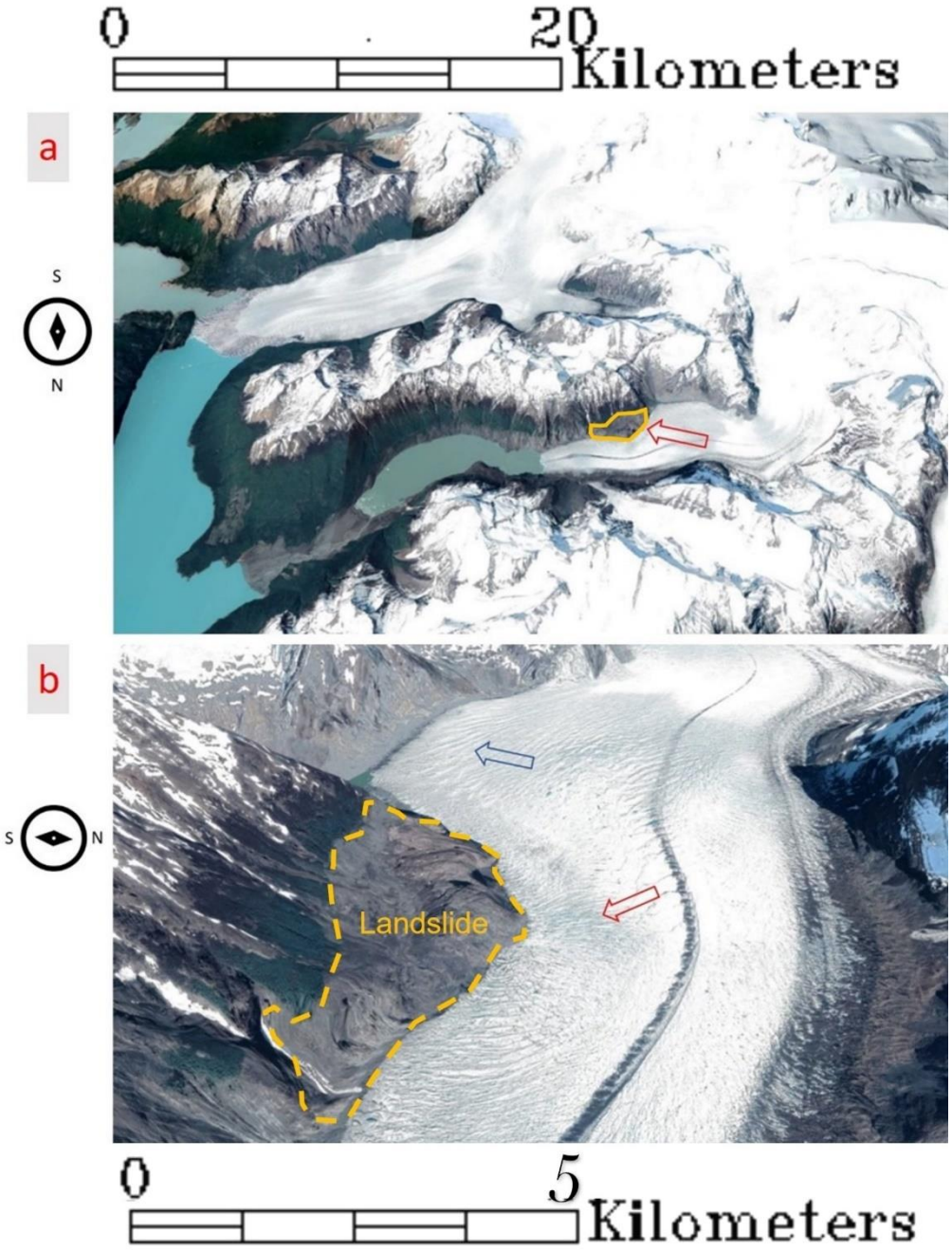

Figure 43. The high-resolution image from CNES Airbus (2020) over the GA and the GPM. A long-existing landslide relic that narrows the GA tongue (Figure 43a). Close examination of the ogives shows a ring-shaped pattern around the landslide relic (Figure

43b, red arrow); no such pattern can be found in the upper region (Figure 43b, blue arrow).

3.5.3.2 AAR ratio, glacier geometry, and others

Based on the preliminary results from Stuefer et al. (2007), Minowa et al. (2015) attribute the contrasting patterns of the GA and the GPM to different accumulation-area ratios (AAR). In their research, the GA has an AAR of 0.45 whereas the GPM has an AAR of 0.73. The researchers concluded that the AAR ratio is the major cause of the contrasting pattern based on the following:

i. the average AAR for SPI the glaciers is 0.71(De Angelis, 2014);
ii. once the AAR is greater than 0.8, calving glaciers are expected to advance regardless of climate forcing and other factors (Post et al., 2011); and
iii. the GPM terminus geometry may contribute to a stable calving front (Minowa et al., 2015).

Therefore, I suggest that these glacier systems are very sophisticated; and that glacier activities and its changes in surface-structure are the result from multiple controlling factors, including climatic forcing, topographic control, tectonic, bedrock conditions, glacier geometry, albedo resistant, relative-mass content (Aniya and Sato, 1995; Naruse et al., 1995; Nick et al., 2009). Thus, for calving glaciers, more factors need to be considered including proglacial-water property (i.e., temperature, salinity, sediment type

etc.), calving-front circulation mechanism, and melting condition of calving ice under water (Bartholomaus et al., 2013; Rignot et al., 2010). Even though AAR can seemingly explain why the GPM terminus is stagnant, it still does not explain why the GPM surface-structure in the glacier tongue shows greater complexity than the GA. My research suggests that even though the GPM has a stable terminus, its surface is extremely active, and this could be because of a continuously down-wasting of the surface and/or fast snow-ice nourishment in the accumulation zone. For the GA, besides the fact that its AAR is extremely low, the orientation of the GA upper ablation zone changed from east-west direction to nearly north-south direction. This sudden change begins approximating the red spot where it is placed in Figure 44 which is around 10 km from the terminus. This orientation shift also significantly influences surface-structure complexity because the link number of the GA has increased ~10km from the terminus (Figure 34 and Table 12). A north-south trending glacier surface receives more solar radiation than an east-west oriented low-reach. This orientation shift can also significantly alter the snow nourishment in the accumulation zone by reducing the influence of winter westerlies.

In conducting this research, I attempted to identify glacier that had similar orientation, similar zone of accumulation zone, similar terminus characteristics (e.., into a lake rather than one on a dry surface and one into a lake), and similar length of travel. The zone of accumulation of GPM is larger than the zone of accumulation of GA. Whereas, difference in the size of zone of accumulation could impact the overall

dynamics of glaciers, I assumed that the size would not have the direct impact on surface change just in the ablation zone.

Figure 44. The GA and the GPM centerlines overlaid on a topographic exposure image. The orientation of the GPM is stable from terminus to the ELA, but orientation of the GA starts to change from the red dot as labeled, which is ~10 km from the terminus position.

Glacier Anomaly and future research

Glacier Anomaly

The IPCC ar4 (Cruz et al., 2007) examined glacier activities in the Southern Patagonia Icefields; however, since then, remote sensing, especially geodetic technology has improved the knowledge about the Patagonian glaciers (Cogley, 2009). IPCC ar5 (Vaughan et al., 2013) acknowledges that glaciers in the Patagonia Icefields show similar glacial anomalies as other coastal glaciers in New Zealand and mountain glaciers in Karakoram and Norway (Solomina et al., 2016). They specially point out that prevalent glacial retreat along with mass loss are occurring in the Patagonia Icefields (Lopez et al., 2010; Davies and Glasser, 2012; Willis et al., 2012; White and Copland, 2013;), however, some glaciers in the Southern Patagonia Icefields exhibit advancing/stagnant characteristics (Muto and Furuya, 2013; Sakakibara and Sugiyama, 2014).

An important question then becomes: is terminus fluctuation the only standard for distinguishing glacier anomaly? As I discovered in this study, even though GPM exhibits a stable terminus, its surface structure has changed dramatically in the terminus area and the glacier tongue. Using the terminus position as the only measure to evaluate glacier dynamics does not adequately reflect what is happening on glacier surfaces. I introduce a new technique to evaluate glacier dynamics by examining the change in surface-structure using object-oriented analysis and graph theory as an alternative to traditional glacier anomaly measures. The characteristics of the new techniques are:

i. it treats the glacier as a system and provides a way to quantify the system properties;

ii. it provides objected-oriented analysis can facilitate configuring the components within the system and map the geomorphological features accurately;
iii. it allows glacier down wasting to be detected; and
iv. it provides a way for change in the glacier surface-structure over time to be effectively represented by graph theory.

Future research

Glaciers can be impacted by climate change. Ten percent of the surface of Earth is covered by glacial ice, and only one percent of glacial ice occurs in mountain ranges (Cuffey and Paterson, 2010). Nevertheless, mountain glaciers have gained a lot of attention recently because these environments are sensitive to global climatic change and can serve as regulators for local climate cascades, such as cooling down the regional weather through increased rates of melting (Benn and Lehmkuhl, 2000; Benn and Evans, 2014). From the North Pole to the South Pole, glaciers have been studied intensively. The Patagonian Icefield still remains, however, a "large blank spot on the map" as the result of minimal research and collaborations. Many fundamental glaciological questions still need specific answers, such as rates of glacier fluctuation, driving factors for Patagonian Glacier Anomalies, glacier-flow dynamics and distribution of supra-glacial debris loads, and mass balance change of the PI as well as its contribution to the rate of

sea level rise. I believe by introducing the new standard in my study, many above mentioned research question can be better addressed in the future.

In addition, glaciers of the NPI and the SPI play a major role influencing water resources and hydroelectric power for South America. But negative impacts also occur. Glacial hazards can also destroy social and economic development of downstream communities. Thus, a better understanding of glacier system by using the new standard in the PI can facilitate urban planning and minimize risk of potential hazards. Bi-national (i.e., Chile and Argentina), and international collaborations are also required for future studies in the Patagonia Icefields.

Conclusions

In this study, I developed a new protocol by using object-oriented analysis and graph theory to evaluate glacier dynamics in the Southern Patagonian Icefield. I first examined the convergence index and its applicability for glacier mapping and feature extraction. Based on the convergence index, I developed an effective approach for segmentation. The segmentation results facilitate the understanding of glacier-surface complexity from a process perspective. The segmentation results are very important input for the two-cascade graph theory analysis in quantifying glacier-surface structure. From a technical point of view, I suggest that:

i. object-oriented analysis and graph theory can be used for mapping glaciers;
ii. network property patterns may be related to down-wasting patterns and ablation;

iii. changes in the temporal patterns of network properties may be related to glacier sensitivity to climate forcing; and

iv. spatial-temporal patterns of glacier topography may be related to glacier dynamics.

In the research I also evaluated how topographic control can influence glacier activities. Even though TOPEX alone cannot sufficiently explain the contrasting patterns between the GA and the GPM, the solar-panel effect, long-existing landslide relic, glacier-orientation shift, along with AAR difference can help to provide a better picture of why such contrasting phenomena occur. Finally, with multiple illustrations, I ascertained that the GPM exhibits more surface changes in the glacier surface than the GA. Thus, using the terminus as the sole indicator of a glacier dynamics is not persuasive. The new technique I introduced to evaluate how changes in the glacier-surface structure over time can be extended into other glaciated areas.

REFERENCES CITED

Aniya, M. and Skvarca, P., 1992. Characteristics and variations of Upsala and Moreno glaciers, southern Patagonia. *Bulletin of Glacier Research*, (10), pp.39-53.

Aniya, M., 1995. Holocene glacial chronology in Patagonia: Tyndall and Upsala glaciers. *Arctic and Alpine Research*, *27*(4), pp.311-322.

Aniya, M. and Sato, H., 1995. Morphology of Ameghino glacier and landforms of Ameghino valley, southern Patagonia. *Bulletin of glacier research*, *13*, pp.69-82.

Aniya, M., Sato, H., Naruse, R., Skvarca, P. and Casassa, G., 1997. Recent glacier variations in the Southern Patagonia icefield, South America. *Arctic and Alpine Research*, *29*(1), pp.1-12.

Aniya, M., 1999. Recent glacier variations of the Hielos Patagónicos, South America, and their contribution to sea-level change. *Arctic, Antarctic, and Alpine Research*, *31*(2), pp.165-173.

Aniya, M., Dhakal, A.S., Park, S. and Naruse, R., 2000. Variations of Patagonian glaciers, South America, using RADARSAT and Landsat images. *Canadian Journal of Remote Sensing*, *26*(6), pp.501-511.

Aniya, M., 2013. Holocene glaciations of Hielo Patagónico (Patagonia Icefield), South America: a brief review. *Geochemical Journal*, *47*(2), pp.97-105.

Bamber, J.L. and Rivera, A., 2007. A review of remote sensing methods for glacier mass balance determination. *Global and Planetary Change*, *59*(1-4), pp.138-148.

Bartholomaus, T.C., Larsen, C.F. and O'Neel, S., 2013. Does calving matter? Evidence for significant submarine melt. *Earth and Planetary Science Letters*, *380*, pp.21-30.

Benn, D.I., Warren, C.R. and Mottram, R.H., 2007. Calving processes and the dynamics of calving glaciers. *Earth-Science Reviews*, *82*(3-4), pp.143-179.

Berthier, E., Dussaillant, I., Brun, F. and Favier, V., 2020, May. Multi-temporal mass balance changes of the Northern Patagonian Icefield from 1975 to 2016. In *EGU General Assembly Conference Abstracts* (p. 18706).

Black, M., 2016. *The atlas of water: mapping the World's most critical resource*. Univ of California Press.

Bolch, T., Pieczonka, T. and Benn, D.I., 2011. Multi-decadal mass loss of glaciers in the Everest area (Nepal Himalaya) derived from stereo imagery. *The Cryosphere*, *5*(2), pp.349-358.

Bradley, R.S., Vuille, M., Diaz, H.F. and Vergara, W., 2006. Threats to water supplies in the tropical Andes. *Science*, *312*(5781), pp.1755-1756.

Bravo, C., Ross, A.N., Quincey, D.J., Cisternas, S. and Rivera, A., 2021. Surface ablation and its drivers along a west–east transect of the Southern Patagonia Icefield. *Journal of Glaciology*, pp.1-14.
Burgess, E.W., Forster, R.R. and Larsen, C.F., 2013. Flow velocities of Alaskan glaciers. *Nature communications*, *4*(1), pp.1-8.

Carey, M., 2010. *In the shadow of melting glaciers: Climate change and Andean society*. Oxford University Press.

Carrivick, J.L. and Tweed, F.S., 2016. A global assessment of the societal impacts of glacier outburst floods. *Global and Planetary Change*, *144*, pp.1-16.

Carrasco, J.F., Casassa, G. and Rivera, A., 2002. Meteorological and climatological aspects of the Southern Patagonia Icefield. In *The Patagonian Icefields* (pp. 29-41). Springer, Boston, MA.

Casassa, G., 1987. Ice thickness deduced from gravity anomalies on Soler Glacier, Nef Glacier and the Northern Patagonia Icefield. *Bulletin of Glacier Research*, (4), pp.43-57.

Casassa, G., Rivera, A. and Schwikowski, M., 2006. Glacier mass-balance data for southern South America. *Glacier Science and Environmental Change*, p.239.

Casassa, G., Sepúlveda, F.V. and Sinclair, R.M. eds., 2012. *The Patagonian icefields: a unique natural laboratory for environmental and climate change studies*. Springer Science & Business Media.

Chen, J.L., Wilson, C.R., Tapley, B.D., Blankenship, D.D. and Ivins, E.R., 2007. Patagonia icefield melting observed by gravity recovery and climate experiment (GRACE). *Geophysical Research Letters*, *34*(22).

Claps, P., Fiorentino, M. and Oliveto, G., 1996. Informational entropy of fractal river networks. *Journal of Hydrology*, *187*(1-2), pp.145-156.

Coudrain, A., Francou, B. and Kundzewicz, Z.W., 2005. Glacier shrinkage in the Andes and consequences for water resources. *Hydrological Sciences Journal*.

Dall, J., Madsen, S.N., Keller, K. and Forsberg, R., 2001. Topography and penetration of the Greenland ice sheet measured with airborne SAR interferometry. *Geophysical Research Letters*, *28*(9), pp.1703-1706.

De Angelis, H., 2014. Hypsometry and sensitivity of the mass balance to changes in equilibrium-line altitude: the case of the Southern Patagonia Icefield. *Journal of Glaciology*, *60*(219), pp.14-28.

Dehmer, M., Kraus, V., Emmert-Streib, F. and Pickl, S., 2014. *Quantitative graph theory* (pp. 1-33). Boca Raton: CRC press.

Dussaillant, I., Berthier, E. and Brun, F., 2018. Geodetic mass balance of the Northern Patagonian Icefield from 2000 to 2012 using two independent methods. *Frontiers in Earth Science*, *6*, p.8.

Frey, H., Paul, F. and Strozzi, T., 2012. Compilation of a glacier inventory for the western Himalayas from satellite data: methods, challenges, and results. *Remote Sensing of Environment*, *124*, pp.832-843.

Gardelle, J., Berthier, E. and Arnaud, Y., 2012. Impact of resolution and radar penetration on glacier elevation changes computed from DEM differencing. *Journal of Glaciology*, *58*(208), pp.419-422.

Gardner, A.S., Moholdt, G., Cogley, J.G., Wouters, B., Arendt, A.A., Wahr, J., Berthier, E., Hock, R., Pfeffer, W.T., Kaser, G. and Ligtenberg, S.R., 2013. A reconciled estimate of glacier contributions to sea level rise: 2003 to 2009. *science*, *340*(6134), pp.852-857.

Garreaud, R., Lopez, P., Minvielle, M. and Rojas, M., 2013. Large-scale control on the Patagonian climate. *Journal of Climate*, *26*(1), pp.215-230.

Georgieva, V., Melnick, D., Schildgen, T.F., Ehlers, T.A., Lagabrielle, Y., Enkelmann, E. and Strecker, M.R., 2016. Tectonic control on rock uplift, exhumation, and topography above an oceanic ridge collision: Southern Patagonian Andes (47° S), Chile. *Tectonics*, *35*(6), pp.1317-1341.

Glasser, N.F., Jansson, K.N., Harrison, S. and Rivera, A., 2005. Geomorphological evidence for variations of the North Patagonian Icefield during the Holocene. *Geomorphology*, *71*(3-4), pp.263-277.

Glasser, N.F., Holt, T.O., Evans, Z.D., Davies, B.J., Pelto, M. and Harrison, S., 2016. Recent spatial and temporal variations in debris cover on Patagonian glaciers. *Geomorphology*, *273*, pp.202-216.

Hata, S. and Sugiyama, S., 2021. Changes in the ice-front position and surface elevation of Glaciar Pío XI, an advancing calving glacier in the Southern Patagonia Icefield, from 2000–2018. *Frontiers in Earth Science*, *8*, p.681.

Heckmann, T., Schwanghart, W. and Phillips, J.D., 2015. Graph theory—Recent developments of its application in geomorphology. *Geomorphology*, *243*, pp.130-146.

Hock, R. and Huss, M., 2021. Glaciers and climate change. In *Climate Change* (pp. 157-176). Elsevier.

Hulley, G.C. and Hook, S.J., 2008. A new methodology for cloud detection and classification with ASTER data. *Geophysical research letters*, *35*(16).

Hubbard, B. and Glasser, N.F., 2005. *Field techniques in glaciology and glacial geomorphology*. John Wiley & Sons.

Immerzeel, W.W., Lutz, A.F., Andrade, M., Bahl, A., Biemans, H., Bolch, T., Hyde, S., Brumby, S., Davies, B.J., Elmore, A.C. and Emmer, A., 2020. Importance and vulnerability of the world's water towers. *Nature*, *577*(7790), pp.364-369.

Iribarren Anacona, P., Mackintosh, A. and Norton, K.P., 2015. Hazardous processes and events from glacier and permafrost areas: lessons from the Chilean and Argentinean Andes. *Earth Surface Processes and Landforms*, *40*(1), pp.2-21.

Jaber, W.A., Floricioiu, D., Rott, H. and Eineder, M., 2012, July. Dynamics of fast glaciers in the Patagonia Icefields derived from TerraSAR-X and TanDEM-X data. In *2012 IEEE International Geoscience and Remote Sensing Symposium* (pp. 3226-3229). IEEE.

Jacob, T., Wahr, J., Pfeffer, W.T. and Swenson, S., 2012. Recent contributions of glaciers and ice caps to sea level rise. *Nature*, *482*(7386), pp.514-518.

Kaab, A., 2008. Glacier volume changes using ASTER satellite stereo and ICESat GLAS laser altimetry. A test study on Edgeøya, Eastern Svalbard. *IEEE Transactions on Geoscience and Remote Sensing*, *46*(10), pp.2823-2830.

Kervyn, M., Ernst, G.G.J., Goossens, R. and Jacobs, P., 2008. Mapping volcano topography with remote sensing: ASTER vs. SRTM. *International Journal of Remote Sensing*, *29*(22), pp.6515-6538.

Lodolo, E., Lozano, J., Donda, F., Bran, D., Baradello, L., Tassone, A., Romeo, R., Paterlini, M., Grossi, M., Caffau, M. and Vilas, J.F., 2020. Late-glacial fluctuations of two southern Patagonia outlet glaciers revealed by high-resolution seismic surveys. *Quaternary Research*, *97*, pp.111-124.

Lopez, P., Chevallier, P., Favier, V., Pouyaud, B., Ordenes, F. and Oerlemans, J., 2010. A regional view of fluctuations in glacier length in southern South America. *Global and Planetary Change*, *71*(1-2), pp.85-108.

Malz, P., Meier, W., Casassa, G., Jaña, R., Skvarca, P. and Braun, M.H., 2018. Elevation and mass changes of the Southern Patagonia Icefield derived from TanDEM-X and SRTM data. *Remote Sensing*, *10*(2), p.188.

Marzeion, B., Champollion, N., Haeberli, W., Langley, K., Leclercq, P. and Paul, F., 2017. Observation-based estimates of global glacier mass change and its contribution to sea-level change. *Integrative study of the mean sea level and its components*, pp.107-132.

Masiokas, M.H., Luckman, B.H., Villalba, R., Delgado, S., Skvarca, P. and Ripalta, A., 2009. Little ice age fluctuations of small glaciers in the Monte Fitz Roy and Lago del Desierto areas, south Patagonian Andes, Argentina. *Palaeogeography, Palaeoclimatology, Palaeoecology*, *281*(3-4), pp.351-362.

Masiokas, M.H., Rabatel, A., Rivera, A., Ruiz, L., Pitte, P., Ceballos, J.L., Barcaza, G., Soruco, A., Bown, F., Berthier, E. and Dussaillant, I., 2020. A review of the current state and recent changes of the Andean cryosphere. *Frontiers in Earth Science*, *8*, p.99.

Meier, M.F., 1984. Contribution of small glaciers to global sea level. *Science*, *226*(4681), pp.1418-1421.

Meier, M.F. and Post, A., 1987. Fast tidewater glaciers: Journal of Geo-physical Research, v. 92.

Mernild, S.H., Liston, G.E., Hiemstra, C. and Wilson, R., 2017. The Andes Cordillera. Part III: glacier surface mass balance and contribution to sea level rise (1979–2014). *International Journal of Climatology*, *37*(7), pp.3154-3174.

Minowa, M., Sugiyama, S., Sakakibara, D. and Sawagaki, T., 2015. Contrasting glacier variations of glaciar perito moreno and glaciar ameghino, southern Patagonia icefield. *Annals of Glaciology*, *56*(70), pp.26-32.

Moholdt, G. and Kääb, A., 2012. A new DEM of the Austfonna ice cap by combining differential SAR interferometry with ICESat laser altimetry. *Polar Research*, *31*(1), p.18460.

Mölg, N. and Bolch, T., 2017. Structure-from-motion using historical aerial images to analyse changes in glacier surface elevation. *Remote Sensing*, *9*(10), p.1021.

Minowa, M., Schaefer, M., Sugiyama, S., Sakakibara, D. and Skvarca, P., 2021. Frontal ablation and mass loss of the Patagonian icefields. *Earth and Planetary Science Letters*, *561*, p.116811.

Naruse, R. and Aniya, M., 1992. *Glaciological researches in Patagonia, 1990*.

Naruse, R., Aniya, M., Skvarca, P. and Gasassa, G., 1995. Recent variations of calving glaciers in Patagonia, South America, revealed by ground surveys, satellite-data analyses and numerical experiments. *Annals of Glaciology*, *21*, pp.297-303.

Naruse, R., Skvarca, P. and Takeuchi, Y., 1997. Thinning and retreat of Glaciar Upsala, and an estimate of annual ablation changes in southern Patagonia. *Annals of Glaciology*, *24*, pp.38-42.

NASA Landsat Image Gallery https://landsat.visibleearth.nasa.gov/view.php?id=90464

Natalia, P., Silvia, F., Silvina, S. and Miguel, P., 2020. Climate change in northern Patagonia: critical decrease in water resources. *Theoretical and Applied Climatology*, pp.1-16.

Neckel, N., Kropáček, J., Bolch, T. and Hochschild, V., 2014. Glacier mass changes on the Tibetan Plateau 2003–2009 derived from ICESat laser altimetry measurements. *Environmental research letters*, *9*(1), p.014009.

Nick, F.M., Vieli, A., Howat, I.M. and Joughin, I., 2009. Large-scale changes in Greenland outlet glacier dynamics triggered at the terminus. *Nature Geoscience*, *2*(2), pp.110-114.

Nuth, C. and Kääb, A., 2011. Co-registration and bias corrections of satellite elevation data sets for quantifying glacier thickness change. *The Cryosphere*, *5*(1), pp.271-290.

Ohmura, A., 2009. Completing the world glacier inventory. *Annals of Glaciology*, *50*(53), pp.144-148.

Paul, F., 2008. Calculation of glacier elevation changes with SRTM: is there an elevation-dependent bias?. *Journal of Glaciology*, *54*(188), pp.945-946.

Paul, F., Barry, R.G., Cogley, J.G., Frey, H., Haeberli, W., Ohmura, A., Ommanney, C.S.L., Raup, B., Rivera, A. and Zemp, M., 2009. Recommendations for the compilation of glacier inventory data from digital sources. *Annals of Glaciology*, *50*(53), pp.119-126.

Post, A., O'Neel, S., Motyka, R.J. and Streveler, G., 2011. A complex relationship between calving glaciers and climate. *Eos, Transactions American Geophysical Union*, *92*(37), pp.305-306.

Quincey, D.J., Bishop, M.P., Kääb, A., Berthier, E., Flach, B., Bolch, T., Buchroithner, M., Kamp, U., Khalsa, S.J.S., Toutin, T. and Haritashya, U.K., 2014. Digital terrain

modeling and glacier topographic characterization. In *Global land ice measurements from space* (pp. 113-144). Springer, Berlin, Heidelberg.

Raup, B., Kääb, A., Kargel, J.S., Bishop, M.P., Hamilton, G., Lee, E., Paul, F., Rau, F., Soltesz, D., Khalsa, S.J.S. and Beedle, M., 2007. Remote sensing and GIS technology in the Global Land Ice Measurements from Space (GLIMS) project. *Computers & Geosciences*, *33*(1), pp.104-125.

Raymond, C., Neumann, T.A., Rignot, E., Echelmeyer, K., Rivera, A. and Casassa, G., 2005. Retreat of Glaciar Tyndall, Patagonia, over the last half-century. *Journal of Glaciology*, *51*(173), pp.239-247.

Paul, F., Hendriks, J., Pellikka, P. and Rees, W.G., 2010. Optical remote sensing of glaciers.

Rignot, E., Rivera, A. and Casassa, G., 2003. Contribution of the Patagonia Icefields of South America to sea level rise. *Science*, *302*(5644), pp.434-437.

Rivera, A., Casassa, G., Bamber, J. and Kääb, A., 2005. Ice-elevation changes of Glaciar Chico, southern Patagonia, using ASTER DEMs, aerial photographs and GPS data. *Journal of Glaciology*, *51*(172), pp.105-112.

Rivera, A., Benham, T., Casassa, G., Bamber, J. and Dowdeswell, J.A., 2007. Ice elevation and areal changes of glaciers from the Northern Patagonia Icefield, Chile. *Global and Planetary Change*, *59*(1-4), pp.126-137.

Rivera, A., Koppes, M., Bravo, C. and Aravena, J.C., 2012. Little ice age advance and retreat of Glaciar Jorge Montt, Chilean Patagonia. *Climate of the Past*, *8*(2), pp.403-414.

Ruel, J.C., Mitchell, S.J. and Dornier, M., 2002. A GIS based approach to map wind exposure for windthrow hazard rating. *Northern Journal of Applied Forestry*, *19*(4), pp.183-187.

Rignot, E., Koppes, M. and Velicogna, I., 2010. Rapid submarine melting of the calving faces of West Greenland glaciers. *Nature Geoscience*, *3*(3), pp.187-191.

Sakakibara, D. and Sugiyama, S., 2014. Ice-front variations and speed changes of calving glaciers in the Southern Patagonia Icefield from 1984 to 2011. *Journal of Geophysical Research: earth surface*, *119*(11), pp.2541-2554.

Schaefer, M., Machguth, H., Falvey, M. and Casassa, G., 2013. Modeling past and future surface mass balance of the Northern Patagonia Icefield. *Journal of Geophysical Research: Earth Surface*, *118*(2), pp.571-588.

Schaefer, M., Machguth, H., Falvey, M., Casassa, G. and Rignot, E., 2015. Quantifying mass balance processes on the Southern Patagonia Icefield. *The Cryosphere*, *9*(1), pp.25-35.
Schaefer, M., Fonseca-Gallardo, D., Farías-Barahona, D. and Casassa, G., 2020. Surface energy fluxes on Chilean glaciers: measurements and models. *The Cryosphere*, *14*(8), pp.2545-2565.

Skvarca, P., Marinsek, S. and Aniya, M., 2010. Documenting 23 years of areal loss of Hielo Patagónico Sur, recent climate data and potential impact on Río Santa Cruz water discharge. In *Abstracts. International Glaciological Conference. Ice and climate change: a view from the South*.

Strecker, M.R., Alonso, R.N., Bookhagen, B., Carrapa, B., Hilley, G.E., Sobel, E.R. and Trauth, M.H., 2007. Tectonics and climate of the southern central Andes. *Annu. Rev. Earth Planet. Sci.*, *35*, pp.747-787.

Stuefer, M., Rott, H. and Skvarca, P., 2007. Glaciar Perito Moreno, Patagonia: climate sensitivities and glacier characteristics preceding the 2003/04 and 2005/06 damming events. *Journal of Glaciology*, *53*(180), pp.3-16.

Tagliaferro, M., Miserendino, M.L., Liberoff, A., Quiroga, A. and Pascual, M., 2013. Dams in the last large free-flowing rivers of Patagonia, the Santa Cruz River, environmental features, and macroinvertebrate community. *Limnologica*, *43*(6), pp.500-509.

Thomson, S.N., Brandon, M.T., Tomkin, J.H., Reiners, P.W., Vásquez, C. and Wilson, N.J., 2010. Glaciation as a destructive and constructive control on mountain building. *Nature*, *467*(7313), pp.313-317.

Viviroli, D., Archer, D.R., Buytaert, W., Fowler, H.J., Greenwood, G.B., Hamlet, A.F., Huang, Y., Koboltschnig, G., Litaor, M.I., López-Moreno, J.I. and Lorentz, S., 2011. Climate change and mountain water resources: overview and recommendations for research, management and policy. *Hydrology and Earth System Sciences*, *15*(2), pp.471-504.

Wang, K., Hu, Y., Bevis, M., Kendrick, E., Smalley Jr, R., Vargas, R.B. and Lauría, E., 2007. Crustal motion in the zone of the 1960 Chile earthquake: Detangling earthquake-cycle deformation and forearc-sliver translation. *Geochemistry, Geophysics, Geosystems*, *8*(10).

Warren, C.R. and Sugden, D.E., 1993. The Patagonian icefields: a glaciological review. *Arctic and Alpine Research*, *25*(4), pp.316-331.

Willis, M.J., Melkonian, A.K., Pritchard, M.E. and Rivera, A., 2012. Ice loss from the Southern Patagonian ice field, South America, between 2000 and 2012. *Geophysical research letters*, *39*(17).

Winsvold, S.H., Kääb, A., Nuth, C., Andreassen, L.M., Van Pelt, W.J. and Schellenberger, T., 2018. Using SAR satellite data time series for regional glacier mapping. *The Cryosphere*, *12*(3), pp.867-890.

Wouters, B., Bonin, J.A., Chambers, D.P., Riva, R.E., Sasgen, I. and Wahr, J., 2014. GRACE, time-varying gravity, Earth system dynamics and climate change. *Reports on Progress in Physics*, *77*(11), p.116801.

Yokoyama, R., Shirasawa, M. and Pike, R.J., 2002. Visualizing topography by openness: a new application of image processing to digital elevation models. *Photogrammetric engineering and remote sensing*, *68*(3), pp.257-266.

Ye, Q., Kang, S., Chen, F. and Wang, J., 2006. Monitoring glacier variations on Geladandong mountain, central Tibetan Plateau, from 1969 to 2002 using remote-sensing and GIS technologies. *Journal of Glaciology*, *52*(179), pp.537-545.

Zhao, P., J. R. Giardino and Gamache, K.R., 2019. *Handbook of environmental engineering*. Chapter 5: Climate Change Impact Analysis for the Environmental Engineer. CRC Press.

Zwally, H.J.R., Schutz, C., Bentley, J., Bufton, T., Herring, J., Minster, J., Spinhirne, R.T. and Thomas, R.H., 2003. GLAS/ICESat L1B Global Elevation Data, Version 33.

4. THE STRATIFICATION OF AUTOMATED SURFACE EXPRESSIONS USING NEW TOPOGRAPHC INDICS AND ARTIFICIAL NEURAL NETWORKS (ANN)

Introduction

Chapter 4 introduces artificial neural network (ANN) and new topographic indices for mapping applied alpine geomorphology via a case study in the San Juan Mountains. The results suggest my protocol can facilitate the mapping and understanding of geomorphic input in the urban planning mechanism (Lehmkuhl et al., 2020).

Geomorphology mapping is fundamental component of urban geomorphology. My research integrates innovative terrain parameters into an Artificial Neural Network (ANN) to first carefully map the basic surface expression and then assess its applicability to urban geomorphology (Lucà, 2020; Nefeslioglu et al., 2021).

Traditional geomorphic mapping requires extensive labor and time. A qualified cartographer must possess the basic geological-domain knowledge to interpret different surface expressions, and also needs to be able to conduct field validation and be skilled in identifying the outline of each surface expression (Huff et al., 2021). Using GIS (Geographic Information System) also requires a cartographer to be able to digitize surface-expression outlines accurately either from aerial photographs or satellite imageries. Many questions still exist for manual mapping, such as an interpreter's bias, drawing error, lack of accuracy, and the difficulty to reproduce. Thus, it is fundamental

to develop an automated mapping protocol for characterizing the surface expression accurately. My hope is that the protocol I have developed will facilitate automated geomorphic mapping protocol to be used in different settings.

Optical remote sensing mapping relies on the spectral differences between different surface expressions; however, understand that background noise could potentially hamper accurate mapping. For instance, a bare-ground ridge during winter may be mapped differently when the ridge is covered by grass in summer. Although pure spectral information can help determine the type of surface material of certain surface expressions, it cannot satisfy the required detail for geomorphic mapping. Whereas, a set of characteristics, such as shape, size, texture, height, gradient, positions, can help to define the type of surface expressions; these characteristics are impossible to retrieve simply by using optical remote sensing. Thus, terrain information must be incorporated to address geomorphic mapping issues (Metelka et al., 2018).

Information from terrain analysis can minimize the above-mentioned issues by revealing the underlying topographic structure to help characterize and detect different surface expressions. Before moving forward, several questions need to be considered. What type of surface expression am I going to map? Is the spatial resolution of available data fine enough to support the mapping task? Can the mapping be automated and used in a variety of geomorphological regions? What processes have produced the current landscape? These are important questions that should be considered before starting any mapping project.

Digital elevation models and the derivatives have been frequently used for geomorphic mapping in conjunction with other remote sensing data. Bolongaro-Crevenna et al. (2005) used a simple topographic index, e.g., slope and curvature to map basic morphometric features as valleys, ridges, peaks and planes. High-resolution DEM retrieved from UAV (Unmanned Aerial Vehicle), or LiDAR (Light Detection and Ranging) significantly enhanced the potential of using terrain analysis for geomorphic mapping; however, the existing terrain-based mapping only focuses on a small number of surface expressions, limiting the mapping capacity in San Juan Mountains which consist of a large spectrum of different types of surface expressions (Latifovic et al., 2018).

Coates (1976) and Cooke (1984) suggest that geomorphology can be used in studies of urban environment by examining the suitability of different surface expressions for physical urban planning, evaluating geomorphic impacts during construction, analyzing the geomorphologic consequences from human-introduced surface expressions, and mitigation of hazard risks. Traditional geomorphological techniques, for instance field surveys, still have merit because of the long-established records (Goudie, 2003). The advent of geospatial technology, e.g., GIS and remote sensing, however, have significantly improved the study of geomorphology from a global-scale perspective (Hengl and Reuter, 2009).

Geomorphometry is the study of the quantitative analysis of the land-surface (Pike, 1995). Qualitative depiction of surface expression evolution has been replaced by numerical analysis approaches since the 1950s. Dramatic changes in geomorphology

have progressed after 1980s as a result of the following technological influences: (1) improved remote sensing platforms offering high-quality acquisition information on the surface of Earth; and (2) development of personal computers and improve computation capacity have significantly stimulated designing innovative and efficient algorithms for solving Earth science problems (Church, 2010).

Geomorphometry is a modern science that obeys basic principles of classic geomorphology. For instance, to characterize the surface of Earth, six classic factors of topography need to be considered: elevation, terrain-surface shape, topographic position, topographic context, spatial scale, and surface expression object (Deng, 2007). With geomorphometry, the first four factors can be properly calculated, and the last two can be effectively analyzed.

The combination of Geographic Information System (GIS) and remote sensing has significantly enhanced the computation capacity to solve Earth science related issues (Goodchild, 1992). Many commercial geomorphometry software exist; however, each employs its own analytical functionality. For example, to calculate a simple geomorphological factor, such as profile-curvature of a slope, different software may yield different results. Thus, recognizing the limitation of different software is as important as understanding the physical nature of the algorithm that is employed.

Various geomorphometry applications exist, including mapping glacier terminus, extracting river channels, assessing terrain for military support, monitoring crop health condition, optimizing urban transportation system, and modeling solar radiation. Coupling GIS with remote sensing significantly enhances the computational capacity of

geomorphometry. Remote sensing can be used to acquire the information from the surface of Earth; GIS can be used to develop relevant functions to aid in the interpretation of the remote sensing data. Thus, it is important to integrate remote sensing and GIS in the study of landform processes.

Traditionally, remote sensing is collecting information from aerial platforms, including airplanes, UAV, and satellites. One advantage of remote sensing is that it can access extremely roughed terrain where human beings cannot. Another advantage of remote sensing is it can provide a chronological record of a specific area, which is very important in the study of geomorphology. Currently, Synthetic Aperture Radar (SAR) and LiDAR are two additional remote sensing technologies used in geomorphometry. SAR is good at penetrating dry materials, such as sand or dry snow. LiDAR is good at delineating land-surface details (Jensen, 2005).

My research will exhibit two case studies of how to incorporate a set of meaningful and innovative terrain analysis layers as input for an Artificial Neural Network (ANN) to map surface geomorphology and as an input for reconnaissance mapping in the Western San Juan Mountains. Using ANN to map alpine geomorphology has not been attempted by other researchers.

Background

Study Area

The San Juan Mountains are the largest mountain range by area in Colorado (Arcusa, 2020). The range covers 13 counties in the southwestern part of Colorado. The

San Juan Mountains are referred to as “Swiss Alps” of America as recognition of the variety of surface expressions with majestic scenery. Thirteen peaks rise to over 4,265 m. Many lakes, waterfalls, and streams exist in this area. The Rio Grande origins from this mountainous area, as well as the Uncompahgre, San Miguel, and Animas rivers (Figure 45).

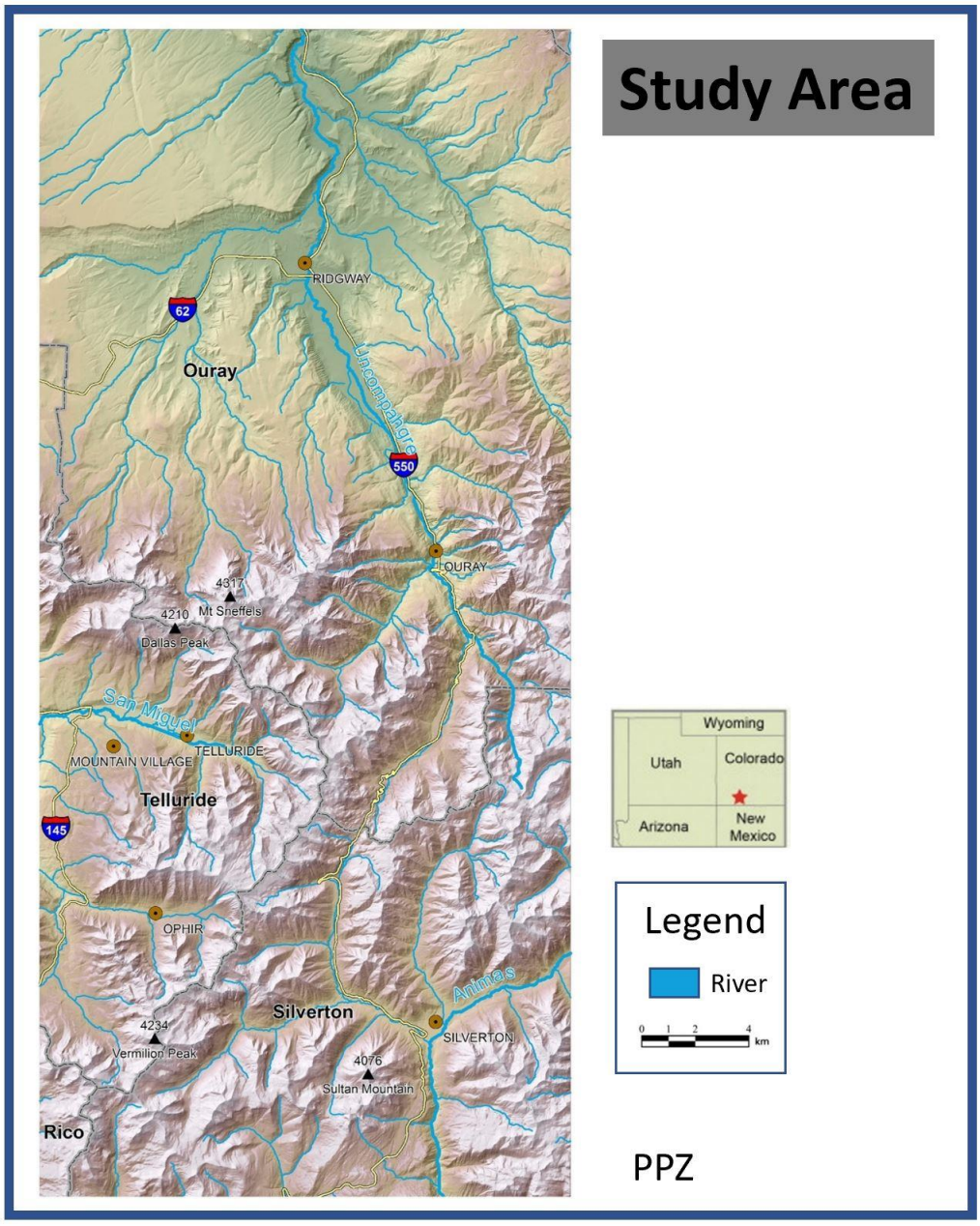

Figure 45. The study area of this research. Map is created based upon shaded relief. The elevations in general increase from north to south of this area.

Six communities in this area include Ridgway, Ouray, Mountain Village, Telluride, Ophir and Silverton. The well-known San Juan Skyway, consisting of U.S. Highways 62, 145 and 550, provides access to this region (Figure 45).

Volcanic processes are dominant in this region from Precambrian to the present, which produced a highly mineralized alpine setting (Hoffman, 1997). Located at the southern extent of the Colorado Mineral Belt, the San Juan Mountains are famous for the mining of gold and silver. Besides volcanic process, the landscape has been sculptured by intense glaciation, fluvial erosion, and mass movement (Moore, 2004).

ANN

Artificial neural networks are a machine learning technique, which can learn relationships between specified input and output variables. Neural networks constitute an information processing model that stores empirical knowledge through a learning process and subsequently makes the adjusted output based on the knowledge training. ANN can mimic a thought process of a human brain to acquire knowledge from the environment through a learning process. A neuron is the fundamental processing unit used in ANNs (Figure 46). A neuron consists of connection links characterized by certain weights. Input is passed from one end of the links, multiplied by the connection weight and transmitted to the summing junction of the neuron (Haykin, 1999). In environmental studies, ANN can facilitate the modeling of cause-effect relationship such as water-quality forecasting (Palani et al., 2008), and rainfall-runoff modeling (Hsu et al., 1995).

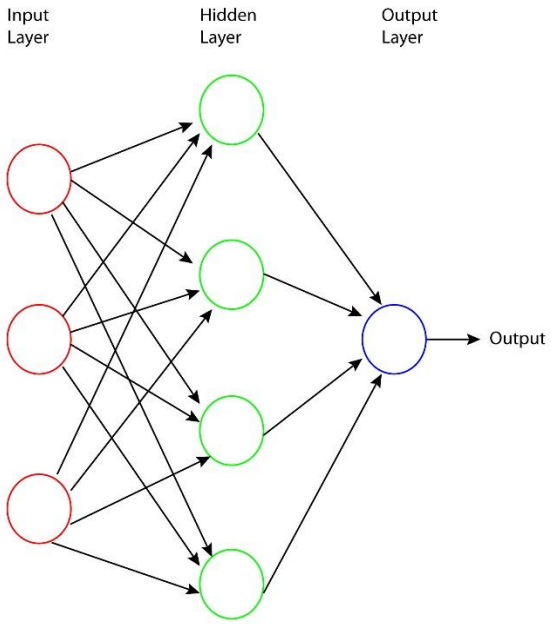

Figure 46. An example of an artificial neural network (Zhao et al., 2018).

For this area I adopted ANN for mapping geomorphology in the San Juan Mountains. This approach allowed a first approximation or reconnaissance-type to be compiled for this area. This technique is both time and cost effective. Kelkar (2017) compiled a detailed map of the geomorphology of this area. I used his map as a substitute for ground truthing the map I derived from the imagery. Kelkar created a mapping cascade of 27 subclasses, of which I generalized these surface expressions into 6 major categories (Figure 47). This fundamental stratification of the geomorphology meets the basic need of mapping at a larger scale.

Outcrop Geology	Glacial
Igneous Outcrops	Arete
Sedimentary Outcrops	Cirque
Glaciofluvial	Glacial Polish
Alluvium	Ground Moraine
Outwash Plains	Lateral Moraine
Valley Train Deposits	Recession Moraine
Gravity	Terminal Moraine
Avanlache Tracks	Morphological
Colluvium	Hillslope
Debris Cone Deposits	Mesa
Debris Flow Deposits	Ridges
Landslide Deposits	Rill and Gully Topography
Talus	Scarps (bare)
Periglacial	Scarps (vegetated)
Patterned Ground	
Rock Glaciers	
Solifluction	

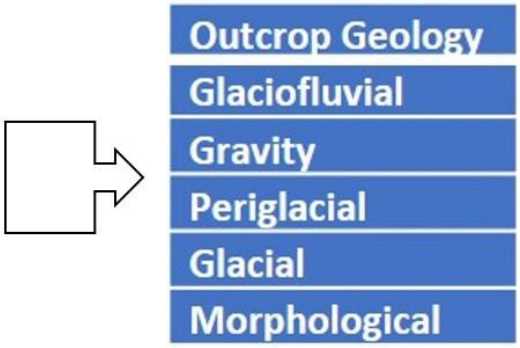

Figure 47. Surface expressions following Kelkar's work (2017).

Geomorphology Mapping

Case description

Kelkar (2017) mapped the surficial geomorphology of the San Juan Mountains at a scale of 1:3,000 using aerial photographs and ground truthing. His map is the first detailed geomorphology map covering this alpine area. In Kelkar's map, surface expressions are mapped into six categories: 1) glacial landforms; 2) glaciofluvial landforms; 3) gravitational landforms; 4) morphological components; 5) outcrop geology; and 6) periglacial landforms (Figure 49). When considering the high potential of mass-driven hazards in alpine settings, such as landslides, snow avalanches and debris

flows, a detailed geomorphic map can assist planners to gain *priori* knowledge and to mitigate damage to real property and plentiful loss of lives. In the future, an accurate geomorphology map of the San Juan Mountains can facilitate environment and engineering, urban planning, and tourism.

Whereas Kelkar's map provides a first approximation of the geomorphology of the San Juan Mountains, manual mapping, however, is subjective, and labor-intensive. It is also challenging to educate a cartographer with the necessary expertise to conduct an accurate mapping task, as Mr. Kelkar did. In this research, I used the ANN (artificial neural network) based upon a careful selection of input layers to optimize the mapping efficiency of surficial surface expressions. It should be noted that some of these input layers are innovative terrain indices and have yet to be applied in other studies. In addition, I tested the possibility of enhancing the mapping accuracy by introducing an input layer based on object-oriented analysis. The mapping protocol in my research is automated and objective; and it can be transplanted conveniently into other areas. The preliminary result is very encouraging when compared with Mr. Kelkar's mapping product.

Data Input

Valid data input determines the accuracy of the mapping outcome. My research incorporates data at different levels, from first-order derivatives of DEMs to very sophisticated data, e.g., topographic shielding. Because the goal of my research is to map surface geomorphology, selecting the data input necessitates choosing data from a

process perspective. After scrutiny, 9 major input layers were chosen as ANN input layers, and these are: elevation, relief, orientation, valley bottom, horizontal distance to river, height above river, convergence, terrain object, and topographic shielding. The following discusses the description of each input layer.

1-DEM integrates all terrain information, which serve as a basic input layer for ANN (Figure 48a). All other input layers are derived from this DEM; however, each represents one physical perspective when considering the process of landform formation.

2-Relief can charactize local topographic change (Figure 48b). It can also serve as an alternative to surface roughness and slope. This index will hightlights landforms whose spatial distributions are highly influenced by gravity, such as landsldie, deposites, talus, and debris flows.

3-Orientation is a quantifable number regarding aspect (Figure 48c). It clearlly differentiates north-oriented slope from south-oriented slope. Because the study area is located in the northern hemisphere, south-facing slopes will reveive more solar solaradiation compared to north-facing slopes. Solar radiation plays a vital role in the rock-weathering process. Thus, this index is fundamental.

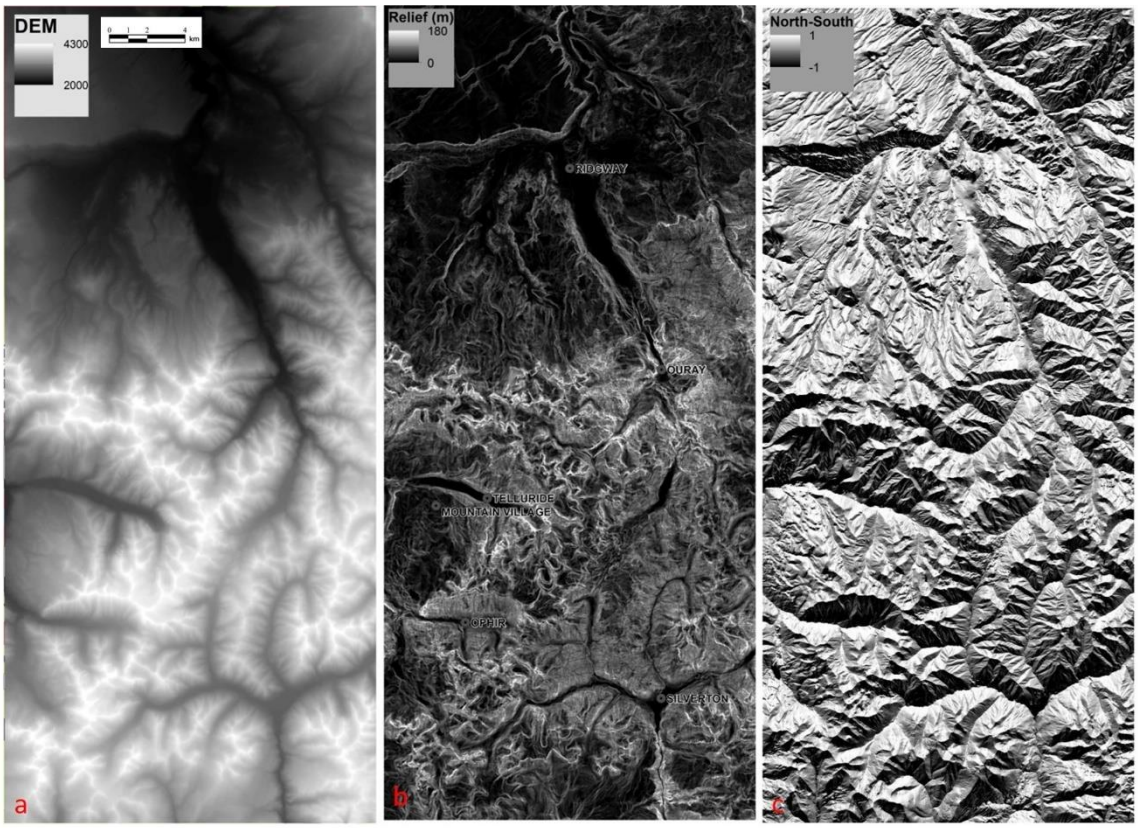

Figure 48. The basic input layers: a) Elevation; b) Relief; c) Orientation.

4-Valley Bottom is the calculation of the Multi-resolution Valley Bottom Flatness (MRVBF) index (Figure 49d; Gallant and Dowling, 2003). This index delineates the flatness and relative height of a landscape at different scales. This index allows one to extract valley bottoms that are relatively low compared to surrounding terrains. This index is essential when working in alpine settings because it can help one to identify u-shaped valley as an indicator of past glaciation.

5-Horizontal Distance and **6-Height above nearest drainage (HAND)** are both related to fluvial processes. Horizontal distance (Figure 49e) is the planimetric distance

from the grid cell centroid to the nearest drainage. Height above nearest drainage (Figure 49f) is the elevational difference from the grid cell centroid to the nearest drainage. The schematic explanation can be viewed in Figure 50 for details. Horizontal distance can serve as measure of the potential of fluvial sediment transfer, whereas Height above river can serve as a measure of potential inundation and erosion.

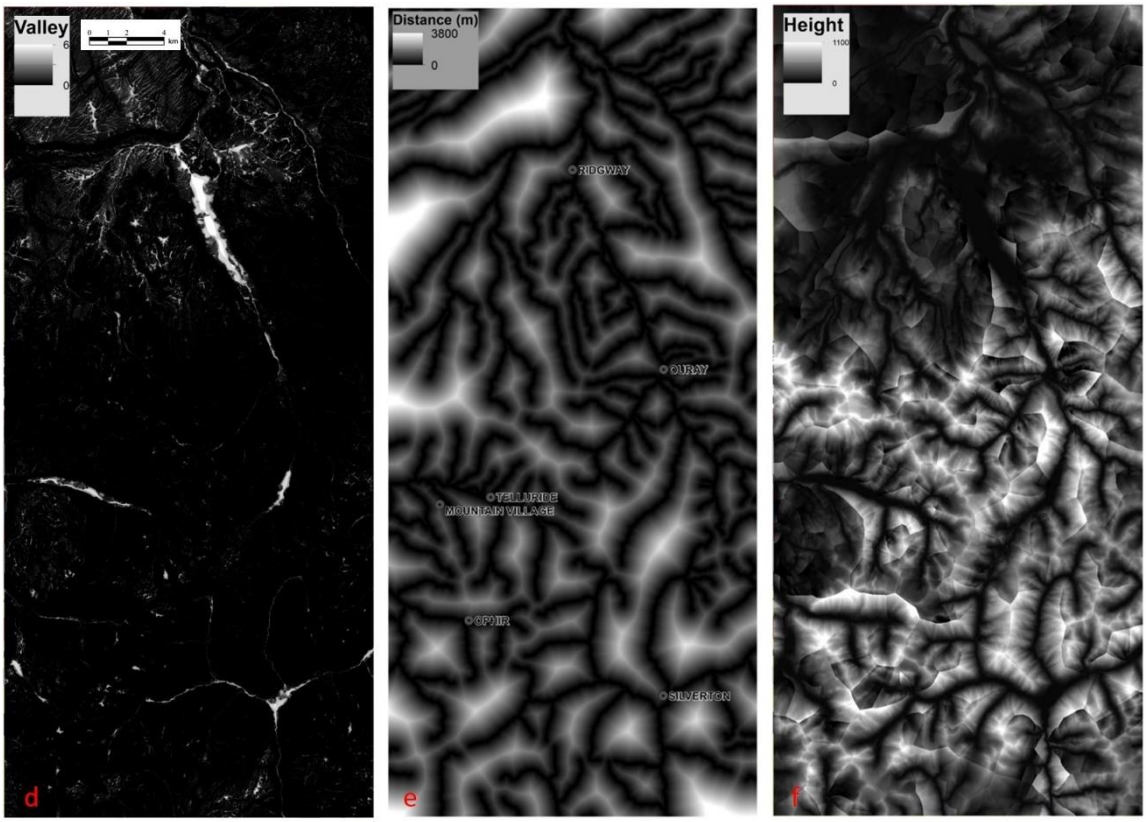

Figure 49. The basic input layers: d) Valley Bottom; e) Distance to River; f) Height above Nearest Drainage.

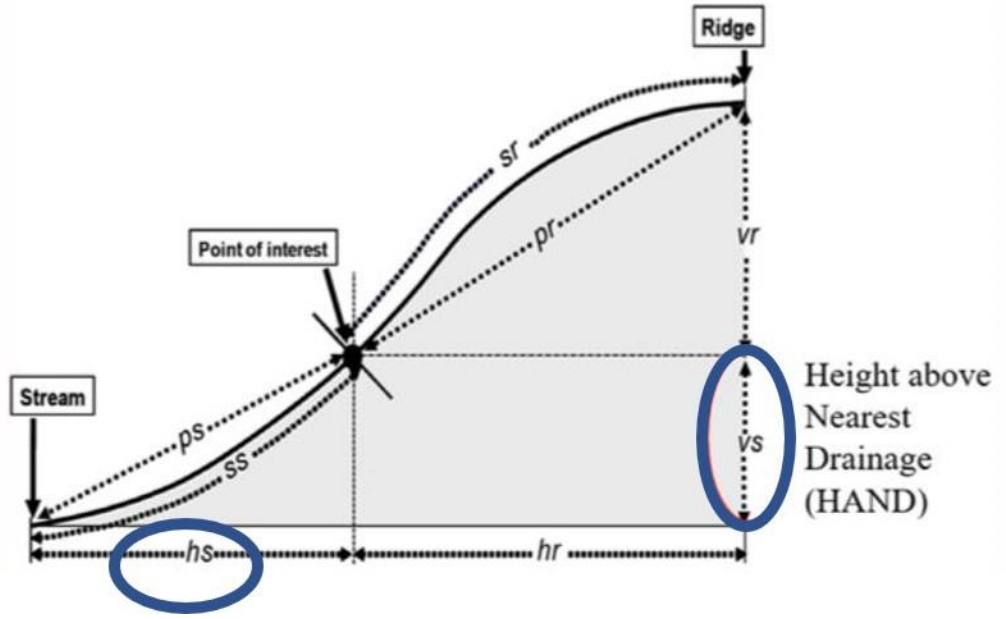

Figure 50. Definition of proximity measures for distances up (to ridge) and down to stream. Height above nearest drainage (HAND) is evaluated using vs, the vertical drop to the stream. hr, horizontal distance to ridge; vr, vertical rise to ridge; sr, surface distance to ridge; pr, direct-transect distance to ridge; hs, horizontal distance to stream; ss, surface distance to stream; and ps, direct transect distance to stream. (Revised from Zheng et al., 2018).

7-Convergence is a valuable resource to show the structure of the topography as a combination of convergent regions (drainage channels) and divergent regions (ridges). This index is based on water flow and improves the existing river-channel extraction algorithm. This new method is cost-effective and can speed up delineating different surface expressions in mountain terrains (Figure 51g; Zhao et al., 2018).

8-Object layer (Figure 51h) is an object-oriented analysis layer based on layer 7 (convergence). I use a threshold of 0.5 to classify regions into either concave or convex. This binary classification generates information about landform objects (i.e., features). Figure 52 illustrates that morphological landform exhibit a totally different patterns from periglacial landforms. This contrast has been found among other landforms as well.

9-Shielding index is also known as topographic exposure (Figure 51i), which is a measure of the surrounding terrain and how it influences routes of wind transfer and incoming solar radiation. Wind and solar energy can influence a landform.

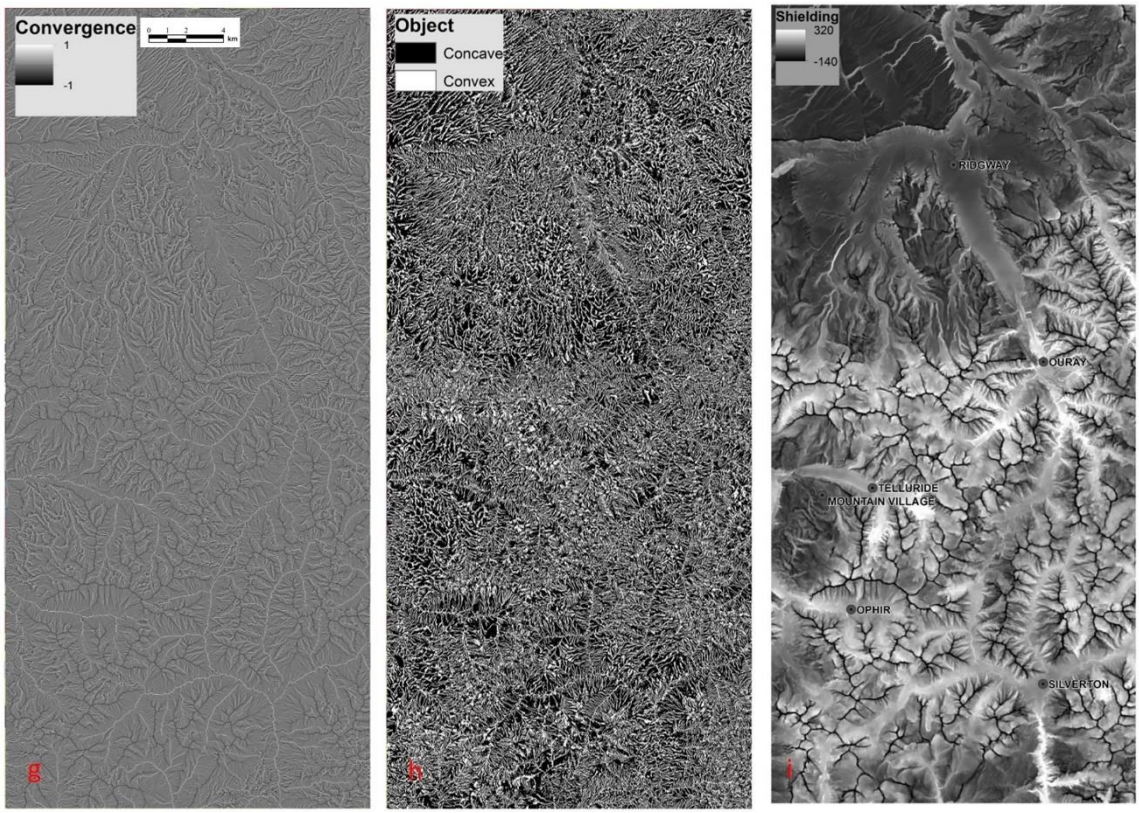

Figure 51. The basic input layers: g) Convergence Index; h) Object Layer; i) Shielding Index.

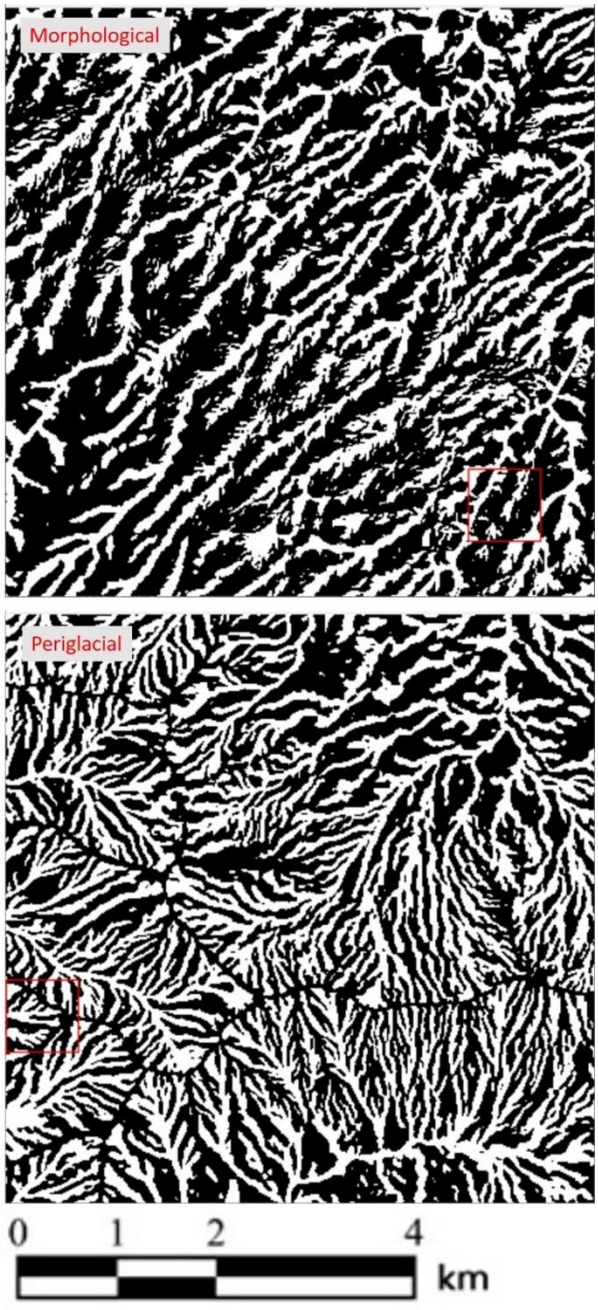

Figure 52. These examples illustrate that different process result in different patterns of surface expression objects. Top image is the pattern of morphological surface expression. Bottom image is the pattern from periglacial surface expression. Note the pattern differences inside each red box.

ANN Training

My research follows three rules for ANN training: 1) take the same number of samples for each surface expression category; 2) all samples should be based on randomly generated points; and 3) all samples should be spread across the region as much as possible.

From these three rules, I randomly pick 1,000 sample points for each geomorphological category. All samples were spread evenly across the region (Figure 53). The dimension of the study area is 2,710 by 5,950 pixels. Thus, the training rate is 0.0372%. This training rate is much lower than most supervised mapping projects, including ANN.

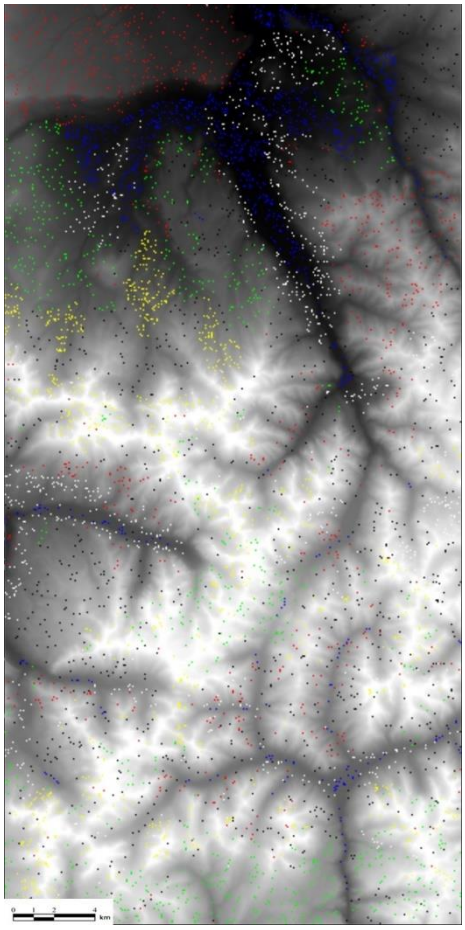

Figure 53. Spatial distribution of sampling points across the region.

Results

After running the ANN based on the 9 input layers, the final output is shown in Figure 54A. From Figure 56A, six categories of fundamental geomorphology classes are captured. By visual comparison with Kelkar's (2017) mapping results (Figure 54B), one can see the close alignment with fluvial and morphological surface expressions. In comparison to Kelkar's map one can see that the ANN mapping overclassified gravity-

related surface expressions and periglacial surface expressions. The ANN mapping also simplified the classification of glacial surface expressions and outcrop.

Overall, however, ANN mapping does show a similar spatial pattern of surface expressions as Kelkar's map. It should be noted that the ANN captured more details of the transition from one surface expression to another, whereas Kelkar's mapping simplifies this transition. Thus, a more heterogenous pattern can be found in ANN mapping.

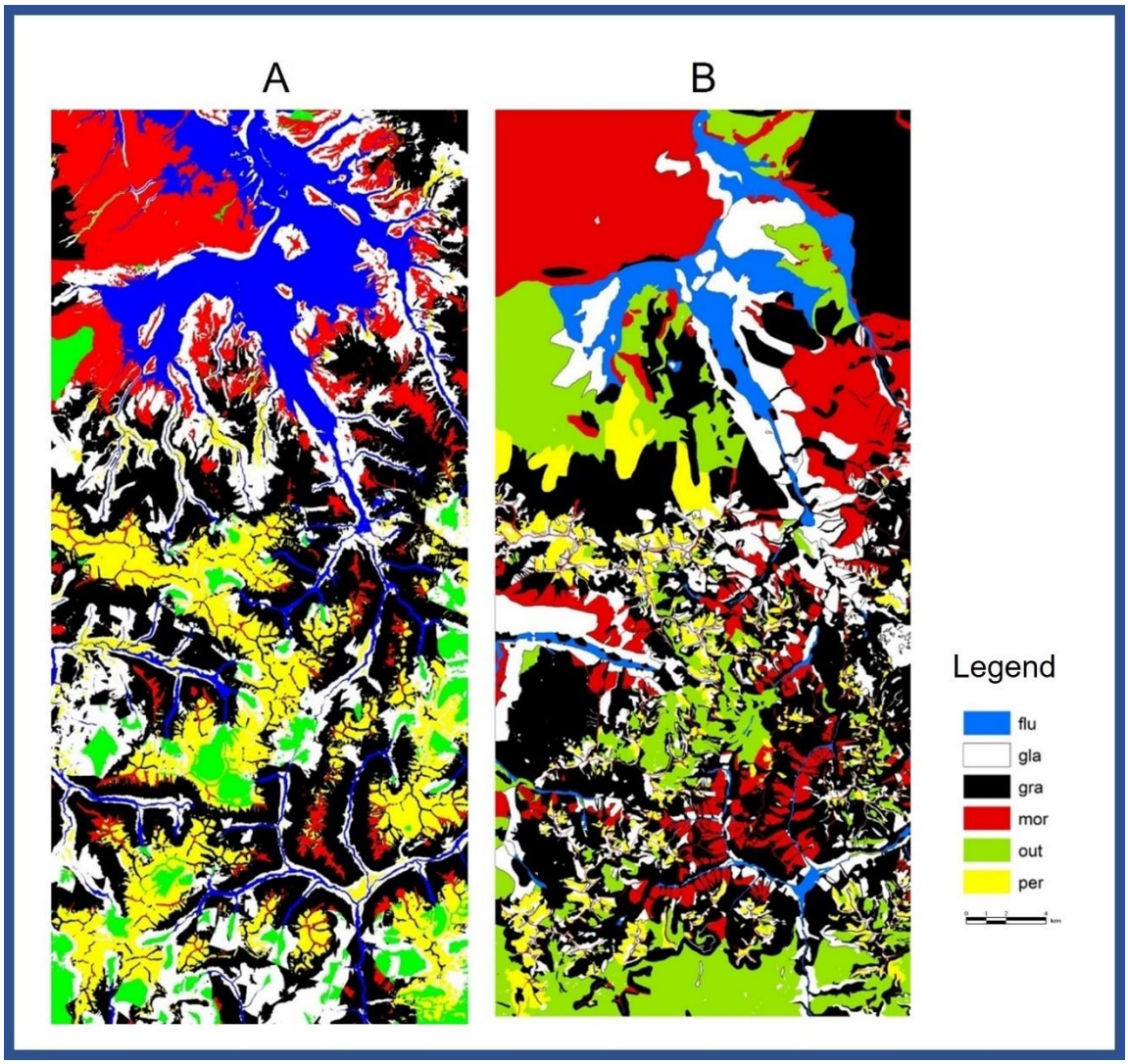

Figure 54. The comparison between ANN mapping (A) and Kelkar's mapping (B).

Discussions

Integrating ANN and innovative topographic parameters have been missing in geomorphic studies. My research used multiple topographic indices as input layers for ANN. The output suggests the integration of ANN and innovative topographic parameters can facilitate geomorphic mapping.

This research demonstrates that automated geomorphic mapping in the San Juan Mountains is achievable. Using a very small number of training sites and limited time to test the mapping protocol, the existing mapping produced accurate results. The ANN mapping was ground-truthed using mapping conducted by Kelkar (2017). Automated mapping can be done within a timeframe of several hours once the protocol is established. On the other hand, field mapping in a complicated alpine region can take from month to years to complete the mapping. The ANN mapping is also cost-effective.

Future ANN mapping protocols will require the following improvements:

i. Evaluate training sites and carefully select training samples to enhance the mapping accuracy. In this research, the training rate is 0.0372% which is significantly small. In the future research, a more rigorous protocol of training sample selection is required.
ii. Scrutinize the stratification of surface expressions in this research. In my research, 6 generalized surface-expression classes were selected. This generalization may reduce details of certain surface expressions; thus, a more scientific stratification is needed in future research.

iii. Develop a rigorous validation method to assess mapping accuracy. In my research, I only used Kelkar's map as a validation dataset; however, the potential human error introduced by Kelkar can be inherent when validating my mapping result. A better validation dataset is needed in future.

iv. Quantify the segmentation image as a new input layer to ANN. In my research, the segmentation exhibits its uniqueness for different surface expression. Because the unique pattern showing in segmentation image is not directly quantified in this research, it is essential to quantify these patterns for a more meaningful input layer to future research.

My research indicates that the use of ANNs would improve remote predictive mapping as an effective tool for remote regions. ANN can be adopted to map surface expressions in the San Juan Mountains. Terrain-based input to ANN can facilitate mapping automation. In this research, controlling factors, such as training site selection, can influence the mapping outcome. Future research will require improve training data to better evaluate accuracy.

Conclusion

This research integrated new topographic indices with ANN to facilitate geomorphic mapping in the San Juan Mountains. The geomorphic mapping results demonstrated the adaptability of the methods proposed in this research. These topographic indices create a

new path to utilize terrain analysis in geomorphology. Thus, it is obvious that this new approach will generation a new research direction. More research is needed in future.

REFERENCES CITED

Arcusa, S.H., McKay, N.P., Routson, C.C. and Munoz, S.E., 2020. Dust-drought interactions over the last 15,000 years: A network of lake sediment records from the San Juan Mountains, Colorado. *The Holocene*, *30*(4), pp.559-574.

Bolongaro-Crevenna, A., Torres-Rodriguez, V., Sorani, V., Frame, D. and Ortiz, M.A., 2005. Geomorphometric analysis for characterizing landforms in Morelos State, Mexico. *Geomorphology*, *67*(3-4), pp.407-422.

Church, M., 2010. The trajectory of geomorphology. *Progress in Physical Geography*, *34*(3), pp.265-286.

Coates, D.R. ed., 1976. *Urban geomorphology* (Vol. 174). Geological Society of America.

Cooke, R.U., 1984. *Geomorphological hazards in Los Angeles: a study of slope and sediment problems in a metropolitan county*. Allen & Unwin.

Dayvault, R.D., 2005. Mines, Mountain Roads, and Rocks: Geologic Road Logs of the Ouray Area, San Juan Mountains, Southwestern Colorado, guidebook 1. *Rocks and Minerals*, *80*(3), p.210.

Deng, Y., 2007. New trends in digital terrain analysis: landform definition, representation, and classification. *Progress in physical geography*, *31*(4), pp.405-419.

Evans, I.S., 2012. Geomorphometry and landform mapping: What is a landform?. *Geomorphology*, *137*(1), pp.94-106.

Gallant, J.C. and Dowling, T.I., 2003. A multiresolution index of valley bottom flatness for mapping depositional areas. *Water resources research*, *39*(12).

Goodchild, M.F., 1992. Geographical information science. *International journal of geographical information systems*, *6*(1), pp.31-45.

Goudie, A., 2003. *Geomorphological techniques*. Routledge.

Haykin, S., 1999. Self-organizing maps. *Neural networks-A comprehensive foundation, 2nd edition, Prentice-Hall*.

Hengl, T. and Reuter, H.I. eds., 2008. *Geomorphometry: concepts, software, applications*. Newnes.

Hoffman, S., 1997. The western San Juan Mountains: their geology, ecology, and human history Rob Blair, editor. *Great Basin Naturalist*, *57*(1), p.14.

Hsu, K.L., Gupta, H.V. and Sorooshian, S., 1995. Artificial neural network modeling of the rainfall-runoff process. *Water resources research*, *31*(10), pp.2517-2530.

Huff, A.E., Nomikou, P., Thompson, L.A., Hooft, E.E. and Walker, I.J., 2021. Applying planetary mapping methods to submarine environments: onshore-offshore geomorphology of Christiana-Santorini-Kolumbo Volcanic Group, Greece. *Journal of Maps*, pp.1-11.

Jensen, J. R., 2005. *Introductory Digital Image Processing*. New Jersey: Pearson Prentice Hall.

Kelkar, K.A., 2017. *Mass Movement Phenomena in the Western San Juan Mountains, Colorado* (Master thesis, Texas A&M University).

Latifovic, R., Pouliot, D. and Campbell, J., 2018. Assessment of convolution neural networks for surficial geology mapping in the South Rae geological region, Northwest Territories, Canada. *Remote sensing*, *10*(2), p.307.

Lehmkuhl, F., Nett, J.J., Pötter, S., Schulte, P., Sprafke, T., Jary, Z., Antoine, P., Wacha, L., Wolf, D., Zerboni, A. and Hošek, J., 2020. Loess landscapes of Europe–Mapping, geomorphology, and zonal differentiation. *Earth-Science Reviews*, p.103496.

Lucà, F. and Robustelli, G., 2020. Comparison of logistic regression and neural network models in assessing geomorphic control on alluvial fan depositional processes (Calabria, southern Italy). *Environmental Earth Sciences*, *79*(1), pp.1-18.

Metelka, V., Baratoux, L., Jessell, M.W., Barth, A., Ježek, J. and Naba, S., 2018. Automated regolith landform mapping using airborne geophysics and remote sensing data, Burkina Faso, West Africa. *Remote Sensing of Environment*, *204*, pp.964-978.

Nefeslioglu, H.A., Tavus, B., Er, M., Ertugrul, G., Ozdemir, A., Kaya, A. and Kocaman, S., 2021. Integration of an InSAR and ANN for Sinkhole Susceptibility Mapping: A Case Study from Kirikkale-Delice (Turkey). *ISPRS International Journal of Geo-Information*, *10*(3), p.119.

Palani, S., Liong, S.Y. and Tkalich, P., 2008. An ANN application for water quality forecasting. *Marine pollution bulletin*, *56*(9), pp.1586-1597.

Pike, R.J., 1995. Geomorphometry-progress, practice, and prospect. *Zeitschrift für Geomorphologie. Supplementband*, (101), pp.221-238.

Zhao, P., J. R. Giardino and Gamache, K.R., 2019. *Handbook of environmental engineering*. Chapter 5: Climate Change Impact Analysis for the Environmental Engineer. CRC Press.

Zheng, X., Tarboton, D.G., Maidment, D.R., Liu, Y.Y. and Passalacqua, P., 2018. River channel geometry and rating curve estimation using height above the nearest drainage. *JAWRA Journal of the American Water Resources Association*, *54*(4), pp.785-806.

5. CONCLUSIONS

Introduction

Traditional GIS mapping framework has four limitations: 1) insufficient geo-computation capacities; 2) incompatible with digital image processing and computer vision; 3) intendency of adapting a tight-coupling GIS setting; and 4) neglect of artificial intelligence. To mitigate the above-mentioned issues in traditional GIS mapping and studying framework, my dissertation integrated geomorphometry with self-designed geospatial algorithms to solve different geomorphic problems in multiple settings. My dissertation sought to achieve three objectives:

- develop a more suitable mapping protocol for alpine and glacial environments,
- evaluate the applicability of integrating ANN and innovative topographic indices for mapping automation, and
- assess using graph theory and object-oriented analysis for glacier dynamics.

To achieve these objectives, I conducted research in the San Juan Mountains in Southwestern Colorado and the Southern Patagonia Ice Field, Argentina. Results from the ANN classification of surface expressions suggests the high potential of combining ANN with new topographic indices for geomorphology mapping in alpine setting. The Geospatial algorithm development proposed in this dissertation illustrate that it can significantly broadens the scope of geomorphology studies. In addition, glacier dynamics can be re-evaluated by the protocol I developed in this dissertation. Finally, the integration of graph theory and innovative topographic indices can help facilitate geomorphology mapping and understanding system dynamics.

Future Direction

Geospatial technology will continue moving on the track of increasing the computational power and the analytical capacity for solving various geomorphic problems. These advancements will significantly alter geomorphologists' understanding of process. But will this 21st century geomorphology undergoes a revolution as dramatic as quantitative revolution in 1960s? I think the answer is no, because the development of modern geomorphology will largely be constrained by three major components: geomorphic flux transport laws, scale dependence of all processes, and complexity of the Earth system.

Geomorphic transport laws dictate how Earth materials can be redistributed, thus, reshaping the landscape. Scales in time and space will limit the understanding of the geomorphological processes and the scope of numerical modelling. System complexity with an emphasis on the non-linear nature of Earth science will further constrain the capacity to thoroughly analyze processes to obtain uniformitarian understandings that can partially explain the above two constraints.

Through my dissertation, I estimate more sophisticated geospatial techniques can somehow ease the constraints in geomorphology, to address scale dependence issues, or to simulate physical processes more accurately.

Future Direction Strengths and limitations of the new protocl

The major contribution of my dissertation is the introduction of a new protocol incorporating graph theory with satellite imagery to examine the structure change of a glacier-surface as an indicator for glacier dynamics. This new protocol has both positive aspects as well as limitations. I think researchers need to know and understand the positive aspects as well as the limitations of my new technique.

The positive points of the technique are:

- the input layer of convergence can uniquely and clearly delineate surface topography on- and off-glaciers;
- the objects-oriented analysis based on the convergence index can well reflect the pro-glacial processes;
- graph theory can mathematically reconstruct the relations of surface structure in a glacial system;
- this protocol challenges the tradition of using terminus position and mass balance as the only indicators for assessing glacier dynamics;
- provides a means to do a global inventory of change on glaciers at a reasonable cost and time period;
- topographic exposure index I developed can be useful for examining micro climate in glacial settings; and
- it allows a relative fast method to compare various locations around Earth.

Researchers also need to be cognizant of some limitations. The limitations are:

- original DEM quality plays a vital role in this protocol; especially the requestion still remains how to reconcile the DEMs retrieved from multiple years with different data sources;
- I adopted a thresholding method for segmentation in this protocol, which is subjective and can influence the size and number of objects generated on a glacier surface;
- it is essential to further evaluate the reproducibility of this protocol in other glacial environments, such as the Himalayas, Alaska, New Zealand and Antarctic;
- atmosphere conditions, i.e., intense cloud cover limits the temporal availability of image selection;
- because of the spatial resolution of various satellite platforms, detection of fine detail on surface of glaciers is limited;
- expense of various imagery whereas not as expensive as field-based observation is still expensive and can limit the options for a researcher; and
- the protocol facilitates detection and comparison of change on surface of glacier; it does not facilitate the calculation of glacier volume.